Development of Sensing Systems for Improving Surgical Grasper Performance

Dominic Paul Jones

School of Mechanical Engineering

University of Leeds

Submitted in accordance with the requirements for the degree of

Doctor of Philosophy

June 2019

Declaration

The candidate confirms that the work submitted is his/her own, except where work which has formed part of jointly-authored publications has been included. The contribution of the candidate and the other authors to this work has been explicitly indicated below. The candidate confirms that appropriate credit has been given within the thesis where reference has been made to the work of others. In all papers listed below, the primary author completed all experimental studies, evaluation of data and preparation of publications. All authors contributed to proof reading of the articles prior to publication.
Papers contributing to this thesis:

- Jones, DP; Wang, H; Alazmani, A; Culmer, PR. **A soft multi-axial force sensor to assess tissue properties in Real-Time**. In 2017 IEEE/RSJ International Conference on Intelligent Robots and Systems Proceedings (pp. 5738-5743). IEEE.
- Jones, DP; Jaffer, A; Alazmani, A; Biyani, CS; and Culmer, P., 2018. **Analysis of mechanical forces used during laparoscopic training procedures**. Journal of Endourology.
- Jones, DP; Kow, JW; Alazmani, A; and Culmer, P., 2018. **Computational Design Tools for Soft Inductive Tactile Sensors**. In IEEE International Conference on Biomedical Robotics and Biomechatronics (BioRob), 2018 7th . IEEE.

For the above Papers, all experimental work and data analysis was completed by myself, with the co-authors responsible for reviewing the papers.

- Wang, H., Jones, D., de Boer, G., Kow, J., Beccai, L., Alazmani, A. and Culmer, P., 2018. **Design and Characterization of Tri-axis Soft Inductive Tactile Sensors**. IEEE Sensors Journal.

For this paper, H Wang was responsible for the majority of experimental work and data processing, I was responsible for the design and experimentation of the final validation study. Myself and all other co-authors were responsible for reviewing the paper.

Dominic Paul Jones

June 2019

Acknowledgements

First, I would like to thank my two supervisors, Pete Culmer and Ali Alazmani, for their support and advice over the past three years. Between them they have always helped me to find the motivation to put in that little extra to push me to greater heights.

To Shekhar, Ata, and the staff at Leeds Teaching Hospitals, thank you for your insights, assistance, and efforts to expand the research through your collaboration and expertise in the surgical field.

Next to my family and friends for always being there to keep me calm and for your unwavering support over the years. Without me talking nonsense at you half of my problems would never have been solved.

Finally to Ellie, my wonderful fiancée, without whom none of this would have been possible. Without your love and support (and copious amounts of cake) I would never have lasted this long. You are my inspiration, motivation, and my best friend.

Abstract

Minimally invasive techniques play a vital and increasing role in modern surgery. In these procedures, surgical graspers are essential in replacing the surgeon's fingertips as the main manipulator of delicate soft tissues. Current graspers lack haptic feedback, restricting the surgeon to visual feedback. Studies show that this can frequently lead to morbidity or task errors due to inappropriate application of force. Existing research has sought to address these concerns and improve the safety and performance of grasping through the provision of haptic feedback to the surgeon. However, an effective method of grasping task optimisation has not been found.

This thesis explores new sensing approaches intended to reduce errors when manipulating soft tissues, and presents a novel tactile sensor designed for deployment in the grasper jaw. The requirements were first established through discussion with clinical partners and a literature review. This resulted in a conceptual approach to use multi-axis tactile sensing within the grasper jaw as a potential novel solution.

As a foundation to the research, a study was conducted using instrumented graspers to investigate the characteristics of grasp force employed by surgeons of varying skill levels. The prevention of tissue slip was identified as a key method in the prevention of grasper misuse, preventing both abrasion through slip and crush damage. To detect this phenomena, a novel method was proposed based on an inductive pressure sensing system. To investigate the efficacy of this technique, experimental and computational modelling investigations were conducted. Computational models were used to better understand the transducer mechanisms, to optimise sensor geometry and to evaluate performance in slip detection. Prototype sensors were then fabricated and experimentally evaluated for their ultimate use in slip detection

within a surgical grasper. The work concludes by considering future challenges to clinical translation and additional opportunities for this research in different domains.

Table of contents

List of figures

Nomenclature

MIS	Minimally Invasive Surgery
ECM	Extracellular Matrix
SITS	Soft Inductive Tactile Sensor
ANOVA	Analysis of Variance
NSRc	Normalised Stress Rate of Compression, $\dot{\bar{\sigma}}$
CoF	Coefficient of Friction

Chapter 1

Introduction

MIS was originally introduced in 1983 [17] and has since become a staple technique around the world. Rather than a single long incision to open the operating site, several smaller incisions (typically 10-20mm long) are made at specific points to allow access the abdominal cavity. The smaller incisions assist in a reduced recovery time, as well as reduced scarring to the patient [18]. Several tooling ports, or trocars, are inserted through the incisions to offer sealable access points for the tools to pass through [19]. The abdomen is then insufflated with CO_2 to provide extra working space for the surgeon. A laparoscope and several long thin tools are then passed through the trocars (Figure 1.1) to provide vision and manipulation at the operating site. Graspers are a key instrument used to manipulate and hold tissue in MIS procedures, in essence replacing the surgeon's fingertips. However, the mechanical nature of these tools coupled with the reducing size of the end effectors amplify the pressures applied to the grasped tissue.

While generally accepted as a superior method for reducing surgical damage, there are some disadvantages. The instrumentation used prohibits the perception of forces, velocities, and displacements of the tissues and the proprioception required for motor performance is distorted [20]. Both manual and telerobotic tools also suffer from losses of haptic feedback to the surgeon, thus increasing the likelihood of grasper misuse [21].

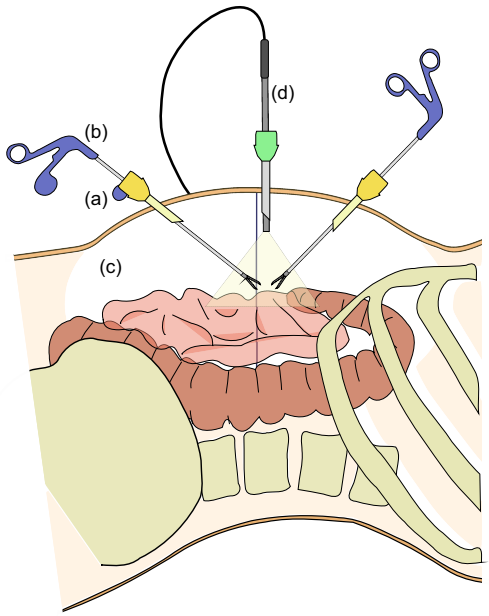

Fig. 1.1 A schematic of abdominal MIS, indicating several key tools: (a) Trocar, (b) Grasper, (c) Insufflated Abdomen, and (d) Laparoscope

The steep learning curve required to overcome these obstacles posed by MIS has long been recognized as a potential hurdle for trainee surgeons, especially given the static training models currently in place. Although virtual reality simulation has the potential to offer important advantages in the area of training for new skills and procedures, evidence on the transfer of skills from the simulated environment to the operating theatre is still limited, especially in advanced surgical procedures [22].

These advanced procedures involve smaller and more delicate structures [23], increasing the demand for enhanced force feedback from the tissue tool interface. While statistics show an increased uptake of telerobotic systems for complex procedures [23], conventional 'hand operated' laparoscopic surgery will continue to be a major component of modern day surgery. The instrumentation for both procedures would benefit improvement and innovation. Therefore there is a clear need for improved instrumentation in both conventional and robotic-assisted laparoscopic surgery.

Many technologies exist which may assist in this sensing increase, however many have not been fully proven for use in this area. For this it is essential to review the existing technologies and to focus the research on those deemed most suitable for the task.

1.1 Project Aim

The aim of the work is to develop and evaluate appropriate sensing technology to optimise grasper usage in MIS.

1.1.1 Research Objectives

The objectives defined to achieve this aim are:

Objective 1 To identify appropriate sensing technologies which may be integrated into a surgical grasper.

Objective 2 To characterise typical grasper use in laparoscopic surgery.

Objective 3 To develop a sensing concept and approach for the improvements of grasping tasks.

Objective 4 To characterise and optimise sensor design parameters using experimental and computational techniques.

Objective 5 To produce and evaluate a demonstrator of the sensing technology in laboratory conditions through clinical input.

1.2 Thesis Overview

This thesis has been divided into 8 chapters. These chapters address each of the objectives before the thesis is concluded with a general discussion and reflection on outcomes and future opportunities.

Chapter 2: Literature Review

The current state of laparoscopic surgery is reviewed to assess potential areas for sensing integration. Next the review presents applicable technologies. Mechanical measurement is concluded as the key technology for tool integration. Different transducer methods are assessed for the fulfilment of sensing within the surgical environment.

Chapter 3: An Analysis of Grasping Forces in MIS

This chapter presents work conducted with clinical partners to characterise the forces and movements used in surgical grasping of delicate tissues. The work was conducted to better understand clinical needs and technical requirements for the sensor system.

Chapter 4: Investigating Methods of Applying Sensing to Improve Grasper Performance

This chapter presents and evaluates two sensing applications intended for use in a grasping environment. This further defined technical requirements for the sensor based on the optimal sensing approach.

Chapter 5: Investigating a Novel Sensing Method to Improve Laparoscopic Grasping Tasks

This chapter uses computational and experimental methods to investigate the design parameters of a novel sensing technique to assess it's fulfilment of the design parameters. This assisted with the final selection of the sensor to be optimised in the subsequent chapter.

Chapter 6: Computational Optimisation of Inductive Tactile Sensors in 3D

This chapter focuses on the optimisation of design parameters through finite element simulation. This produced the optimum sensor geometries for increased resolution.

Chapter 7: A Sensor for Slip Detection within a Grasper Jaw

This chapter focuses on assessing the capabilities of a prototype sensor to assess it's concordance with the design limitations and requirements. The sensor was used to fulfill criteria established in previous chapters.

Chapter 8: General Discussion & Conclusions

The concluding chapter g.presents a general discussion of the outputs and findings from this work in the context of the wider research field of surgical robotics and sensing systems. The research objectives are then reviewed, and potential future pathways for the research are established.

Chapter 2

Literature Review

This review presents a critical analysis of the literature relevant to the clinical problems associated with laparoscopic graspers. In particular the lack of force feedback increasing the chances of incorrect force application in tissue retraction is identified as a significant problem. Initially, current advances to MIS grasper technology are presented, before identifying the key properties of tissues which may be measured. The main body of the review focuses on a variety of tactile sensing methods which may be integrated within a grasper face. The aim of this chapter is to communicate a significant clinical need for grasper optimisation and the methods which may be used to assist this optimisation. The review is concluded with the selection of a sensing technique and a series of technical requirements which must be met.

2.1 Minimally Invasive Surgery

Existing research seeking to reduce damage in MIS graspers has considered the geometry and characteristics of the grasper jaw. In general, sharp jaws are used to prevent cases of tissue slip [24], however sharp edges and corners on the grasping face increase the magnitude of point stresses applied to the tissue [25] . These stresses can be reduced by rounding of the geometries [26] in an effort to reduce damage, although excessive rounding can increase the chances of tissue slip [27]. Other groups have looked toward soft graspers as a method of stress reduction [1]. Instead of a large variance of elastic modulus between the tool and tissue (found in grasper jaws made from stainless steels), a soft grasper would deform under higher forces, applying much lower stresses to the tissue. Such a grasper would deform to the geometry of the tissue providing a higher contact area to increase friction along the tissue-tool interface, reducing the chances of slip [1].

2.2 Soft Tissue Properties

In open surgery, a surgeon may use several tissue properties to assess the quality of tissues as they may be easily accesses and manipulated. Within MIS however there is little sensing available for the surgeon, generally limited to visual feedback via the laparoscope and basic haptic feedback transmitted through the tool mechanisms. In order to increase this available sensing, the properties of tissue must first be assessed. Several properties may be used to characterise tissues, presented in 2.1

Table 2.1 Various quantifiable measures to assess tissue quality

Mechanical	Surface	Thermal	Electrical	Chemical
Elasticity	Roughness	Temperature	Conductivity	pH
Hardness	Coefficient of	Conductivity	Capacitance	pO_2
Density	Friction		Reactance	Hydration
Tensile Strength				

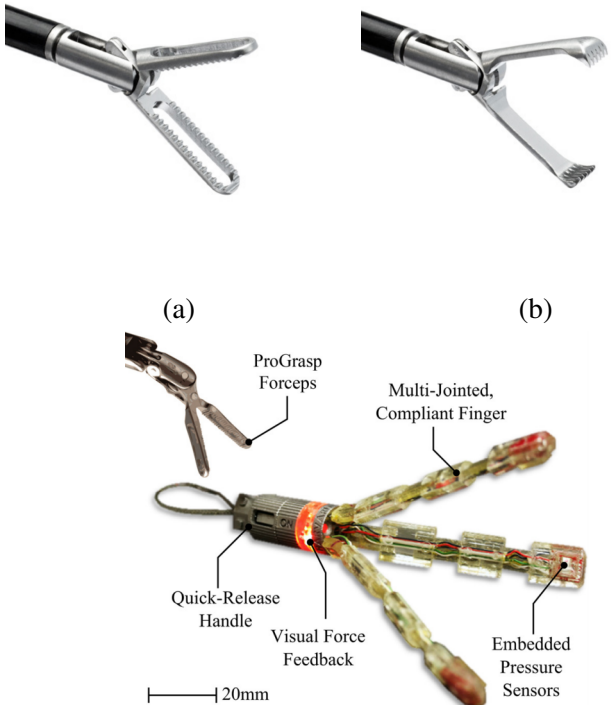

Fig. 2.1 Examples of Surgical grasper tips, (a) Short fenestrated and (b) Fine toothed forceps (Surgical Innovations, Leeds, UK); and (c) Hammond's soft atraumatic grasper, from [1]

The tissue properties available for analysis cover many fields, but several are unsuitable for intra-operative sensing. The predominant properties to be assessed in this review are mechanical, electrical and electrochemical, each giving a different insight into the composition and structure of different tissues. Each property was chosen for its potential for use within a a surgical grasper, as well as previous work within the research group to be potentially adapted for such use.

2.2.1 Biological Constitution of Soft Tissues

Due to their complex compositions, soft tissues exhibit many different properties depending on the constituents and their orientation. The main constituents of tissue are cells and the extracellular matrix (ECM) which control the function and structure of the tissue, respectively.

The ECM consists predominantly of collagen and elastin and is saturated in ground substance [28] (Figure 2.2).

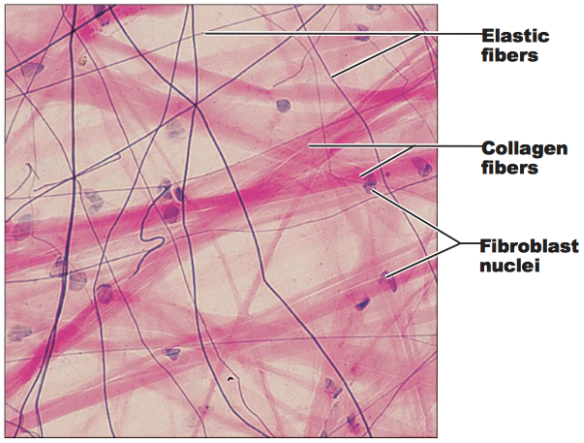

Fig. 2.2 Diagram of connective tissue structure, indicating the matrix of collagen and elastin. Fibroblast cells are also present within the matrix, from

Collagen(I) is the most abundant protein in the ECM, forming the bulk structure. It is a helical protein organised into strands, giving varying isotropic and anisotropic mechanical properties dependent on their orientation [29]. Tendons, for example, have an extremely organised and tightly packed structure, leading to a strong axial tensile strength, but an extremely weak radial strength. Stromal tissue, conversely, is composed of a web of collagen, leading to isotropic tensile strength [2] 2.3.

Elastin is the secondary protein of the ECM, giving the tissue its elastic properties at low strain [30]. At these lower strains, the bulk elastic modulus of tissue is dominated by the modulus of elastin, due to the low modulus of coiled collagen. Once the helical structure of the collagen straightens, the bulk elastic modulus is shifts to be dominated by collagen, preventing over-extension of the elastin [28]. The fibres of the ECM are saturated in ground substance, an amorphous gel-like substance containing water, proteins, and sugars [28]. It is secreted by cells, and forms the base for the production and repair of molecules within the matrix.

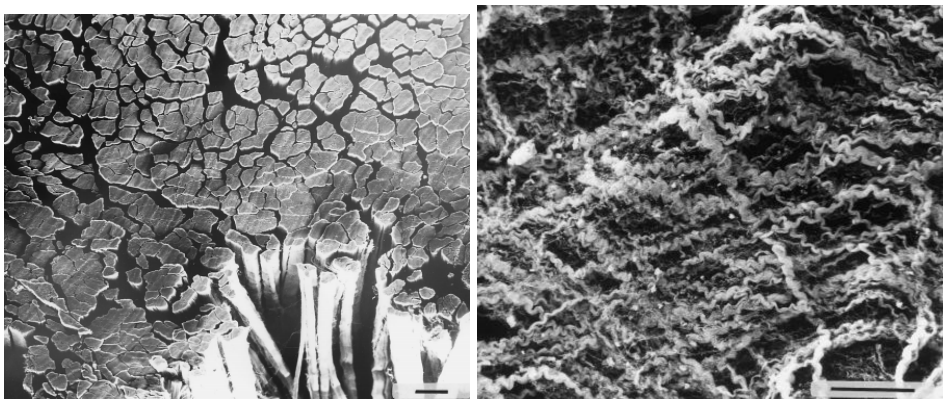

(a) (b)

Fig. 2.3 Collagen microstructures of different tissues: a) Tendon, displaying parallel orientation and b)Stroma of the small intestine, showing a web-like structure, from [2]

2.2.2 Electrical Properties

For over a century, the electrical properties of tissue have been studied [31]. Two properties by which issue can be electrically categorised are capacitance and conductance [32]. The relative permittivity and Dielectric conductivity are heavily influenced by the internal physiology and chemistry of the cells, with typical variances for different and diseased tissues, giving potential for the use of such measurements as diagnostic methods [31, 33].

The mechanisms of conduction through electrolytes are not as simple as the models used for solid conductors. In solid conductors, the transfer of electrons is direct through the substance itself. In an electrolyte, charge is transmitted through the physical movement of ionic particles through their solvent. This movement varies with ionic size as well as the viscosity of the solution [34], and so limits the lower limit of the resistance of the solution, and generates a time-dependent effect for the overall perceived resistance. The charges are transferred to the circuit by their oxidation and reduction at the surface of the electrodes, meaning the electrical assessment of tissues is linked with the field of electrochemistry. Methods of electrical sensing have been proposed for surgery, however mainly focus on the detection of benign regions [35], location of sub-surface structures [36] or detecting muscular impulses [37].

2.2.3 Electrochemical Properties

Electrochemistry is a field of study specialising in the relationships between chemical reactions and electric charge. Typically, this refers to the reactions based at the surface of an electrode in contact with an electrolyte [34]. Redox reactions at the boundary cause the transfer of electrons between the ionic compounds dissolved in the electrolyte and the conductive electrode. The rate of transfer of electrons from a particular solution is affected by the reactivity of the electrode in question. This can be measured as the electrode potential of a material, measured in reference to a hydrogen electrode, with a standard potential of 0V at all temperatures [38]. Two geometrically identical electrodes of different materials, connected electrically and ionically via circuitry and a salt bridge, will produce a current between them, with potential equal to the difference in standard potentials. In surgery, analysis of the electrochemical properties has shown promise in tissue discrimination [39], health assessment [40] and external biosensors to detect molecules present in the blood [41]. The main issues with such sensing methods are electrode reactions with the contacted tissue, resulting in ions dispersed within tissues [42].

2.2.4 Mechanical Properties

The bulk mechanical properties of tissues are a widely researched area in biomechanics, and so their use in future surgical interventions could be key. Unlike solid mechanics, soft tissues do not respond in a Hookean manner to external forces. The non-linear nature of tissue is dependent on several factors but is mainly based on the constituents of individual tissues, as well as their arrangements [28, 43]. This is particularly true for the detection of cysts and cancers, due to their tissues exhibiting a greater hardness than surrounding tissues [44]. Tissues may also display an orthotropic nature, with tissues such as blood vessels possessing highly arranged layers of collagen, preventing radial expansion, yet giving little axial strength [45]. In addition to this, tissue exhibits a time-dependent viscoelastic nature [3] (Figure 2.4), whereby the viscous extracellular fluid may move throughout the ECM [46]. Due to this,

tissue exhibits stress relaxation, where a constant applied strain will induce a time-dependent decrease in stress, which must be accounted for in real-time models of tissue analysis [47].

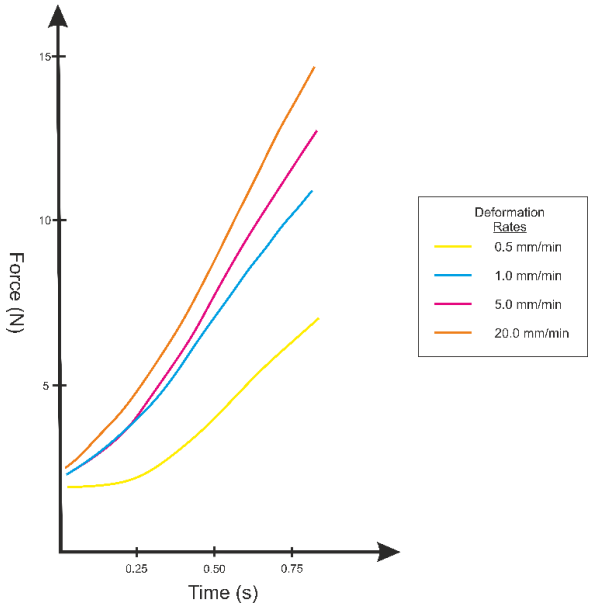

Fig. 2.4 The influence of deformation speed on the viscoelastic properties of tendon, showing increased elastic modulus at increased speed. Adapted from [3]

2.3 Current Surgical Graspers

Graspers are a key instrument used to manipulate and hold tissue in MIS procedures, in essence replacing the surgeon's fingertips. However, the mechanical nature of these tools significantly impedes the sensation of force feedback to the surgeon, thus increasing the likelihood of tissue over-compression and damage [21]. Up to 66% of damage in MIS can be attributed to grasping forceps [48], showing a significant clinical need for improvements in surgical tools to deliver force feedback and limit tissue trauma. The forces at which over-compression occurs may be seen as an upper bound of grasping forces [4], above which tissue will always be damaged. Conversely, a lower bound of compressive force may be established at the point where tissue begins to slip from the grasper jaw (Figure 2.5) [49]. This creates a 'safe zone' for grasping at which the grasper will perform optimally.

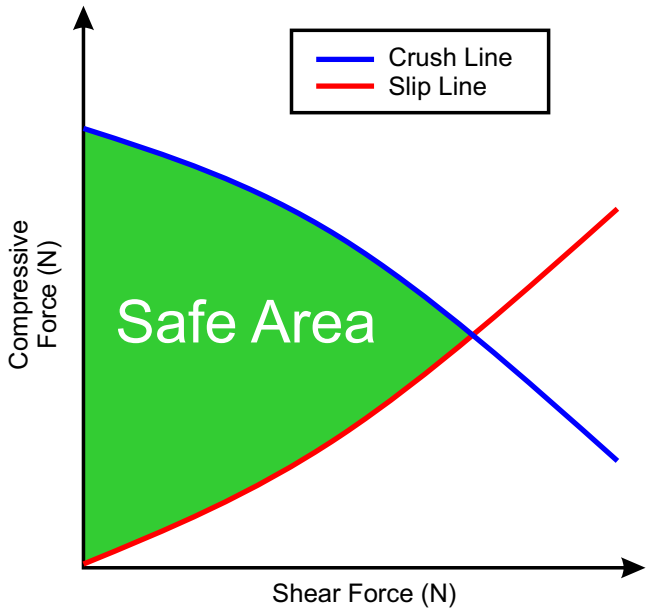

Fig. 2.5 Indication of the 'safe' grasping forces bounded by slip and crush forces, adapted from [4]

There are two main limitations that may be improved upon [21, 50–52]:

1. The risk of tissue slipping from the grasper jaw (causing abrasion) due to insufficient compressive forces.
2. The risk of excessive force application, effectively crushing the tissue.

These limitations all may be rectified with an increase in the availability of force sensing. In particular, mechanical force measurement will allow rectifications of all limitations stated. Therefore future investigation will focus solely on force, specifically tactile, sensors.

2.3.1 Placement of sensors

MIS graspers present several areas in which force sensors may be integrated which fall into two main categories: internal and external sensors. Each of these have significant differences in their advantages and disadvantages for an effective sensor.

- **Placement within the actuation method**
  of a grasper, either within the mechanical linkage or handle [25, 53–55], removes the size constraints from any sensing module. The signal, however, is affected by friction and backlash in the mechanism [53]. This can cause overestimation of grasping forces in some cases [56].

- **Proximal placement on the instrument shaft**
  has little size constraint, however the force readings will be affected by reaction forces imparted on the tool by the trocars during movement [57]. Therefore other sensing must be present in the system to compensate this error and make the method feasible.

- **Distal placement on the instrument shaft**
  is free from the interferences of shaft flexion experienced further up the shaft , and has the potential to measure multi axis force and torque on the end effector [6]. The main disadvantage, however, is the size constraint. The sensor must be small enough to pass through the trocar while being fixed upon the surface of the shaft. Generally, the maximum diameter of trocar used is 15mm [58] offering an extremely small space for instrumentation.

- **Placement on the grasper face**
  has even more extreme size constraints than the lower shaft, with a maximum width equal to that of the shaft diameter. There is a major benefit in this method is the direct measurement of the tissue-tool interface with isolation from external interference. This also allows direct measurement of multi axis contact force but the difficulty of torque measurement is increased. The sensor, however, must fit on the extremely small face requiring a miniaturised technology.

Direct measurement of the tissue tool interface through sensing at the grasper tip will offer the highest fidelity measurement of applied forces to the tissue, and so will be the main focus in the research.

2.3.2 Tissue-tool Interaction Pressures in Grasping Tasks

Before requirements for the sensor can be produced, first the force ranges for the tactile sensors must be established. The existing research using instrumented laparoscopic graspers provides much information on the forces applied during general tasks, such as knot tying [59], but is limited in the application to soft tissue. Brown's BlueDRAGON indicated a maximum compressive force of 68.17N applied by surgeons [60]. This is not sufficient for the measurement of the tissue-tool interface however, as the tips of graspers come in many sizes, and surgeons will grasp with varying percentages of the face. To adequately correlate between different grasping faces, the force must be converted to a contact pressure. De's motorised endoscopic grasper (MEG) used this force as reference, and applied various contact pressures up to 240kPa to liver tissue [25]. Barrie used an instrumented grasper to analyse the forces applied to porcine colon in a simple handling task [54], and deduced a maximum applied pressure of 300kPa.

2.4 Mechanical Measurement in a Grasping Environment

The intrinsic properties of tissue can be analysed to provide methods of characterisation. This characterisation would allow the differentiation between different tissue types within a surgical environment. One main feature of many of the potential technologies is the ability to display data to a surgeon in real-time, allowing precise movements within the body to be monitored effectively. Of the above properties, mechanical measurement offers the best potential for integration into a grasper. Therefore, several methods of mechanical assessment are assessed in comparison to current techniques.

2.4.1 Techniques in open surgery

Palpation is a common technique for assessing tissues within open surgery. It is generally performed by two techniques, either sliding the fingers across the tissue or probing individual points of interest. This gives a surgeon an overview of the tissue they are examining, with less elastic tissue structures, such as tumours and scarring, being easily detected below the surface by the human finger [61]. As the fingertips can sense both compressive and shear forces, texture and friction may also be sensed. In order to replicate such sensations, and sensing method chosen must possess multi-axis force sensing.

2.4.1.1 Mechanics of Fingertip Sensing

Before assessing appropriate tactile sensing technologies, first the gold standard of current surgical sensing must be assessed: The human fingertip. Fingertips are capable of sensing compression, shear, friction, temperature and texture. In particular, the sensing of shear and friction allows highly dextrous handling of objects, in particular soft wet surfaces [62]. If the sensations observed at the fingertip could be replicated in a robotic sensor, manipulators would be capable of 'smart' gripping that is more accurate imitation of human grip.

The structure of the fingertip offers an insight into it's sensing capabilities. Four types of mechanoreceptor are dispersed through the soft tissue, each sensing individual segments of the overall sensation [5, 63].

- **Meissner's Corpsucles** are located superficially and detect dynamic forces. They are particularly useful in the detection of slip of a grasped object.
- **Merkel's discs** are located superficially and detect sustained compressive forces. They assist in the perception of shape and texture in a grasped object.
- **Pacanian corpsucles** are located deeper into the tissue and detect high frequency vibrations.

- **Ruffini Ccorpsucles** are located deep within the fingertip and along the finger. They operate independently to applied forces and allow the detection of finger position.

Various free nerve endings also exist in the upper layers of the skin in order to detect temperature and pain. Of the above receptors, the Meissner's corspucles and Merkels's discs account for around 40% and 25% of the total receptors in the fingertip [5]. They also are responsible for the sensations most used in palpation of tissues in open surgery. If a tactile sensor can accurately replicate the functions of these receptors, it can be seen as an adequate replacement for a surgeons fingertips in MIS.

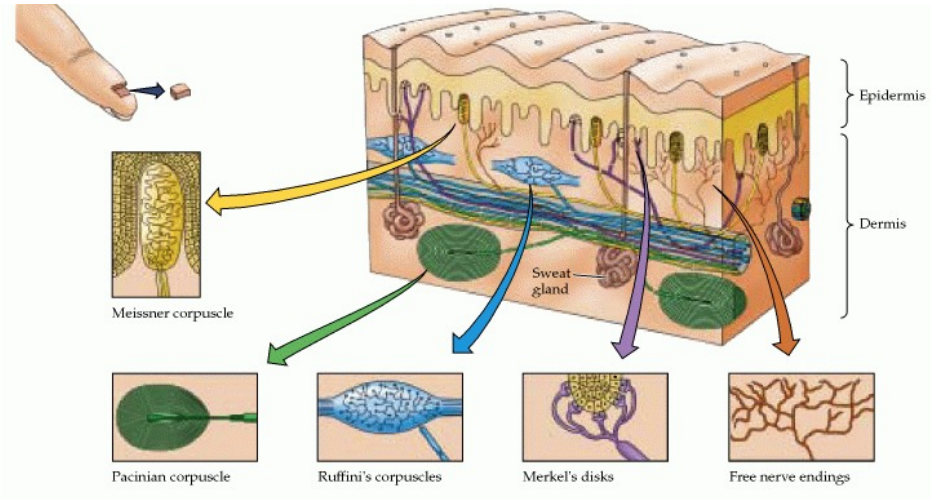

Fig. 2.6 Schematic of the location of various mechanoreceptors in the fingertip, from [5]

2.4.2 Resistive sensors

2.4.2.1 Strain Gauges

Strain gauges are one of the most common technologies used to sense forces. They consist of a thin metal wire, typically in a parallel zig-zag pattern, upon a flexible polyimide substrate (Fig 2.7a). Once bent, the electrical resistance of the wire changes, which can then be calibrated to force. While a standard strain gauge is limited to a single DoF, several

orientations exist which allow multiple DoF, such as the Stewart Platform [6] and the Maltese cross [7] (Fig 2.7).

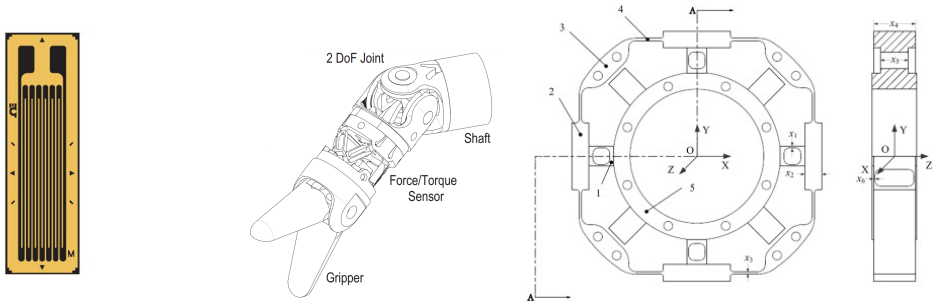

(a) (b) (c)

Fig. 2.7 (a) Example of a 1D strain gauge, (b) Stewart Platform arrangement (labelled Force/Torque Sensor) [6], (c) The Maltese Cross arrangement [7]

In literature, there are several examples of strain gauges being used within a surgical grasper. The simplest implementation of strain gauges is to use a commercial load cell within an existing tool. This technique was used by De and Barrie [25, 54] to measure contact force at the tool tip by implementing a single-axis load cell within the grasper mechanism. Rosen [64] also used a similar method, incorporating a single-axis cell within the grasper handle to detect tensile forces in the mechanism. These graspers are able to achieve good resolutions of contact force, however show limitations in the error level of the measurements (up to 30% of the true force value [64]). These limitations stem from the location of the load cell, as the measurements experience errors through backlash and friction in the mechanism [54, 64]. Therefore for the precise measurement of contact forces through analysis of mechanism forces is insufficient for use in grasping.

Because of this, some groups have incorporated strain gauges to the distal end of the grasper mechanism. This reduces the mechanism effects above and theoretically gives a more accurate value of tip forces. Kubler *et al.* [6, 65] introduced a stewart platform load cell arrangement to the distal end of the grasper to detect the forces present on the end effector under grasping. Due to the cable-driven actuation of the end effector, contact forces were also measured. The device exhibited high sensitivity, 0.25N in z, 0.05N in x,y, however suffered from interference in the contact force measurement. This was caused by the same axis of

force (z) recording both the tension in the mechanism as well as any pull forces applied. For such a sensor to perform in the grasping task this would need to be calibrated out through use of other sensors. Strain gauges also suffer in their performance with exposure to high temperatures and pressure. Typical responses are an increase in hysteresis and drift. For use within a surgical tool, this must be rectified to allow sterilisation by autoclave. Trejos [66] investigated an encapsulation method for strain gauges designed to prevent these effects from the autoclaving process. Results show that the hysteresis error caused by sterilisation is reduced, however the encapsulated gauges have a limited survival under repeated sterilisation, generally surviving only 5 autoclave cycles [66].

Strain gauges show potential for multi-axis surgical sensing, as they are innately contained and can function in wet environments. The major disadvantage, however, is the manufacturing complexity of the structures needed to increase the DoF are relatively high. Therefore they must be fully sealed before use on the end-effector to prevent contamination with external biomatter [67].

2.4.2.2 Piezoresistive Sensors

Piezorestors are defined as materials which exhibit a varying resistance under applied stresses. Two main classes exist: doped silicon and nanocomposites. Doped silicons act in a similar manner to strain gauges, yet have a higher sensitivity and measurement range. Takashi et al. [8, 68] developed a triaxis force sensor using pairs of doped silicon beams in multiple directions to sense axial and shear forces in a 10 x 10 mm package (Fig. 2.8). The sensor allowed measurements upt to 400 kPa (40N) normal,and 10N shear force. The sensor-specific bandwidth is not stated, however other similar sensing methods have achieved around 100 Hz [69]. The main problems with such sensors is a hysteresis up to around 15% [70], as well as the complex manufacturing methods required to produce them.

Nanocomposites consist of a soft elastomer substrate doped with conductive fillers to produce a piezoresistive effect. Contact between individual particles of the filler produces

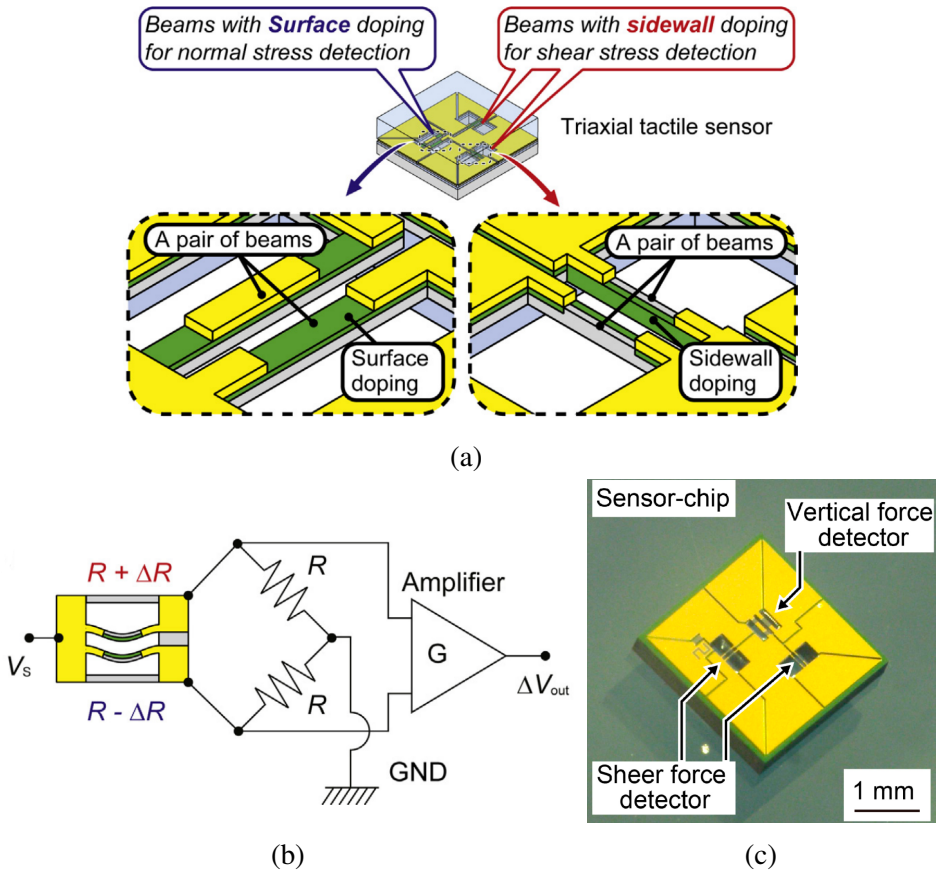

Fig. 2.8 Takashi's piezoresistive triaxis tactile sensor: (a) Schematic indicating silicon beams, (b) the bridge used for measurements [8], and (c) photo of the full sensor design [9]

a complex conduction pathway with relatively high resistance (Fig. 2.9a). As a pressure is applied, the filler particles are forced closer together and more contact is created. This causes more direct conduction paths, and reduces the observed resistance [71]. Typically fillers are metal- [72, 73] or carbon-based [71, 74]. Carbon fillers are generally will give better mechanical properties in the resulant nanocomposite, as some metal can have adverse effects on the flexibility of the final structure.

Nanocomposites are omniaxially conductive, and in a basic structure will only offer a single axis of force data. There are some examples, however, of structures to allow multiple degrees of freedom form soft piezoresistive materials. Li [10] produced a triaxis tactile sensor using a carbon black doped film as the resistive element. The sensor used a 'seesaw' like model to detect non axial forces (Fig. 2.9c), whereby a shear force would cause uneven

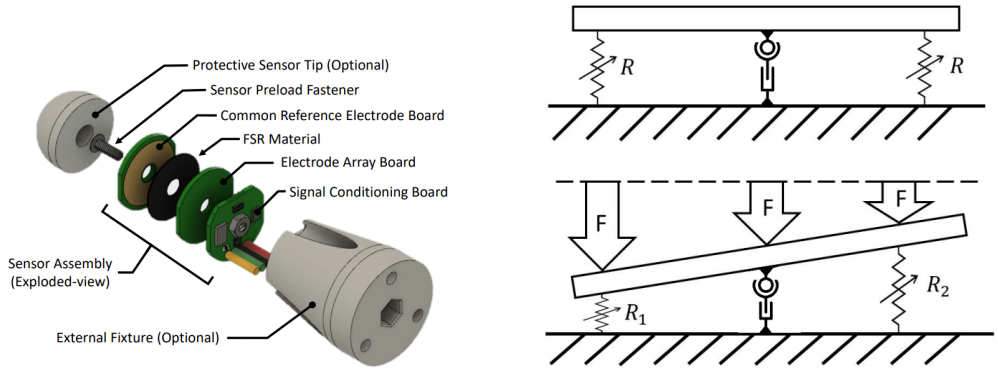

(a) (b)

Fig. 2.9 (a) Li's triaxis tactile sensor [10]; (b) Operating principle of Li's sensor [10]

compression of the film about the pivot. The sensor performed comparably to an off the shelf multi-axis load cell in testing, at a fraction of the cost. The sensor suffered from repeatibility issues over extended use, as well as significant drift from the carbon black film used.

Piezoresistive sensors are widely used transducer method in tactile sensing. While generally precise and robust, manufacturing complexity of both micromachined silicon beams and nanocomposites is high. Therefore such sensors would be relatively expensive both in time input and cost.

2.4.3 Capacitive Sensors

Capacitive sensors rely on the deformation of a dielectric substrate between two electrodes as the transducer mechanism for the detection of force [75]. Generally, they have a high spatial resolution and good frequency response, however are susceptible to crosstalk between channels [76]. Many examples of capacitive sensors have been produced in recent years, both in array and multi-axis forms. As an array, capacitive sensors rely on scanning the intersection points of several perpendicular electrodes electrodes, separated by a dielectric layer [11, 77, 78] (Fig. 2.10a). In this manner, a capacitive array can be used as a 'sensing skin'. Such skins have been developed for both anthropomorphic [79, 80] and surgical manipulators [81] offering single-axis sensing in a similar manner to that of the human

fingertip. Other arrangements of capacitive nodes can offer 3-axis sensing. Wang [82] and Lee [12] both used 2 × 2 arrays of capacitive nodes with soft structures placed above the centre axis (Fig 2.10b). A 'hard' version of the sensor has been produced by Asano [83] using a CMOS circuit with a 3-axis node of 2.5 × 2.5 mm. Using additive and differential signals from the nodes, both normal and shear forces may be calculated.

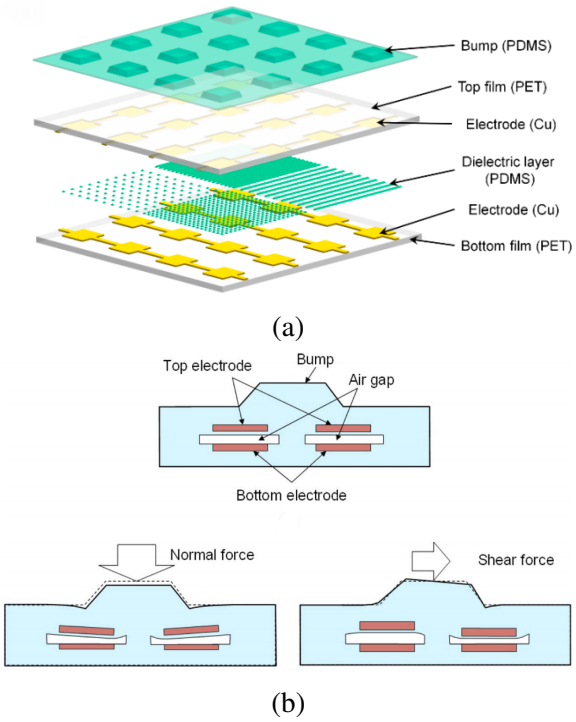

Fig. 2.10 (a) Schematic of a Capacitive tactile array, indicating two layers of perpendicular electrodes, from [11], and (b) Multiaxis capacitive tactile sensing principle, from [12]

Such sensors offer better frequency response and sensitivity than that of resistive sensors, however suffer from a vulnerability to electromagnetic noise and crosstalk between channels. While the sensing nodes are relatively compact, complex manufacturing processes are used to produce them.

2.4.4 Computer Vision

With advances in neural networks and machine learning, computer vision is becoming a robust method for determining compressive and shear loading. In this field there are two

main sensors relying on similar methods. Bristol University's 'TacTip' tracks the changes in the size and spacing of regularly spaced markers within an elastomeric dome to detect deformation of the surface [13]. Several versions have been produced including one designed as a grasping surface with the ability to dexterously handle objects [84].

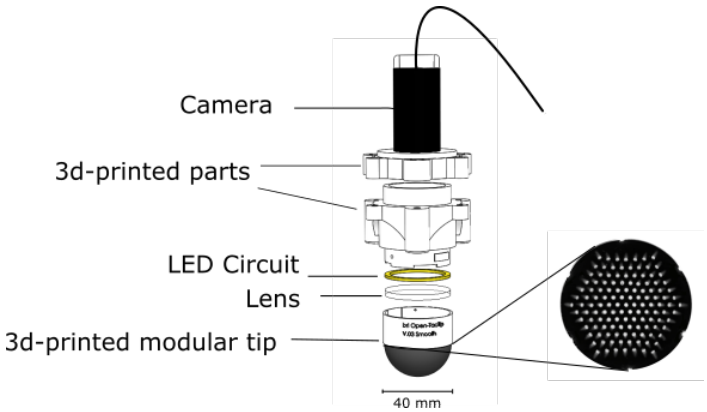

(a)

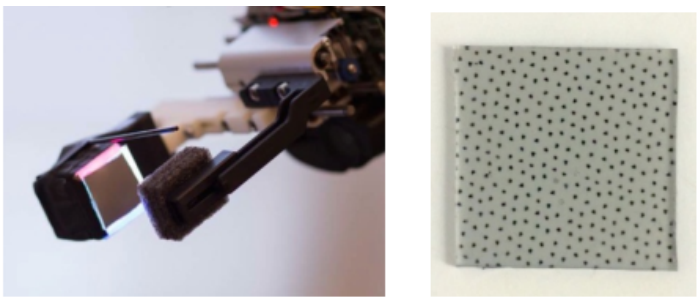

(b)

Fig. 2.11 (a) Bristol's TacTip and internal view of displacement markers [13], (b) Gelsight sensor and shear measurement markers [14]

MIT's GelSight can detect the surface topography of a sample using the shadows from three coloured light sources. In a similar manner to the TacTip, estimations of three axis forces can also be produced by calculating the change in size and position of a random array of dark markers on the sensing surface. While both sensors offer three axis force sensing with relatively good accuracy, their main problem with the use in a surgical setting is the cameras used in sensing. The size of the sensing body is fully reliant on the size of the camera, from which high resolution images are needed. Also the use of computer vision

for real-time sensing is difficult, with sensing being reliant on the 60 Hz frame-rate of the cameras used for sensing.

2.4.5 Optical Fibre Sensors

Fibre Bragg sensors make use of distributed Bragg reflectors along a section of optical cable to prevent the transmission of certain wavelengths along the cable. The Bragg grating reflects a particular wavelength of light while allowing all other wavelengths to pass. This wavelength is dependent on both the refractive index of the grating and the distance between reflectors in the grating (grating period). As stress is applied to the fibre the grating period changes, thereby creating a measurable change in the reflected wavelength [85, 86].

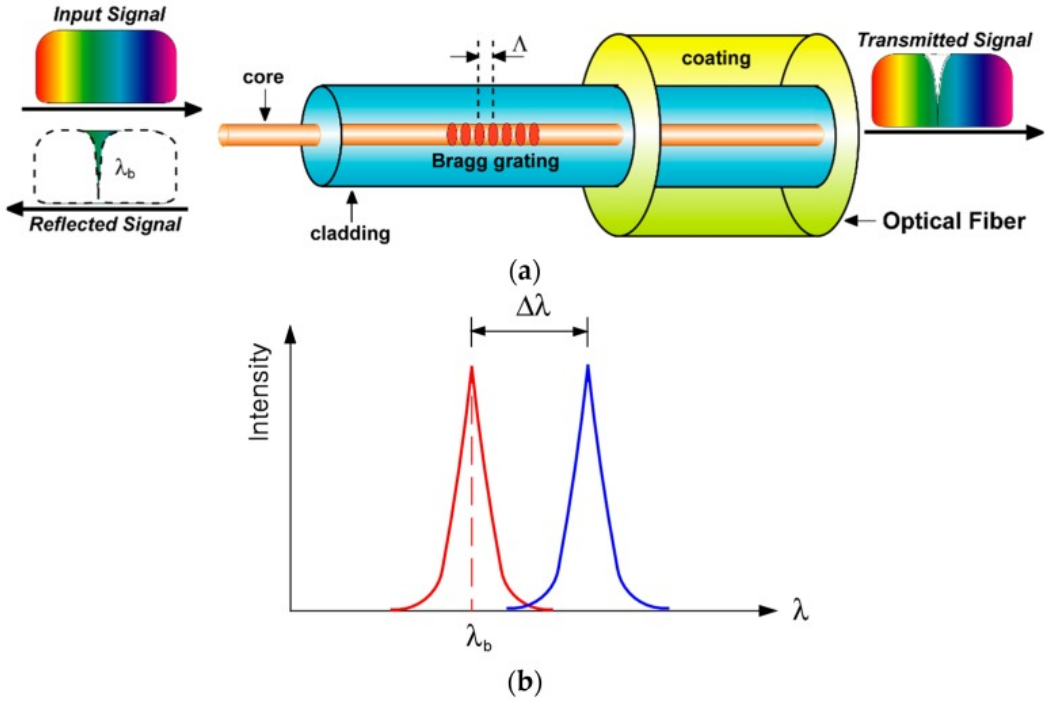

Fig. 2.12 (a) Principles of the fibre Bragg grating (b) indicating the absorption wavelength change under stress, from [15]

FBG-based sensing is a promising technology for healthcare, particularly useful is the immunity of the fibre optics used to the electromagnetic fields in MRI scanners [87]. A main disadvantage of the technique is the effects of temperature on the grating. Thermal

expansion of the fibre will also cause a shift in the reflected wavelength causing a significant source of error. Some groups have mitigated this through use of redundant gratings which do not experience stresses from applied forces, using a shift across all gratings to calculate the temperature change [88–90]. Others have taken advantage of the ability to locate the electronics distant to the sensing surface to create various surgical tools with multi-DoF force sensing capabilities at the tool-tip [88, 91]. Zarrin *et Al.* developed a electrical discharge machined grasping surface with two embedded FBGs to detect compressive and pull forces in surgery [92]. Each grasper face consisted of a sliding platform to measure axial forces, with a soft surface to measure normal force. The sensorachieved ranges of 10N and 6N compressive and axial forces, respectively. The sensor bandwidth is dependent on the external interrogator used, up to 500 Hz with the stated model (SM130, Micron Optics Inc., USA). Generally FBG tactile sensors have shown high sensitivity with resistance to many external factors such as moisture [93] and magnetic fields. The main limiting factors in the technology are based in the electronics needed to measure the changing absorption wavelength. FBG interrogators are generally quite large, and as such cannot be mounted to a grasper directly [94]. As the fibre must be physically connected to the interrogator, and such graspers would require a cabled connection to an external sensing bank. While this problem would be less significant in robotic surgery, the application to non-robotic graspers would be difficult.

2.4.6 Other Transducer Methods

2.4.6.1 Hall Effect based Sensors

Magnetic field based sensors are a relatively new method of force sensing providing multi-axis force measurements through the detection of a changing magnetic field. The technique exploits recent advances in MEMs Hall-Effect sensors to provide high performance, multi-axis force sensing at a low cost. Wang et al [16, 95] present a tactile sensing node and a full analysis of it's design parameters. In the sensor, a fixed magnetic field source, such as a neodymium magnet, is fixed above a soft silicone substrate. As forces are applied, the

magnet displaces in 3D, causing a change in magnetic field in the sensor below (Fig. 2.13). This displacement can be calibrated to the force input, and is dependant on the mechanical properties of the soft substrate. As such, the sensing characteristics can be readily 'tuned' through adaption of sensor design variables, principally the geometry and material properties of an elastomer core which deforms with applied load. The specified design was a 12 mm diameter cylinder of elastomer with 6 mm height. Using Ecoflex 00-30, the calibrated forces were 4 N and 0.5 N in normal and shear, but may be varied with differing erlastomer stiffness. The sensor bandwidth was 100 Hz, with a hysteresis of 3.4%. The main disadvantage of such sensors is the interference caused by disturbances to the magnetic field. These disturbances can originate as the result of a changing external field, or by the presence of a ferromagnetic mass morphing the local field.

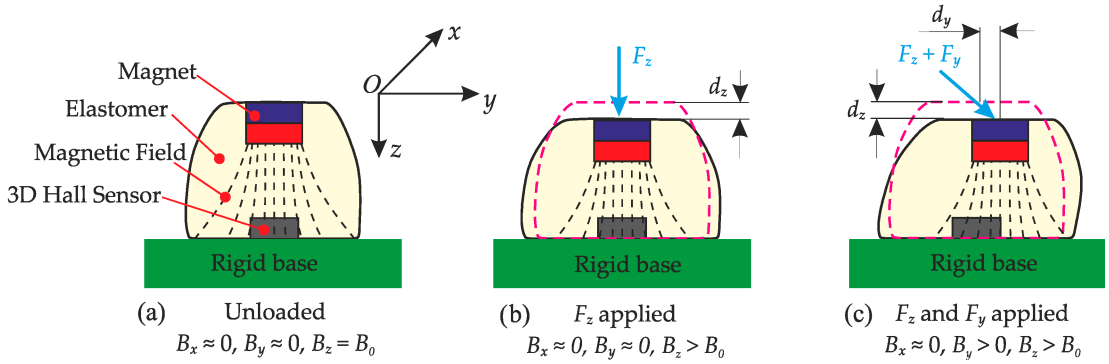

Fig. 2.13 Wang's MagOne, indicating the applied force deforming the sensor, and therefore the sensed magnetic field, from [16]

2.4.6.2 Inductive Tactile Sensors

Inductive tactile sensors use the varying inductance of a coil to determine force changes. This variance may be caused by several effects, including varying coil geometry [96, 97], magnetic resistance [98] and the eddy current effect [99–101]. Most inductive sensors use a deformable elastomer as a substrate to moderate the inductance change and to calibrate the change to a known force. In a similar manner to other elastomer-based sensing techniques, the resolution and range of the sensor may be varied dependent on the material properties

of the substrate used. Multi-axis configurations may be produce by increasing the number of coils present in a single sensing module. Du's three coil [102] and Wang's four coil [99] three axis configurations present both high and low force range sensors.

Such sensors have been shown to be highly resistant to external influences and extremely robust, even functioning in a fully submerged environment. Wang's sensor showed a bandwidth of 500 Hz, with hysteresis of 5.4%. The sensors have been shown to exhibit long-term drift over several weeks of functioning [103], however this was below 7% over an 8 hour period. While showing potential in sensing, the design parameters of existing sensors are not well understood, with most papers not considering the design characteristics of the sensor.

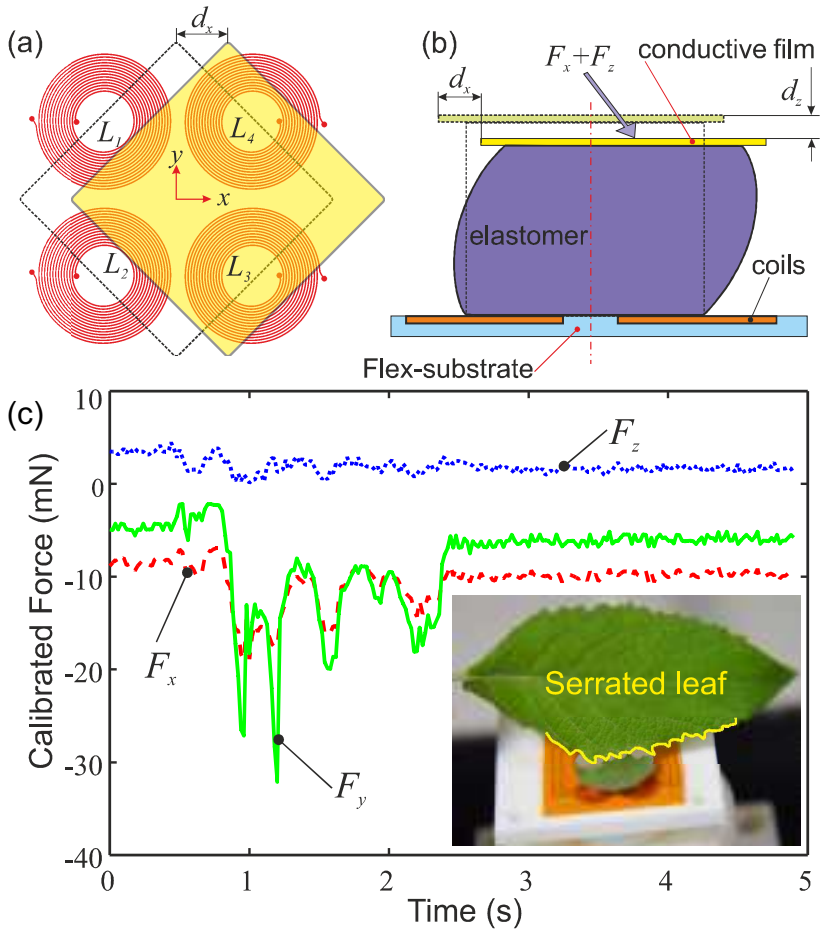

Fig. 2.14 Working principles of Wang's three axis SITS (a) target movement and (b) Elastomer deformation; and (c) SITS achieving mN precision under contact with a leaf.

2.5 Summary of Literature

This review has investigated the limitations in the performance of surgical graspers, and methods which may improve their usage. In summary there is a distinct clinical need for increased sensing capabilities within surgical graspers for both manual and telerobotic laparoscopy. Prevention of slip and over-compression have been identified as important issues to the clinical community which may be solved by incorporating tactile sensing within the grasper.

A series of requirements have been identified from the literature, based upon the parameters expected in a surgical environment and standard tactile sensing principles:

- **Sensor Location**

  The sensor must be located directly on the grasper face rather than a more proximal location on the instrument shaft or mechanism. This will reduce measurement errors and improve reliability through the removal of both mechanism losses [57]. This creates a tighter constraint on the sensor geometry, the sensor must be able to fit within the size constraints of the grasper jaw to measure the direct tissue-tool interface. Generally the jaw of a grasper is around 5 mm width, and between 10 - 30 mm long [104].

- **Real-time feedback (Bandwidth)**

  The sensor must be able to relay information on the changes of the measured property to the user in Real-Time. If not, the lag introduced by the sensor could increase surgery times and increase patient risk [105]. For such measurement to occur, a minimum bandwidth of 100 Hz is suggested, with an optimal value of 500 Hz. This allows for the detection of both mechanical properties of the tissue, as well as slip events [106].

- **Pressure Range**

  An approximate pressure of 300 kPa has been proposed as the upper limit of grasping pressure. Coupled with the grasper size constraint of 5 $\times$ 10 mm, this gives a force

range of up to 9 N for a sensing body equal to the full size of the grasper face [54]. The shear force range is yet unknown, and so should be investigated. While some research has been performed into the pressures applied during MIS procedures, there is a need for further investigation. Existing research has either focused on shaft forces [60] or with single participants [54]. To fully understand the pressures applied, a study should be performed across different surgeon experiences to understand the range of forces applied. Sensor hysteresis should also be kept to a minimum, to prevent error over multiple grasping actions.

- **Multi-axis Measurement**

  To reduce the chance of incorrect force application through MIS graspers, the 'safe area' proposed by Heijnsdijk may be further investigated. Both the upper bound of tissue crushing, and lower bound of slip prevention must be investigated to find the tissue response under compressive and shear forces and to find the better technique for assisting in grasping tasks. For this, a multi-axis force sensor will be needed on the face of the grasper, to measure the forces applied to the tissue.

Typical parameters of the reviewed sensing methods are presented in Table 2.2. From the sensing requirements, the Soft Inductive Tactile Sensor proposed by Wang [100] fits the requirements well, as it is applicable to a range of forces, has a sufficient bandwidth, and it's function as a multi-axis sensor has been shown. The main disadvantage of the sensor is it's size. For use in a grasping environment, inductive sensors would require miniaturisation to fit within the 5 x 10 mm constraint of the grasper face. The reviewed inductive sensors are early prototypes, and as such there is a significant gap in the research on their optimisation and miniaturisation.

Before this occurs, the mechanics of grasping must be further established. In particular, further data must be acquired and analysed to assess the 'safe' bounds of grasping. For this, typical grasping pressures will be needed. Next, the mechanical response of tissue will be analysed in further depth along each of the bounds to define both the normal and shear

ranges required for the sensor. After this, the sensor may be miniaturised to fit within the size constraint, and optimised using the parameters obtained.

Table 2.2 Typical key parameters of various sensing techniques

Sensing Type	Force range	Bandwidth	Size	Sensing Axes	Hysteresis	Other Notes
Strain Gauge (Stewart Platform)	±2.5N - all	-	10 x 10 x 5 mm	6-Axis	∼1%	Difficult to mount to face in current configuration [6]
Piezoresistive	40N - normal 10N - shear	∼100 Hz	10 x 10 x 1 mm	3-Axis	15%	[8, 68]
Computer Vision	-	15 Hz	40 x 40 x 160 mm	3-Axis	-	Designed for contact shape measurement [13]
Fibre Bragg Grating	10N - normal 6N - shear	500 Hz	3 x 6 mm	3-Axis	4%	Requires external interrogator; [92]
Hall Effect	4 N - normal 0.5 N - shear	∼100 Hz	12 x 12 x 6 mm	3-Axis	3.4%	Force range varied with elastomer stiffness [16]
Inductive	15 N - normal 0.5N - shear	∼500 Hz	14 x 14 x 1 mm	3-Axis	5.4%	Force range varied with elastomer stiffness [100]

Chapter 3

An Analysis of Grasping Forces in MIS

In this chapter, an analysis of surgical grasping forces is performed to inform the pressure applied in the later chapters. This section aims to define the mechanical forces applied to tissues by surgeons using minimally invasive graspers. This force will give a guideline for the forces applied to tissue in future chapters. An existing instrumented laparoscopic grasper [54] was used to record the forces of thirty-four participants of various skill levels with laparoscopic tools. Significant differences were observed between low and high experience surgeons, with higher experience showing a more consistent grasp force. This work is used to inform future chapters, as an upper bound for pressures in parametric tissue compressions, and to help define the requirements for potential sensing technologies.

Work contributing to this chapter was published in the Journal of Endourology:

Jones, DP; Jaffer, A; Alazmani, A; Biyani, CS; and Culmer, P., 2018. Analysis of mechanical forces used during laparoscopic training procedures. Journal of Endourology.

3.1 Introduction

During open surgical procedures, the surgeon receives direct haptic feedback when manipulating tissues and is, therefore, able to regulate the amount of exerted forces, so that they are sufficient to prevent tissue slipping out of the instrument, yet not excessive to prevent tissue damage. Moreover, direct vision and 3D visual cues are available; hand–eye coordination is, therefore, preserved. With the advent of MIS, long rigid instruments have been introduced between the surgeon's hands and the tissue, and, therefore, the direct feedback of mechanical forces are inhibited. The current instrumentation obstructs the perception of forces, velocities, and displacements of the tissues and the proprioception required for motor performance is distorted [2]. With direct haptic feedback, the trainee is able to perform laparoscopic tasks more consistently [107]. This is likely to be a result of better differentiation of tissue types with the use of direct vision as well as tactile feedback [108]. The direct feedback from tissue handling is diminished in MIS and, therefore, the discrepancy between 'safe' and potentially 'traumatic' mechanical forces applied to tissues is far more discrete as compared with traditional approaches in surgery.

3.1.1 Chapter Objectives

In order to fully understand the mechanics of surgical grasping, it was first needed to asses the forces applied by surgeons through graspers. This section details the investigation into grasping forces in order to inform future research into sensor development. The following objectives were identified:

Objective 3.1 To define a methodology for the measurement of laparoscopic grasping forces.

Objective 3.2 To investigate the relationship between surgeon experience and applied grasping pressure.

Objective 3.3 To define a range of forces used by a typical surgeon in MIS grasping tasks.

Objective 3.4 To define the clinical and technological requirements for tactile sensing technologies.

3.2 Recording Surgical Grasping Forces

While previous studies have aimed to define the forces used in surgical grasping tasks [25, 54], the definitions of applied force are limited to two specific tissue types: colon and liver. While this gives an insight into the forces used to define the clinical requirements of a force sensor, further investigation is required on different tissue types to fully understand them. To investigate this, a study of grasping forces was proposed on ex vivo porcine ureter. The research was collaborative with a consultant urologist (Leeds Teaching Hospitals NHS Trust) and was conducted at a training event for junior doctors at St James' Teaching Hospital (Leeds, UK). An existing pair of instrumented graspers [54] were used to record the normal forces applied to tissue under various grasping conditions.

3.3 Materials and Methods

Thirty-four participants with varying levels of experience in MIS participated in the experiment. The skill levels were defines by the number of years experience a participant had with the use of surgical graspers. Novices were defined as junior doctors with no specialist (1-2 years experience in medicine), intermediates as surgeons who were in surgical speciality training, and experts were defined as surgeon who had completed their training (Consultant level in the UK).

3.3.1 Instrumented Laparoscopic Graspers

To perform the experiment, first it was needed to record force data using an existing sensing laparoscopic grasper. Horeman [109] states that the main parameters required to be measured

in MIS graspers are the compressive pressure and face angle. To measure these, the tools produced by Barrie [54] were used. The device consisted of commercial modular grasper, with a sensing module added between the shaft and handle of the grasper (Figure 3.1). The sensing module consisted of a 200N tension load cell positioned in-line with the existing mechanism to measure grasp force; and a hall effect sensor coupled with a moving magnet to measure the movement of the mechanism, thereby measuring the grasper face angle. The sensors were calibrated across a range of values, and achieved resolutions of 0.005N and 0.1deg respectively. The module was enclosed in a 3D printed housing, with the full instrumentation module weighing 90g.

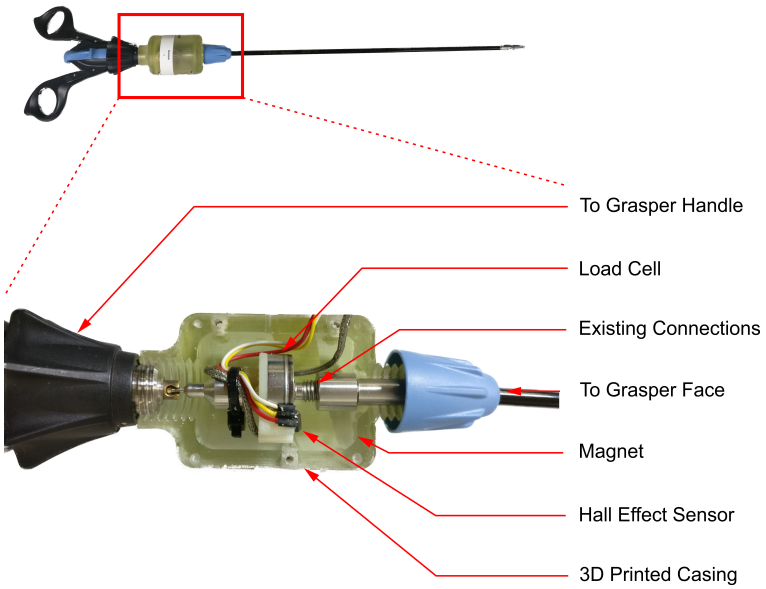

Fig. 3.1 A photo of the instrumentation module of the grasper, indicating the key components

3.3.1.1 Grasper Mechanism Effect

While the recording of force would allow a comparative metric between different surgeons, it does not fully reflect the forces applied to the tissue for all graspers. For this, the shaft

forces must be converted to face pressures. This allowed a direct comparison between forces applied by different grasper jaw types, making the metric significant beyond the graspers used in this study. Russell [53] proposed a mathematical model for the conversion of shaft forces to a tip force for a scissor-style laparoscopic grasper (Equation 3.1). Using the grasper face angle and shaft tension, the results can be converted to a point force at the tip.

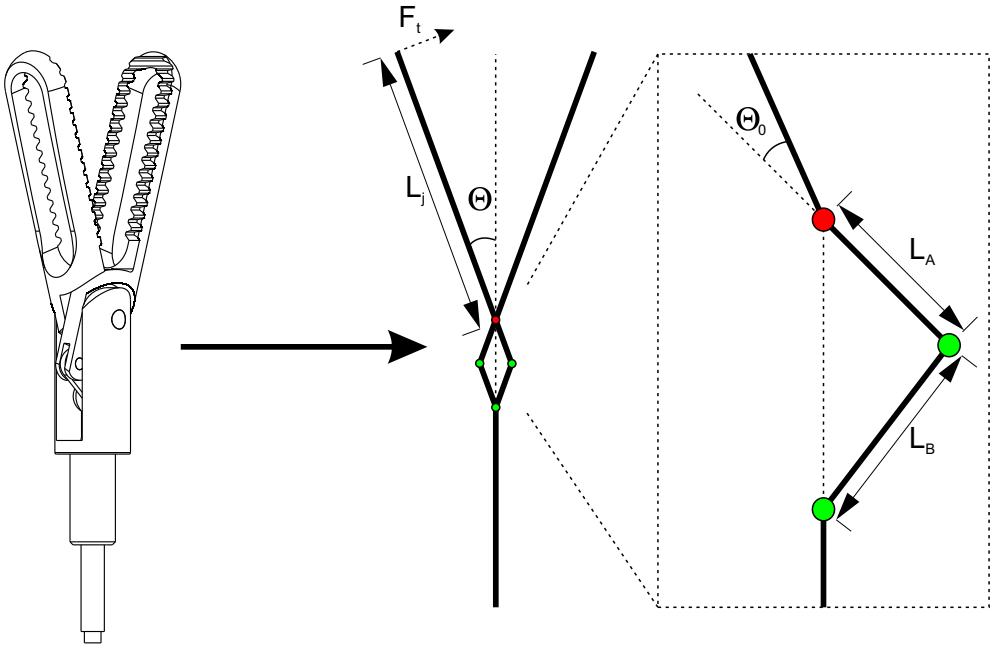

Fig. 3.2 Schematic diagram of the grasper mechanism used to calculate the tip force: F_t - Tip Force, L_j - Jaw Length, Θ - Jaw angle, Θ_0 - Jaw Angle Offset, $L_{A,B}$ - Mechanism Linkage Length

$$F_t = \frac{L_A}{2L_j}\cos\left(\Theta+\Theta_0+\sin^{-1}\left(\frac{L_A\sin(\Theta+\Theta_0)}{L_B}\right)\right)\ldots \\ \ldots\cos\left(\sin^{-1}\left(\frac{L_A\sin(\Theta+\Theta_0)}{L_B}\right)\right)F_{IN} \tag{3.1}$$

The values in table 3.1 were substituted into the equation, taken from the geometry of the grasper mechanism. To simplify this calculation, it was assumed that under grasping conditions the face angle was 0°. Once substituted, this gave Equation 3.2.

Parameter	Symbol	Value
Jaw Offset Angle	Θ_0	21.80°
Linkage 'A' Length	L_A	3.770 mm
Linkage 'B' Length	L_B	3.200 mm
Jaw Face Angle	Θ	Assumed 0°

Table 3.1 Values quantified from the grasper mechanism

$$F_t = \frac{0.333A}{L_j} F_{IN} \tag{3.2}$$

From the tip force, it was then required to calculate a contact pressure. For this, contact area between the grasper and tissue sample was needed. As this could not be measured directly, it was estimated to be between one- and two-thirds of the total jaw length. A grasp area of less than one third gives a non-secure grip on the tissue, whereas areas greater than two-thirds from the tip experience higher pressures closer to the hinge. Using these two values, the upper and lower bounds of a grasp were calculated (Figure 3.3). For the later results, only the higher bound of pressure is discussed, giving a 'worst case' scenario for each grasping task.

3.3.2 Experimental Procedure

The instrumented graspers were used to analyse the grasping forces in a simulated surgical environment. A portable laparoscopic box trainer (Eosim) was used in combination with a high definition webcam (C920 HD Pro, Logitech) and PC screen to replicate the visual environment of MIS (Figure 3.4). Samples of porcine ureter (frozen and defrosted) were divided in to 50mm sections, and spatulated from the distal end. The samples were then pinned to the base of the simulated environment at the proximal end. The grasping study consisted of 34 participants, split between 8 experts, 10 intermediates and 16 novices. Participants were asked to grasp the sample in three positions with each hand on the corresponding edge of the

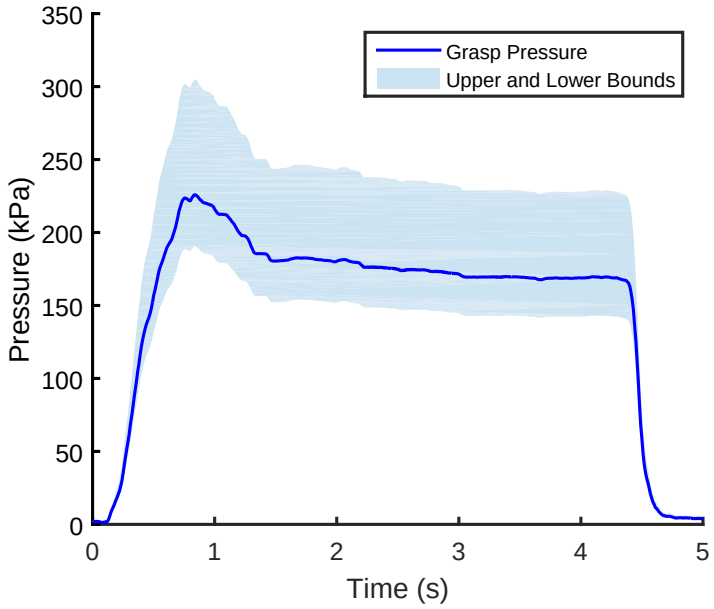

Fig. 3.3 Example grasp data obtained by the instrumented graspers. The upper and lower bounds of calculated pressure (rangeing between 1/3 and 2/3 of the face) are indicated.

sample. Each of these positions was designated to be grasped either 1, 5, or 10 times. The grasp forces and grasper face angle were recorded, along with a video of each task.

3.3.3 Data Processing

The data was post-processed using a custom LabVIEW VI to identify the force and duration of each grasp, where the force and angle passed two thresholds. For each grasp, the peak pressure (P_{MAX}) was identified and mean pressure (P_{RMS}) was calculated (Figure 3.5). To eliminate the bias of hand dominance, an Edinburgh Handedness survey was completed by each participant.

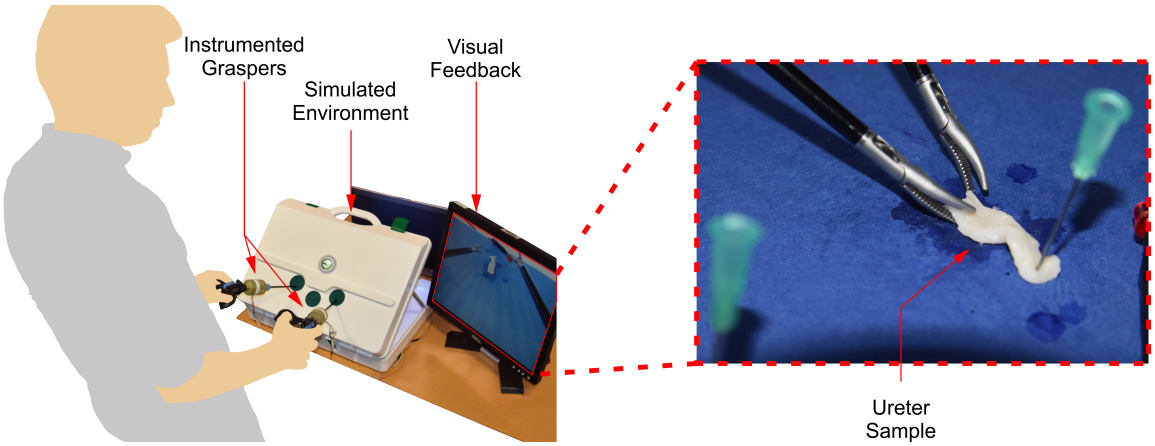

Fig. 3.4 The test setup in use, showing the simulated environment and positioning of the participants

3.4 Results

Each participant performed the three tasks with both their dominant and non-dominant hand, totalling 32 grasps. Example shaft force profiles for a single grasp are presented in Figure 3.6. Novices show an erratic profile, with an inability to hold a consistent force. Intermediates apply a similar magnitude of force, holding the tissue more consistently but still showing fluctuations in force. Experts use the least force, and under holding the force trend resembles a perfect stress relaxation of soft tissue [110]. The average grasp for each training level is presented in Figure 3.7. The average grasps indicate some further general characteristics of the force applied by the different training levels. Novices used a mid-range force, which once again showed major fluctuations. Intermediates used a greater force which was reduced to a lower level relatively quickly. Experts however used a low force and held a very consistent grasp. The expert group also grasped much slower than the the others, indicated by the lower rate of force increase.

To establish the correct metric at which further results will be compared to, the differences between peak (P_{MAX}) and mean (P_{RMS}) force were assessed. Figure 3.10 presents the mean P_{MAX} and P_{RMS} values for each skill level. Significant correlation was observed between

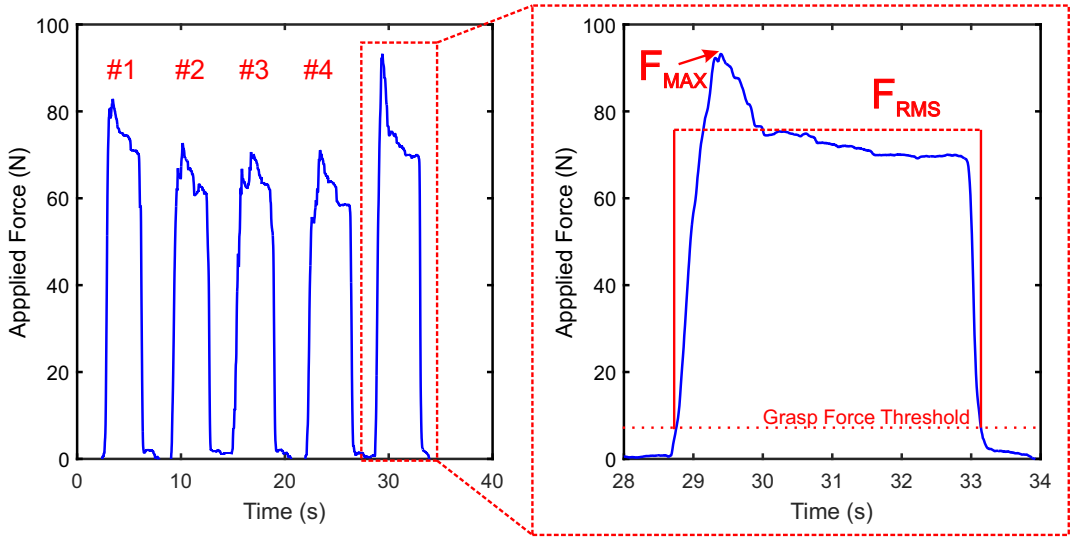

Fig. 3.5 Example of idealised Grasping data, not from experimental use. Indicates the Peak Force (F_{MAX}), average force (F_{RMS}) and the force threshold at which grasps were detected

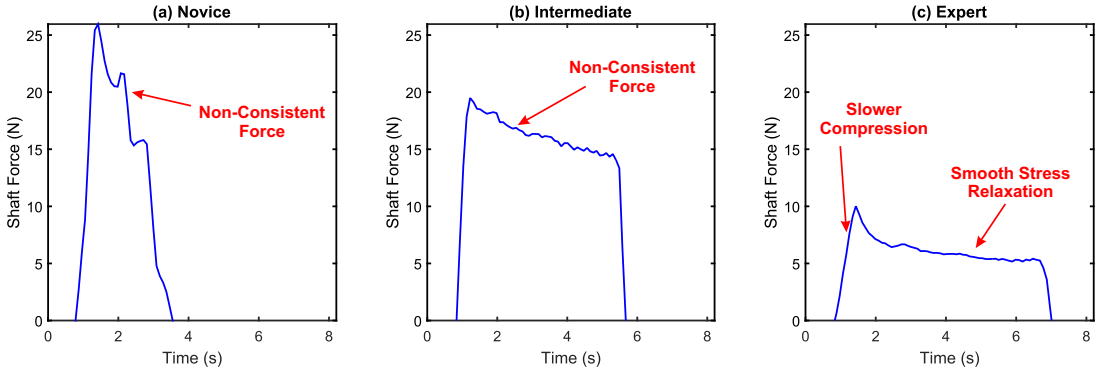

Fig. 3.6 Example grasp traces for (a) Novice, (b) Intermediate, and (c) Expert participants

P_{MAX} and P_{RMS} (Pearson Correlation, r=0.97, p<0.0005) (Fig. 3.8). Owing to this, the reported results only focus on P_{MAX}.

Figure 3.9 shows a summary of grasps across tasks for the three skill levels separated by task. While the intermediate and expert groups applied similar forces between all tasks, the novices seem to apply slightly lower forces under tasks with a greater number of actions. A one-way analysis of variance (ANOVA) was conducted to compare the effect of the three different tasks on peak force, yielding no significant differences (F(2,1084)=0.28, p=0.753). Separated by training level, there were no significant differences between tasks, with significance p=0.836, 0.859, 0.387 for the novice, intermediate and expert groups.

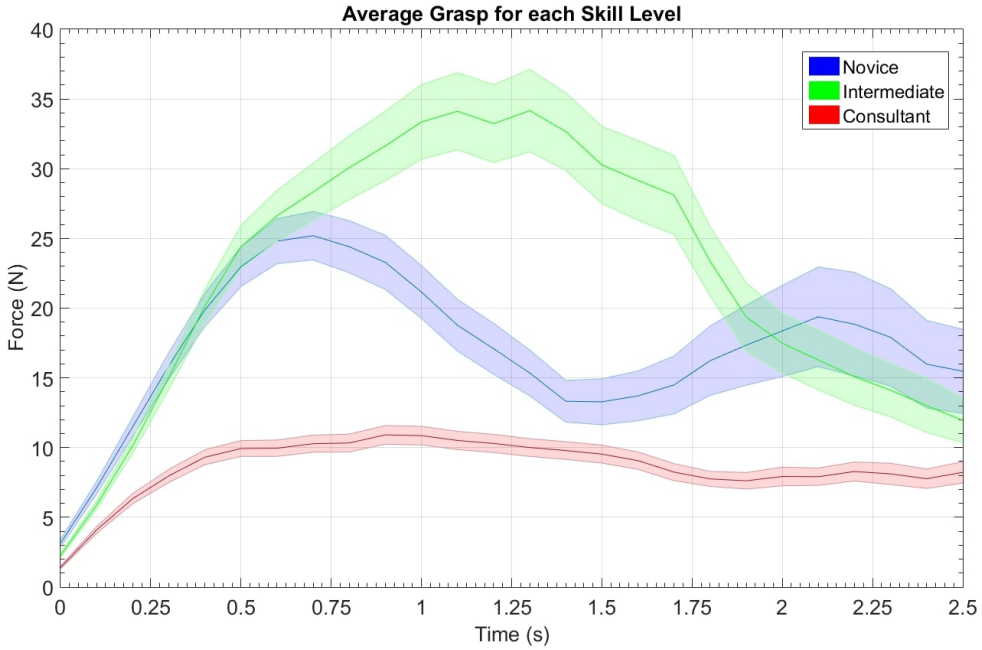

Fig. 3.7 The average grasp profile for each training level ± SEM

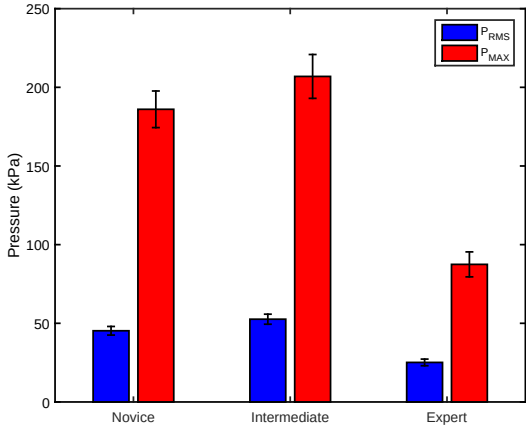

Fig. 3.8 Mean P_{MAX} and P_{RMS} separated by experience level

The difference in forces between skill levels is also shown. Novice and intermediate participants are shown to apply a similar level of forces, while experts are shown to apply lower force. This indicates both a greater degree of dexterity and a more precise ability to discern forces, gained the the increased experience with the tools. The statistics echoed this, one-way ANOVA showed that there was a statistically significant difference with those more

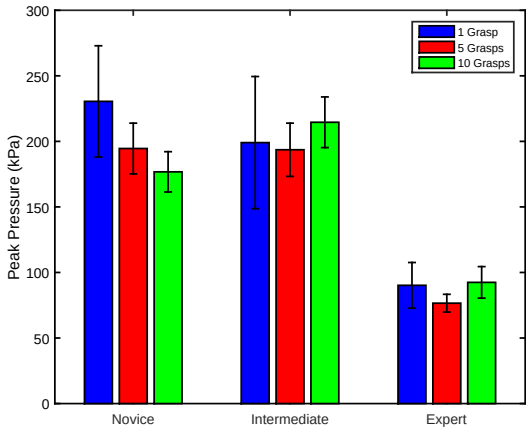

Fig. 3.9 Mean peak pressures for each task, separated by experience level

experienced applying consistently lower mechanical forces (F(2,1084)=21.36, p<0.0005), with no significant difference between the lower training levels (p = 0.422) (Figure 3.9).

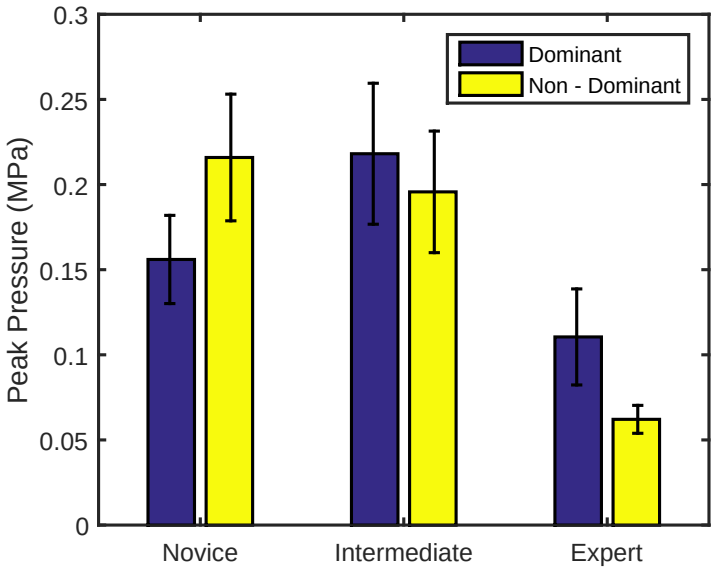

Fig. 3.10 Average maximum pressure $\pm$ 95% confidence interval for each training level

The relationship between handedness and surgeon skill was also assessed and presented in Figure 3.10. Handedness alone did not show a statistically significant interaction (F(1,1084)=0.06, p=0.806), but the interaction effect (training X hand) was (F(2,1084)=5.66, p=0.004). Therefore it was investigated whether handedness was significant in individual

groups. Figure 3.10 clearly shows a lower peak force for the novice dominant hand, whereas the expert group's dominant hand was higher. These relationships are present in the statistical analysis. The intermediate group showed no significant difference between the hands, but the effect of dominant hand is significant in the novices (significantly lower,$F(1,510)=6.70$, $p=0.010$) and experts (significantly higher,$F(1,250)=9.601$, $p<0.020$). In particular for the expert case, discussions with the clinician participants revealed that the non-dominant hand is favoured for grasping tasks, further cementing the effect of experience increasing control over grasping forces.

3.5 Discussion

The reduced haptic feedback from laparoscopic surgeries as compared with conventional open techniques [111, 112] places a significantly greater upon surgeons in training to be able to differentiate between the subtleties of safe and excessive mechanical forces. There is evidence to suggest that experience is the most important factor in allowing the surgeon to develop a safer sense of mechanical forces applied to tissues [113]. This evidence was echoed by the results obtained in this chapter, wherein it is shown that there are significant discrepancies in the mechanical forces applied to tissue between novice/intermediate trainees as compared with experts. Horeman et al [109] also observed similar findings. Whereas the novice/intermediate groups were applying significantly higher forces onto tissue with increased variability over grasp time,the expert group showed a far greater level of force consistency with significantly reduced levels of forces applied as shown in Figure 3.10.

In vivo, there is a direct, graded response between forces applied and tissue damage with liver and small bowel being most susceptible and ureter most robust [25]. In addition, certain laparoscopic complications can be attributed directly to tissue handling. One study analysing the errors during laparoscopic cholecystectomies showed that graspers were the most frequently involved instrument in erroneous task performance: 70 out of 189 errors (37%) in 20 procedures. Importantly, 14 out of the 70 grasping errors (20%) were due to excessive

forces while 40 out of 70 (57%) resulted from insufficient applied force to hold tissue [114]. A further study investigating erroneous task performance during 977 laparoscopic operations performed by 20 surgeons, graspers came third in frequency of causing complications (53%), after coagulators and dissectors. The threshold of safe mechanical pressure that one can apply is dependent on the type of tissue surface and therefore further work is required to firstly identify these thresholds to inform future research on sensing within the grasper face.

The average pressure applied across all groups was 169 kPa, however outlying results from the expert category were up to around 300kPa. This was comparable with previous results as found by De et al. [25] using a different instrumented grasping system. While 170 kPa gives a good estimate of the pressures that will generally be exerted, future chapters will use 300kPa as a maximum threshold for applied pressure.

3.6 Chapter Summary

In this chapter the pressures applied by surgeons in grasping conditions are identified. An existing pair of instrumented graspers with sensing at the proximal end of the shaft was used to record pressures applied by doctors at various stages along the training pathway. Typically, surgeons across all skill levels will apply around 170kPa on average under grasping conditions. While this will encompass most cases, outlying data showed forces up to around 300kPa. As such, future sensors in the research will be required to apply up to 300kPa to be valid for the full training pathway, while should maintain sufficient sensitivity at the levels applied by experts - around 50kPa.

Chapter 4

Investigating Methods of Applying Sensing to Improve Grasper Performance

This chapter aims to assess sensing applications for the use within a surgical tool. From the analysis of literature, it was evident that the mechanical measurement of tissue properties showed the most promise for integration, yet the application of the increased sensing was not defined. Therefore metrics based on contact and shear force were tested for their efficacy in either the prediction of damage or the optimising of grasping mechanics. Firstly, the Normalised Stress Rate of compression (NSRc) was analysed. Initially proposed by Chandler et al. [115], the NSRc was intended to allow the analysis of a tissue's quality during the initial compression stage. Secondly, the prevention of slip was identified as a potential damage prevention method. As both over-compression and slip were identified as major causes of trauma [48], a slip prevention method would allow the minimum compressive force to be applied while maintaining traction on the grasped tissue.

Work contributing to this chapter is to be published in the Preceedings of IEEE conference on Intelligent Robots and Systems

Jones, DP; Wang, H; Alazmani, A; Culmer, PR. **A soft multi-axial force sensor to assess tissue properties in Real-Time**. In 2017 IEEE/RSJ International Conference on Intelligent Robots and Systems Proceedings (pp. 5738-5743). IEEE.

4.1 Introduction

The previous chapter has helped define an appropriate pressure range for surgical grasping, however use of the instrumented grasping system highlighted some problems for use in analysis. The scissor action of the grasper caused non-normal forces to be applied to the samples in simple compressions, and the grasper mechanism varied the tip forces dependant on the face angle. This highlighted the need to make use of a simplified automated grasping environment allowing parametric conditions to be replicated in a controlled environment.

Previous work in our group has proposed a set of metrics with the potential to detect tissue damage in real time through the assessment of applied stress and strain rate [115]. A discrete differentiation of the changing pressure on a tissue sample was correlated with histological signs of damage. Others have attempted to prevent tissue slip with specialised sensors [116, 117] to detect when tissue starts to slip from the grasper jaws. Such analyses could allow a new generation of 'smart' surgical tools with the ability to detect approaching tissue damage and help prevent it from occurring by providing the controlling surgeon with appropriate feedback.

4.1.1 Chapter Objectives

This chapter assesses the potential of two metrics for use in real-time analysis of the forces recorded from a grasper. The following objectives were identified:

Objective 4.1 To define force sensing applications for use within a grasper jaw.

Objective 4.2 To parametrically analyse the sensing metrics using *ex vivo* porcine tissues.

Objective 4.3 To investigate the efficacies of the measurement techniques for potential use in a grasping system.

Objective 4.4 To define the clinical and technological requirements for future sensing technologies.

4.1.2 Sensing Applications for Grasper Usage Optimisation

Previous studies into the detection of damage in MIS have identified force thresholds as the main method of damage prevention [25, 54]. While this gives a basic indication of grasping conditions, there is a more complex relationship in the tissue-tool interaction. While over-compression is a major symptom of grasper misuse, tissue slipping with the grasper jaws has also been shown to be a significant problem [48, 118]. In essence it is the inverse of over-compression, if a surgeon does not grip with sufficient force there will not be enough friction on the tissue surface to maintain grip.

Visser proposes a different view of safe grasping forces [4]. While the upper bound of grasping forces remains, the level at which insufficient force and therefore insufficient traction causing slip, is also measured. This established a 'safe zone' for grasping with a lower chance of causing trauma. While this gives a general view for the grasping forces, the thresholds are not universal and will vary based on grasped tissue type. Advancements to these measures are therefore required to allow an optimisation of grasping on any tissue.

4.1.2.1 Normalised Stress Rate of Compression

Because of the viscoelastic nature of soft tissues in the body [119], a force threshold is insufficient as an upper bound for grasping. The mechanical response under compression is extremely complex and relies on many environment-specific variables, in particular the compression speed. Previous research within our group has looked to establish a predictive metric for tissue trauma [115]. The NSRc (Equation 4.1 & Fig 4.1) was developed to

use easily accessible measurements from a grasper face (load and position) to predict the occurrence of damage independent of tissue type. In particular it detects the momentary stiffening of the tissue, mostly independent of it's material properties, which reduces the physical recovery of the tissue when the grasp is released. The method uses a measured stress (σ) and position (x) discretely differentiated by comparison to data stored m and n points previously and the sampling time step Δt.

$$\dot{\tilde{\sigma}} = \frac{(\sigma_i - \sigma_{i-n})/n\Delta t}{(x_i - x_{i-n})/m\Delta t} \tag{4.1}$$

To analyse the metric's efficacy as a predictor to damage, a measure of damage was also needed. After tissue damage is incurred its internal structure is changed [28] causing change in the viscoelastic properties. A quantitative histological analysis of the stress relaxation was performed by Chandler et Al. [115] and found significant correlations between post-grasped tissue deformation and Normalised Stress Relaxation ($\overline{\Delta\sigma}$; Equation 4.2, Figure 4.1), where the relaxed stress ($\Delta\sigma$) is normalised by the peak grasp stress (σ_{MAX}). Therefore the relaxation will be used as a measure of tissue damage.

$$\overline{\Delta\sigma} = \frac{\Delta\sigma}{\sigma_{MAX}} \tag{4.2}$$

4.1.2.2 Tissue Slip Prevention

Similarly to the upper bound of forces, the slip line proposed by Visser [4] is insufficient as a lower force bound because of the varying surface properties between tissues [120]. Under the same compressive forces, the slip force will vary between different tissues requiring a more advanced method for detecting the lower bound. For this, a more advanced measure is required. In tribology, the varying level of the Coefficient of Friction (μ) is commonly used to detect the instance of slip [121]. The Coefficient of Friction may be calculated as follows:

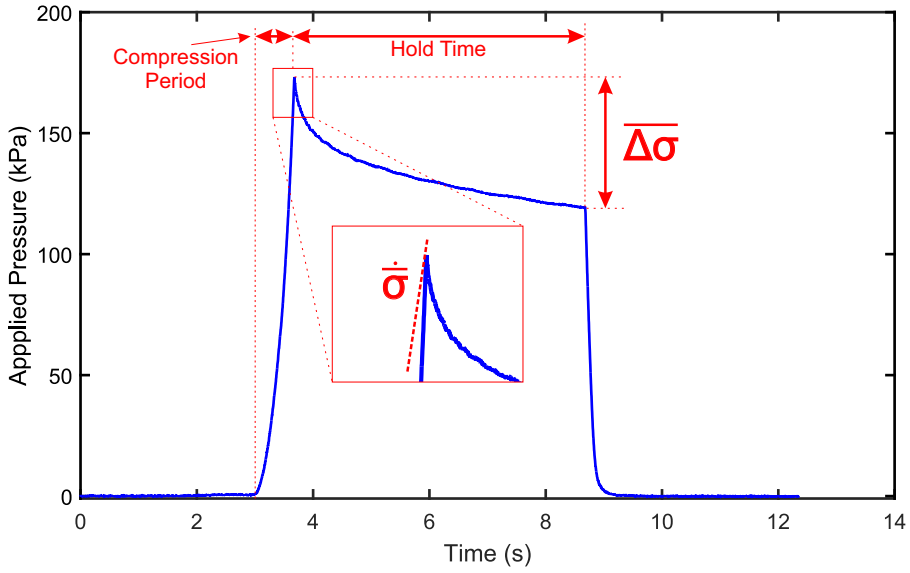

Fig. 4.1 Parameters calculated from the compression tests. $\dot{\bar{\theta}}$ = Normalised Stress Rate of Compression, $\overline{\Delta\sigma}$ = Normalised Stress Relaxation

$$\mu = \frac{F_{Shear}}{F_{Normal}} \tag{4.3}$$

Slip is observed at the first peak of the coefficient of friction, also defined as:

$$\frac{d\mu}{dt} < 0 \tag{4.4}$$

Once a value of slip is established, the sensor may be used to modulate the compressive force of the grasper jaw, thereby keeping the coefficient just below the slip value and minimising the applied force to the tissue.

4.2 Materials and Methods

In order to fully assess the sensing application methods, they must first be parametrically investigated to assess their potential for damage prevention. Two experimental procedures

were defined to fulfil the stated aims. In particular, the testing focused on colon and ureter tissues, each being an example of a relatively hard and soft tissue [25]. Porcine specimens were selected as an analogue to human tissues due to the similarities in size and morphology [122].

4.2.1 Porcine Specimen Preparation

All measurements were conducted of fresh ex vivo porcine tissues (ureter and colon), which were bred and sacrificed in accordance with UK Home Office regulations (Animals [Scientific Procedures] Act 1986). The excised specimens were obtained from a local abattoir and stored in a saline (PBS) solution. Three porcine colons and fifteen ureters were obtained and tested on within 24 hours of sacrifice.

The colon was sectioned to obtain samples of sigmoid and descending colon. This was due to the wall thickness being similar across the two sections [123]. This was then sectioned into 3cm wide samples and randomised for the below testing procedure (Fig 4.2a). The ureters were spatulated and trisected laterally. This revealed the mucosa and replicated the grasping conditions of urological surgery (Fig 4.2b).

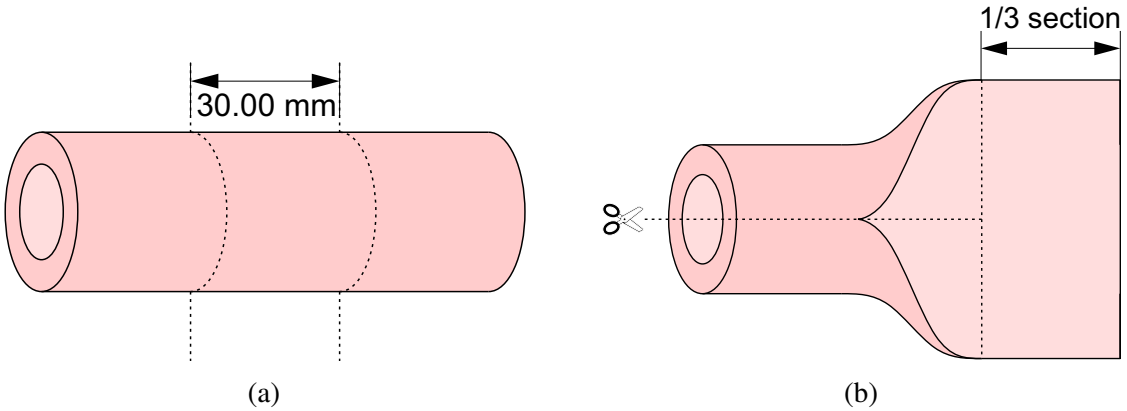

(a) (b)

Fig. 4.2 The sectioning method of the (a) colon and (b) Ureter samples

4.2.2 Experimental Equipment

To perform the parametric study, a simulated grasping environment [115] was used to compress ex-vivo porcine samples. The apparatus allowed extremely precise control and measurement of the force and displacement of the grasper faces at high frequency (1kHz). Detailed in Figure 4.3, two linear actuators with integrated encoders (LCA 50-025-721F3, SMAC) were used to replicate the normal and shear forces applied to the tissue. Each stage was fitted with a high precision tension/compression link load cell (LCM-703-25, Omega). Measurement and control of the system was performed using an NI MyRIO running a modified version of Chandler's control program (Fig. 4.5 & 4.4). The resolutions of the encoders and load cells were 0.1 μm and 0.03 N, respectively. Data was pre-processed with a low-pass filter (second order Butterworth with a 50 Hz cut-off frequency) to reduce high frequency noise, and processed with custom Matlab scripts.

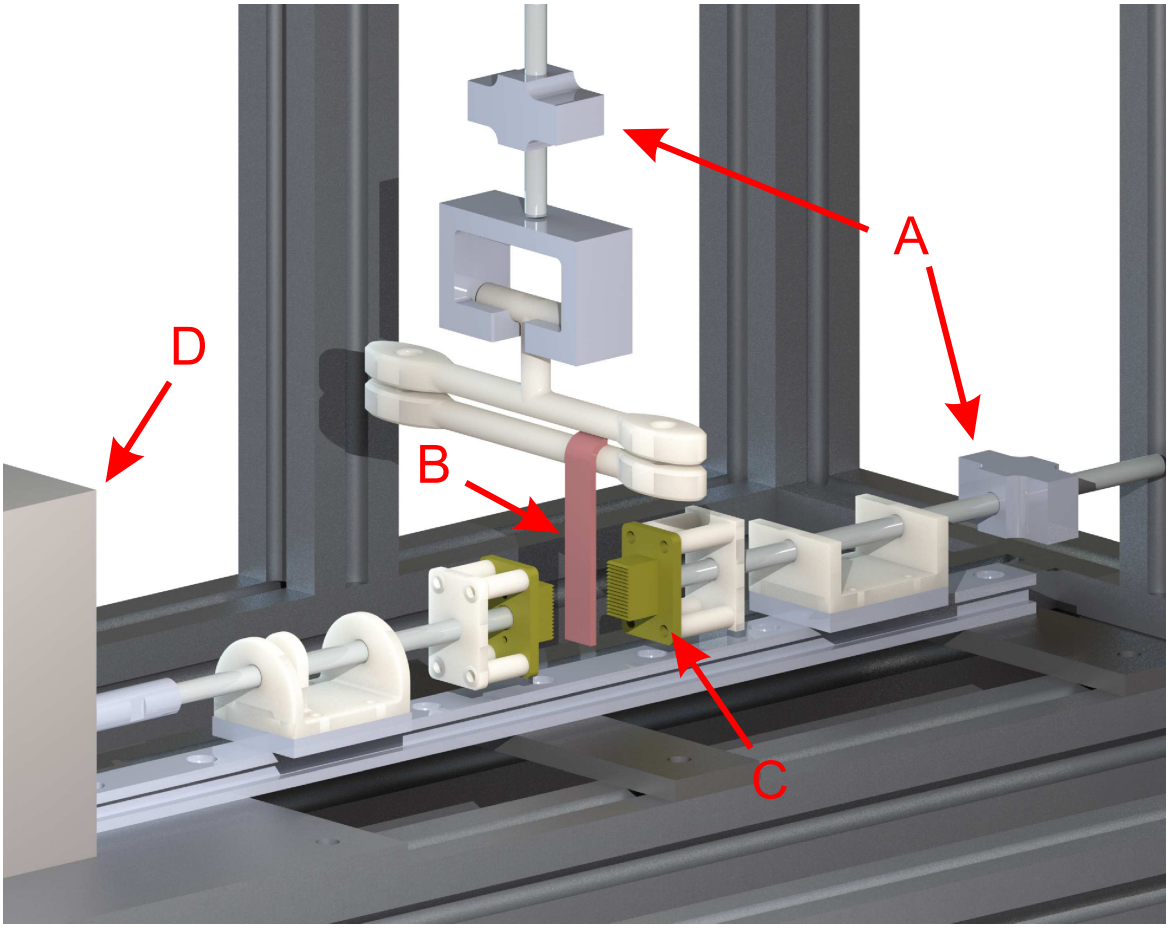

Fig. 4.3 Diagram of the simulated grasping Environment: A -Load Cells, B - Tissue Sample, C - 3D Printed Grasper Face, and D - SMAC Linear Actuator

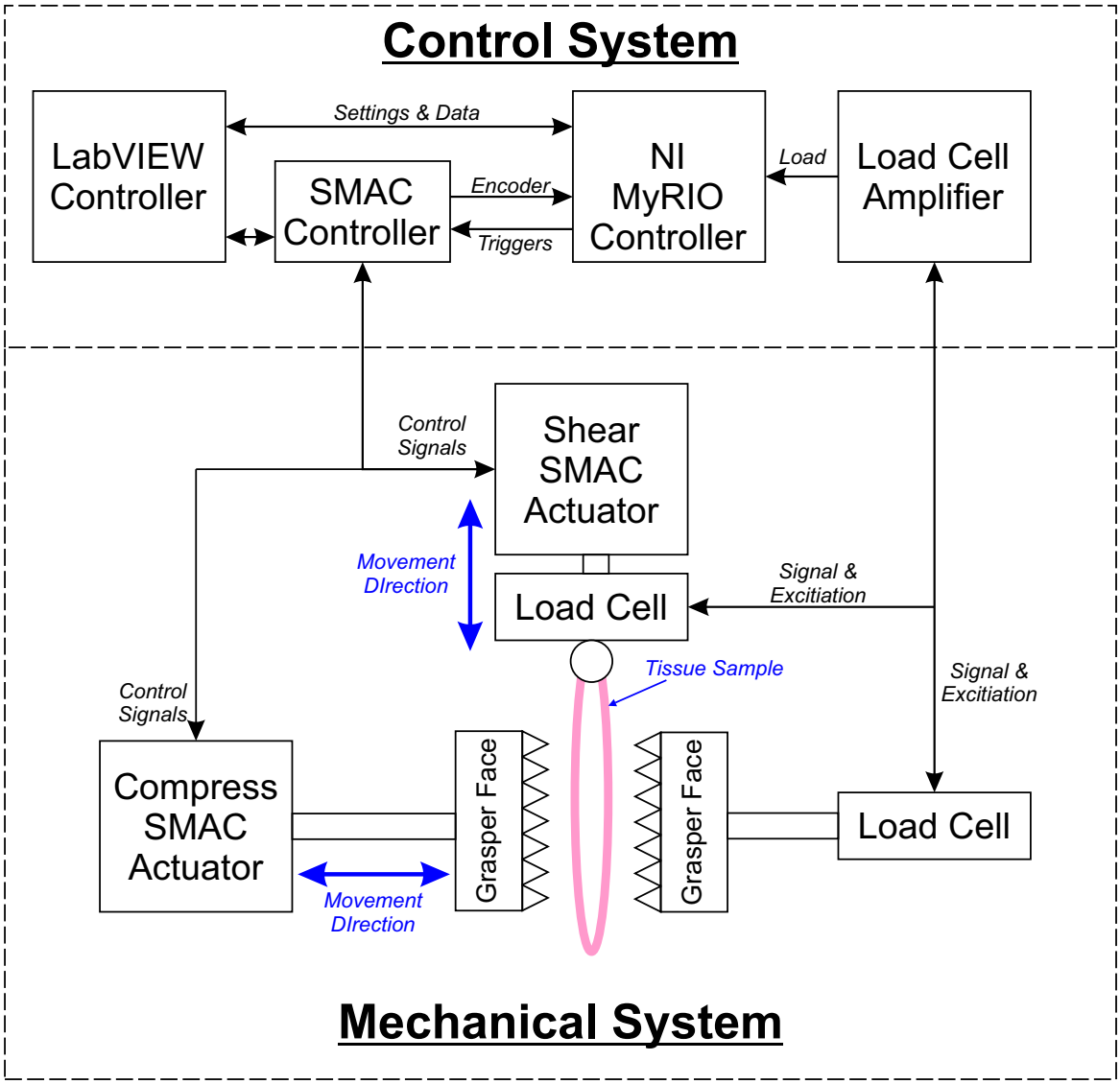

Fig. 4.4 Schematic diagram of the controlled grasping system

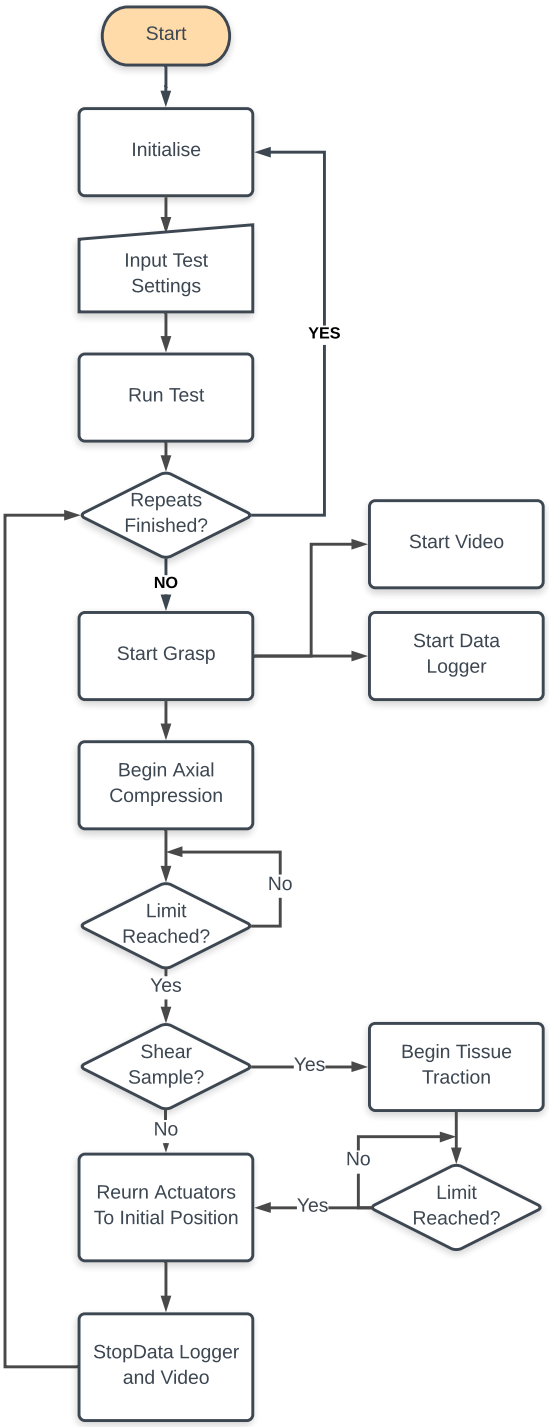

Fig. 4.5 Flowchart of the control method of the simulated grasping system.

4.2.3 Experimental Methodology

4.2.3.1 Normalised Stress Rate of Compression

To investigate the NSRc as a measure for the upper bound of grasping forces, the simulated grasping environment was used to apply specified target pressures to the samples at different speeds. The parameters used are shown in table 4.1. The parameter values were selected based on both Chandler's findings and the output of Chapter 3. The applied pressured focused on the upper bounds of the surgeon grasping results, from the average grasp (169 kPa) to the maximum applied pressure (323 kPa). The speeds selected focused on the lower end of Chandler's grasping speeds, where a greater difference was seen [115]. Each individual combination of parameter values was explored, such that the total number of cases was 15. Each sample was grasped 5 times to investigate the effects of multiple grasps to the same surface. Each condition was repeated 5 times (n = 75). To ensure the efficacy of the metric between various tissue types, both porcine colon and ureter were analysed.

Table 4.1 Parameters used in the NSRc experiments

Compression Force/Pressure, N (*kPa*)	Compression Speed (mms^{-1})
20 (*167*)	2
25 (*208*)	4
30 (*250*)	6
35 (*292*)	
40 (*333*)	

4.2.3.2 Tissue Slip Prevention

The simulated grasping environment was once again used to apply the forces to the tissues. The procedure was to apply a varying initial compression to the tissue at a constant rate (1 mm/s), and to then apply shear through moving the tissue vertically at different speeds. The parameters are shown in table 4.2. After this, the Coefficient of Friction (CoF) was calculated as the ratio between the shear and normal forces. The slip data was analysed to find the

first peak in the data, or the point at which the differential ($d\mu/dt$) first became negative, at which the CoF was recorded. If this did not happen the test was defined as 'No Slip'. Each condition was repeated over 5 samples.

Table 4.2 Parameters used in the slip experiments

Compression Force/Pressure, N (*kPa*)	Shear Speed (mms^{-1})
5 (*43*)	2
10 (*86*)	4
15 (*129*)	6

4.3 Results

The results of both compression and slip testing are presented in this section, along with statistical analysis to indicate variances between test conditions.

4.3.1 Normalised Stress Rate of Compression

A total of 5 repeats were completed for each condition of the compression testing. To ensure no effects were present between test repeats, a one way ANOVA was performed, yielding no significant differences ($F(5,293)=1.89$, $p=0.96$).

Figure 4.6 shows example data from two typical grasps on a typical colon sample. In the compression stage, the applied pressure rises to the target level, and relaxes over the hold time as expected. During the relaxation period, a small change in face displacement (Δd_{Relax}<0.2mm) was observed in the first grasp of each sample. This was smaller in higher pressures, and reduced to near zero in subsequent grasps. This may be explained by the tissue 'squeezing' out of the faces [110]. Statistical analysis of the effect of multiple grasps was investigated, with five grasps being applied to the same position of tissue for each condition. Variance in both NSRc and relaxation was observed with both showing a

significant difference between grasp 1 and grasps 2-5 ($p<0.0005$ in all combinations), with no significant differences between grasps 2-5 ($p>0.85$ in all combinations).

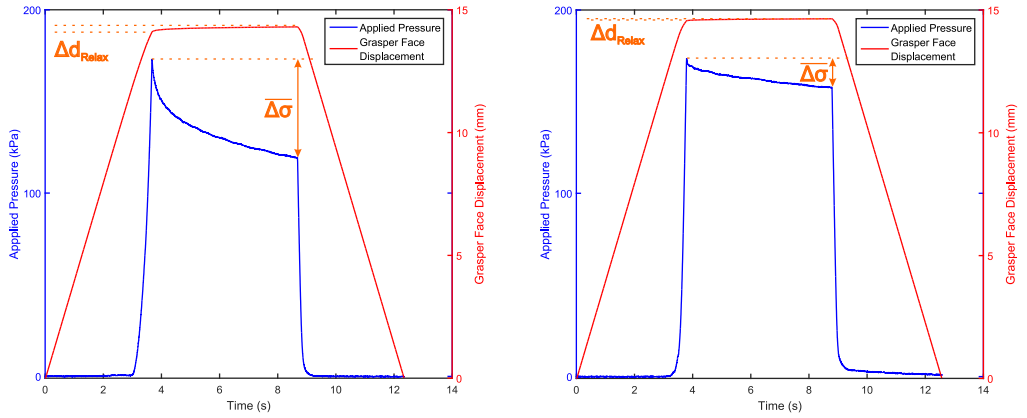

(a) (b)

Fig. 4.6 Example presure and displacements data from a single colon sample (a) Grasp 1 (b) Grasp 5

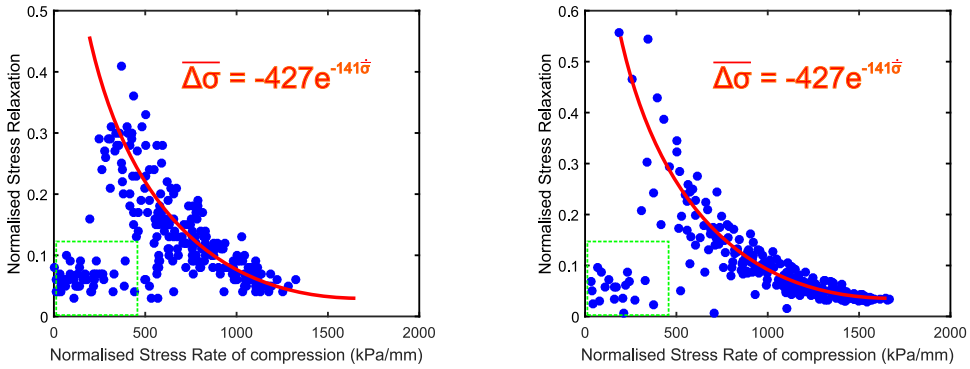

(a) (b)

Fig. 4.7 NSRc vs Relaxation for all grasps recorded for (a) Colon and (b) Ureter. The regression fit for the full dataset is shown, with anomalous readings indicated by the green box

Presented in Figure 4.7, the relationship between NSRc and Relaxation was observed. For both ureter and colon, there were patches of data with both low relaxation and NSRc . These patches of data (highlighted in Figure 4.7) corresponded to all grasps on three ureter samples (4% of cases) and four colon samples (5.3% of cases). During experimentation it

was observed that these samples had a different texture to most, being softer and slimier than other samples. Because of this difference, coupled with the variation in mechanical measurements, the samples were treated as 'non-standard' and excluded from the analysis. A logarithmic relationship was observed between NSRc and Relaxation, defined as:

$$\overline{\Delta\sigma} = ae^{-b.\bar{\sigma}} \tag{4.5}$$

Therefore to correlations were made between NSRc and ln(Relaxation) to achieve a linear relationship. Pearson correlations were observed for both Colon (r=-.896, n=191, p<0.0005) and Ureter (r=-.940, n=289, p<0.0005). The data for both tissue types was combined and a linear regression was performed to discern the values of the coefficients in equation 4.5. The resultant equation ($R^2 = 0.806$, $p < 0.0005$) was:

$$\overline{\Delta\sigma} = -427ae^{-141.\bar{\sigma}} \tag{4.6}$$

4.3.2 Tissue Slip

For slip analysis, 5 repeats were also performed. A one way ANOVA was performed to ensure no effects between repeats, yielding no significant differences (F(4,44)=0.12, p=0.87). Slip was achieved in 71% of the 45 cases tested. In all cases, normal force increased to a peak at the instant the shear was applied. The force then reduced until sufficient tension was applied to the tissue, when normal force increased to a higher level than before. The shear force increased gradually under tension until a plateau (Figure 4.8)

A two way ANOVA was conducted to determine the effects of retraction speed and target force on the peak CoF. No significant differences were observed between speeds (F(2,31) = 0.4, p=0.65), target forces (F(2,31) = 2.60, p=0.10), or the interaction effect (speed x force) (F(4,31) = 0.01, p=0.63). The mean value of CoF at slip was 0.42±0.05 (95% CI). Figure 4.9 presents the mean coefficient of friction for the three applied pressures.

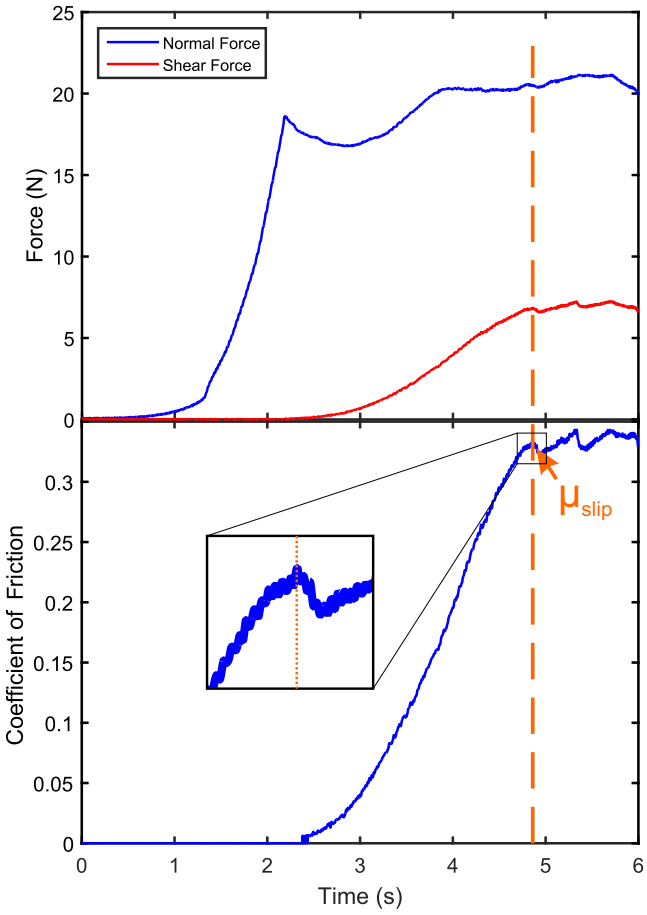

Fig. 4.8 Normal and Shear forces alongside the calculated coefficient of friction, μ. The point of slip, μ_{slip}

4.4 Discussion

The results presented above indicate a complex relationship between the mechanical properties of tissue and two potential methods of damage prevention. The two metrics presented were of opposing methods to reduce damage. The NSRc was designed to find an upper bound of safe grasping force, dependent upon compression speed, before damage occurred. Slip prevention was deduced as a method of keeping the grasping force to a minimum, while still maintaining a definite grip on the object. This would prevent damage by both overcompression and abrasion by the grasper tip.

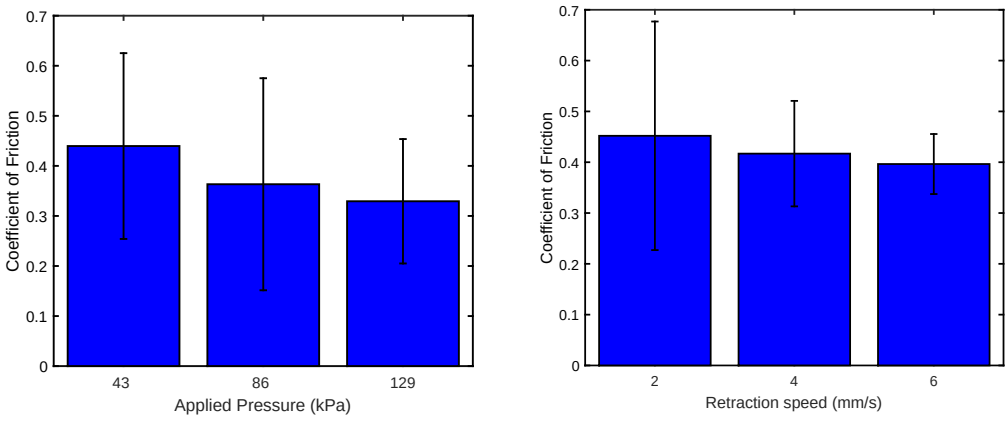

(a) (b)

Fig. 4.9 Mean coefficient of friction $\mu \pm SD$ for each (a) loading case and (b) speed. No significant difference is observed ($p<0.05$ in all cases)

NSRc exhibited a linear relationship with the logarithm of relaxation, with subsequent grasps on tissue samples showing a higher NSRc and lower relaxation. This was present across all levels of force and compression speed, so therefore without histological analysis performed by Chandler [115] cannot directly correlate to a chance of damage. While this is the case an assumption can be made that a decrease in relaxation indicates mechanical trauma through variation of the viscoelastic response of the tissue. This may be a result of fluid migration out of the compressed area but would still increase the amount of load borne by the solid components of the tissue [124], thereby increasing the risk of mechanical damage to the underlying structures.

An interesting observation was with the anomalous samples not included in the correlation. For each colon and ureter there were a small amount of samples that did not follow the above trend between consecutive grasps. Both the relaxation and NSRc observed were lower in the samples, potentially caused by a degraded tissue sample. A practical use of this factor would be be the detection of tissue areas with abnormal mechanical properties, an indicator malignancy [125, 126] Further experimentation will be needed to show this however.

The slip experiments also showed consisted results between compressive force and retraction speed. Across all grasps, the average coefficient of friction at the point of slip

was 0.42. This shows promise as a damage prevention metric, as keeping the coefficient below this level during a grasping action would prevent and damage caused by the slip of the grasper. This value is only true for the simulated grasping environment, however. In particular the jaw profile (currently a 1mm pitch triangular profile) and jaw angle of the grasper (currently parallel plates) will affect the level at which grasping can be considered 'safe'. Therefore future experimentation must be conducted with parametric study on these factors to fully understand the frictional relationship of the grasper jaw.

Both sensing methods were selected as advancements to current methods of grasping improvement, which are currently limited in their application within a surgical environment. Both metrics may be used to enclose a range of 'safe' grasping forces across a range of tissues, however they differ slightly in the technical requirements of sensor and the benefits the bring to optimise the grasping task. NSRc requires two sensing inputs, a single axis force sensor and a position sensor for the face position. Tissue slip requires only a two-axis force sensor for a single axis retraction which, while more complex, offers a better alternative for preventing grasp errors. NSRc ony focuses on a single grasping error, the prevention of overcompression, while tissue slip offers more flexibility in the prevention of multiple errors. On these grounds, the tissue slip will be the focus for the requirements of the sensor in this research, however further investigation of NSRc is advised for future research.

4.5 Chapter Summary

This chapter presents an investigation into analysis methods for a potential grasper integrated sensor. Two methods are presented and investigated for their use, each of which presents different sensing requirements which must be addressed by any resultant sensing. Both the normalised stress rate of compression and tissue slip present advantaged for use in a grasping environment. Under laboratory conditions, the NSRc has proven links to improve a single error in grasping, whereas slip prevention may improve upon multiple aspects of the grasp.

To assess the slip in it's simplest regard, in the case of a single dimension retraction, a two axis force sensor is required for the analysis.

Chapter 5

Investigating a Novel Sensing Method to Improve Laparoscopic Grasping Tasks

This section details the initial investigation into the use of a simulated environment as a design tool for the SITS. Previous experimentation [100] has used set target parameters to indicate function, however a full optimisation has not been performed. The use of computational models can help speed this process and minimise the need for timely empirical design methods. Here we present the use of computational multi-physics modelling as a design tool for Soft Inductive Tactile Sensors (SITS) which use variation in electromagnetically-induced eddy-current effects as a transducer mechanism. We develop and experimentally validate 2D models which extend existing understanding to provide insight into the configuration of sensing elements for measurement of multi-axis forces and rejection of unwanted environmental disturbances.

Work contributing to this chapter is to be published in the Preceedings of IEEE conference on Biomedical Robotics and Biomechatronics

Jones, DP; Kow, JW; Alazmani, A; and Culmer, P., 2018. Computational Design Tools for Soft Inductive Tactile Sensors. In IEEE 7th International Conference on Biomedical Robotics and Biomechatronics (BioRob), 2018 .

5.1 Introduction

For many tactile sensing technologies, modelling tools were developed to assist in the design and optimisation of soft tactile sensors. Many of these covered both the physical deformation and transducer physics within the simulation [127–132]. In the resistive, capacitive, and piezoresistive models, the physics models are fully dependent on the varying geometry of the substrate acting as a conduction pathway. In multi-axis hall effect dome models, the physics is decoupled from the substrate, however the complex geometries require simulation of the deformation to fully optimise the sensor response [95].

From the conclusions of the review presented in Chapter 2, Soft Inductive Tactile sensors (SITS) [100] were presented as an area of particular interest for sensing within a surgical system. They use the eddy current effect to detect the position of a conductive target in relation to an electrical coil through variation in the inductance of the coil. The change in inductance is dependent on several parameters, including varying target and coil geometries [99]. The sensor can be calibrated to relate the measured inductance with applied force [100]. This mode of sensor has a number of attractive qualities for use in surgical graspers; it is physically robust, can achieve a high dynamic range and can be configured to obtain multi-axis measurements [99]. However, designing and optimising the sensor configuration is challenging due to the complexity of the associated electromagnetism calculations [133]. Tools for this specific application are limited to software provided by Texas Instruments for designing sensors which use their inductance to digital converter chips [134]. However, this is limited to a single coil and precludes exploration of multi-coil configurations for multi-axis measurement (Figure 5.1).

To address the current paucity of design tools for inductive tactile sensors, this chapter aims to develop and validate computational models which facilitates easy exploration of the design-space related to SITS, with the ultimate intention of creating a tool for their design and optimisation. We use the case study of a two-axis SITS, introducing the working principle

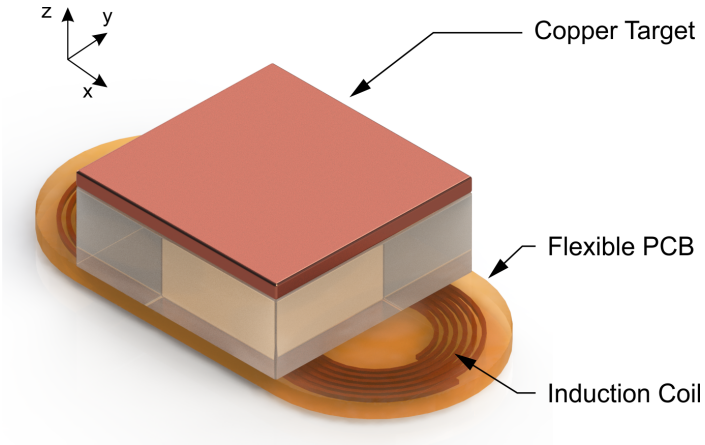

Fig. 5.1 A two-axis SITS. Two inductance coils are positioned below a copper target and silicone elastomer to detect forces in the z and x axes.

of this system before deriving computational models and validating them against physical prototypes. We then use the model to identify and explore key design parameters.

5.1.1 Chapter Objectives

In order to fully understand the design parameters and their effects to SITS measurement range and resolution, an initial investigation into the effectiveness of a simulated design tool was proposed. This section details the investigation, and aims to fulfil the following objectives:

Objective 5.1 To produce a 2D finite element model of a 2-axis SITS.

Objective 5.2 To validate the response of the model through the use of experimental data.

Objective 5.3 To assess the effects of target movement on the sensor response

Objective 5.4 To deduce a set of geometric parameters to be assessed in future chapters

5.2 Working Principle

The SITS uses the eddy current effect to detect the changing position of a conductive target above a number of sensing coils. When excited by AC current, the coils generate an alternating magnetic field, which in turn induces eddy currents in the conductive target (Figure 5.2a). The eddy currents induce an opposing magnetic field, thus reducing the magnetic flux around the coil and serving to dissipate energy [135]. This effect causes a measurable decrease the inductance and increase in reactance of the coil. The effect is increased by two main methods:

1. Reducing the distance between the coil and conductive film, thereby increasing the magnetic flux and eddy current density in the conductor [135].
2. Increasing the coverage of the coil with a larger conductive film, increasing the available area in which eddy currents may be generated [135].

In this manner, the displacement of a conductive target may be measured using the variance in the inductance of one, or several, coils. When placed upon a soft substrate, such as silicone, the changing inductance can be calibrated directly to the applied force on the target.

The operating principle underpinning single-axis SITS can be extended to achieve multi-axis measurements by coupling multiple coils with a single target [99]. In this instance, a two-axis sensor is developed in which the inductance of two coils (L_{c1} & L_{c2}) is combined using additive and differential forms to determine normal and lateral displacements of the target respectively. Using a deformable layer to modulate target displacement then enables force calibration as a function of the coil inductances for both normal (F_z, Equation 5.1) and shear (F_x, Equation 5.2). The resolution of such a sensor is dependent on the properties of the sensing coils, target, and elastomer. This chapter presents only the exploration of variance in the target properties.

$$F_x = f(L_{c1} - L_{c2}) \tag{5.1}$$

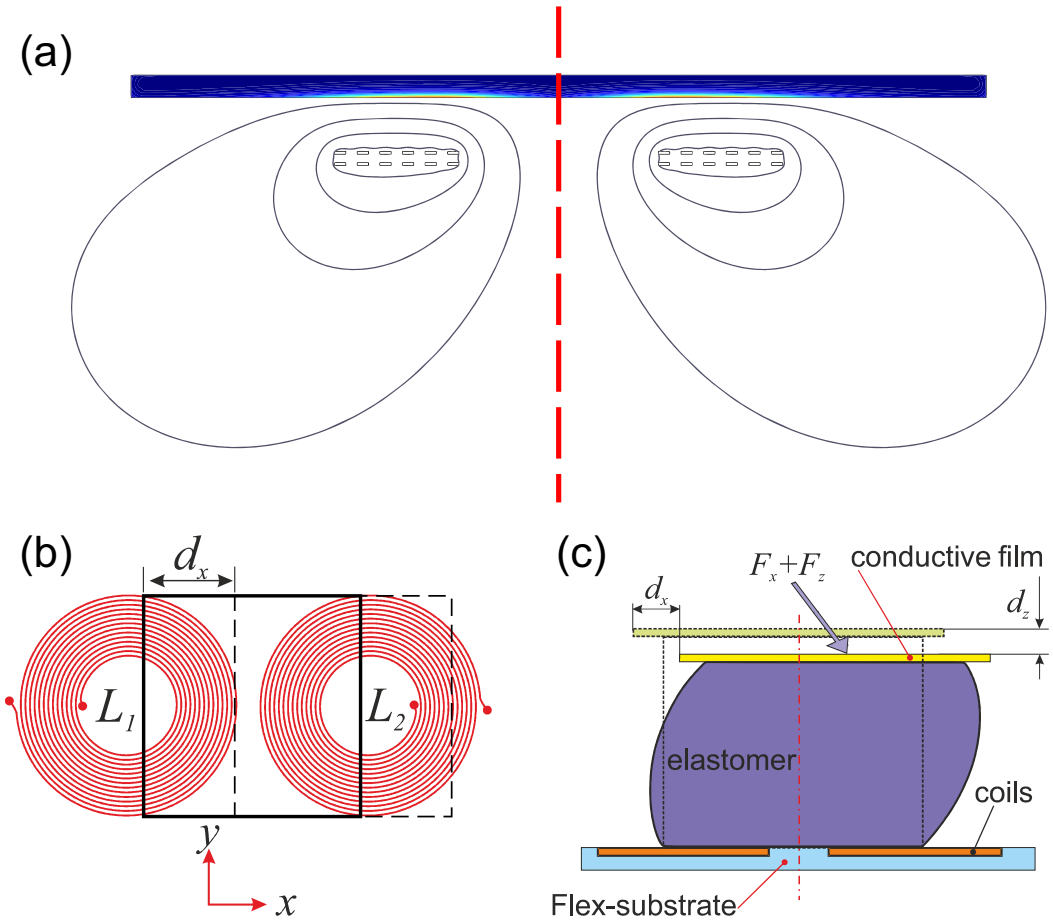

Fig. 5.2 Working principles of the single and multi axis SITS. (a) Magnetic field coupling between the coil and copper target: Shaded region = eddy current density in target, contours = Field strength; (b) Schematic of target displacement in a 2D SITS with a (c) side view of elastomer deformation

$$F_z = f(L_{c1} + L_{c2}) \tag{5.2}$$

Considering this as a 2D case with rigid target and coil elements, movement of the target can be defined using three parameters: horizontal (shear) movement d_z, vertical (normal) movement d_x, and rotation α, discussed further in section 5.3.3. The sensor aims to determine d_z and d_x while α is considered an unwanted disturbance resulting in measurement noise.

5.3 Methods

A combination of computational modelling and experimental evaluation was used to develop and validate a computational SITS model and then investigate it's efficacy as a practical design tool.

5.3.1 Sensor Response Calculation

The lowest level method of sensor response prediction is to use standard inductance equations to calculate the response. However using this method is difficult, as many equations exist only for specific portions of the system [136]. The combination of these equations would rapidly increase the complexity of the system, therefore an alternative method is required. Finite element modelling presents a solution in the ability to parametrically analyse a complex system with little overhead in the setup of the simulation.

5.3.1.1 Computational Modelling

Finite Element models of the coil-target electromagnetic system can be achieved using one of three main approaches of increasing complexity, from 2D axisymetric and lumped parameter models, through 2D planar approximations to a full 3D representation. The full 3D enables modelling of complex (e.g. asymetric) coil and target geometries and configurations. However, this comes at the expense of computational cost, with detailed models requiring many hours to compute on a high-performance PC. Therefore simplification of the model is desirable to provide a pragmatic design tool (in which the designer may wish to evaluate multiple iterations of a design). 2D axisymmetric and lumped parameter models require symmetry about a central axis which limit their applicability to single coil-target systems. However, 2D planar models enable simulation of multiple coil-target cross-sections and while this requires simplification of spiral coil geometries, the resultant computational time is reduced from hours to minutes.

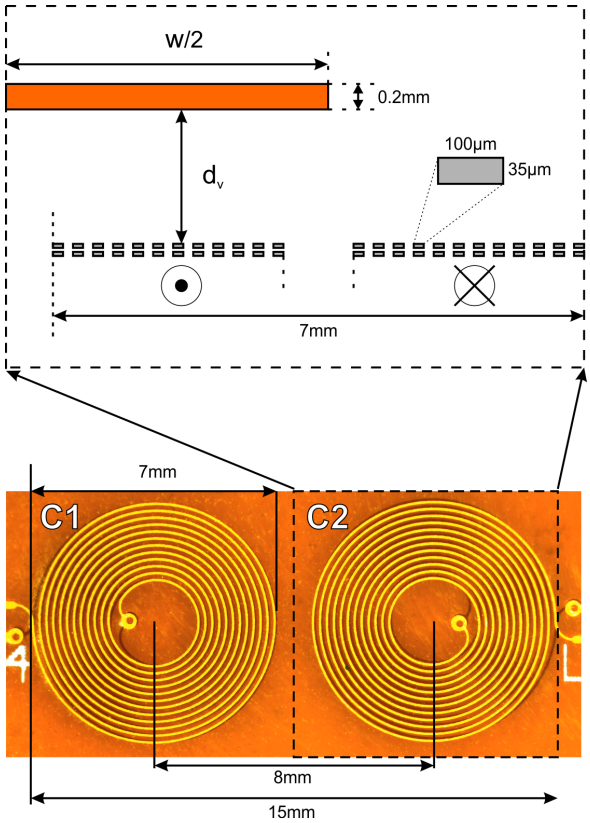

Fig. 5.3 Diagram of the geometry of the computational simulation. The diagram indicates a half of the simulated two coil cross-section. Each coil was represented by two 2 × 12 arrays of wires separated by a 2.2mm gap representing the centre of the coil. Each wire section was modelled as a rectangle of dimensions 100 μm × 35 μm. One half of each coil had current directed into the plane, while the opposing side current out of the plane.

As an initial investigation, a 2D planar simulation of the 2-axis SITS was developed using multi-physics FEA software (COMSOL Multiphysics [137]). The model focuses on the electromagnetic aspects of SITS operation and so neglects physical aspects (e.g. deformation of the elastomer layer which modulates target movement on application of an input force). This method effectively takes a cross-sectional representation of the system, approximating each coil as a paired array of straight parallel wires. For each coil, the left and right hand groups of wire carry electric current in opposite directions to emulate the behaviour of the spiral windings. The geometry of the model is based directly on the physical prototype (Figure 5.3). The wire size of the coil was approximated to be 100 μm wide and 35 μm thick. The wires were positioned in four 12 × 2 arrays, each representing a half of the 12

turn, 2 layer spiral coil. The coils were excited with a 5kHz AC supply, with an applied drive current of 1.017 *mA*.

The main disadvantage of the 2D planar simulations is the missing geometric attributes of the coils. In the spiral coil prototype used for validation (Figure 5.3), the field will be present around the full coil. In the 2D simulation however, a 'dead spot' will be present in the centre of each coil where this continuous field is not simulated. Due to this limitation, the results obtained for the simulated inductance of the coils was of a different order of magnitude relative to the validated value. Therefore the models were validated on the percentage change from the inductance value of the coils when no target was present. This value was 3.21μH & 3.19 μH in validation coils 1 & 2 respectively, and 0.43 μH in the simulated coils. This allowed a direct comparison between the simulated and validated results.

5.3.2 Experimental Configuration

An experimental prototype of the 2-axis SITS was developed using two spiral coils fabricated on a thin Kapton film with 100 μm track width and 100 μm spacing, as shown in Figure 5.4. Each coil is 7 mm in diameter, with two layers and 12 turns per layer. Copper targets of variable size and 0.2 mm thickness were located above the coils and their position relative to this datum was controlled using two linear micro-positioning stages Figure 5.4. The inductance of the coil pair was measured for a range of experimental conditions (defined below) using a digital inductance converter (Texas Instruments LDC1614) connected to an data acquisition device (National Instruments MyRIO). The coils were excited sequentially by the chip (Figure 5.4b) to negate the chance of crosstalk between the adjacent coils. Each coil was driven by a 5 MHz excitation current using the LDC1614, selected based on empirical design guidance [99].

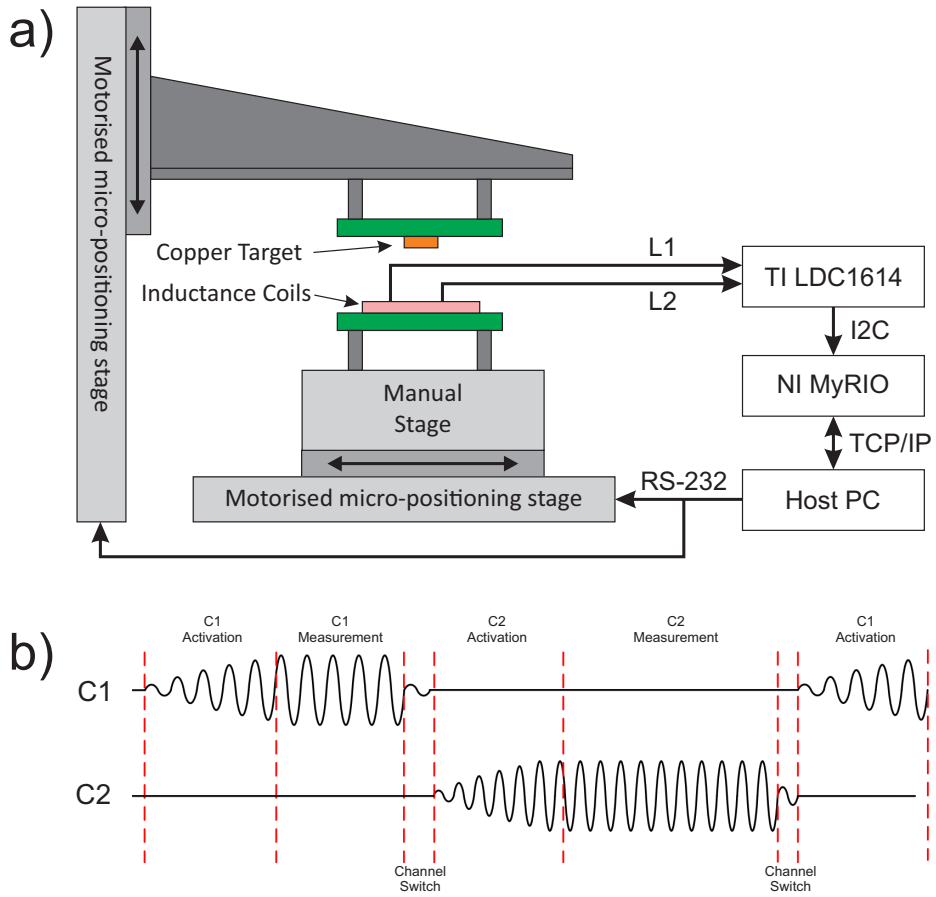

Fig. 5.4 a) The experimental test platform used to evaluate the 2-axis SITS and the inductive coil pair used in the system. b) Operation principle of the TI LDC1614. Each channel is operated sequentially, such that only one coil is activated at any one time.

5.3.3 Parametric Study

A parametric study of key design variables was conducted using experimental testing and the computational model, firstly to validate the computational model and secondly to explore its efficacy as a practical design tool to investigate the effects of individual design parameters on inductance. The parameters, illustrated in Figure 5.5, were selected to relate to physical aspects of the sensor and its interaction with the external environment across a range of values selected through preliminary studies:

- Target vertical displacement $d_v = 1 : 5mm$
- Target horizontal displacement $d_h = 0 : 5mm$

- Target rotation $\alpha = 0 : 20°$
- Target size (width) $w = 8 : 22mm$

A fixed coil geometry and AC excitation configuration, described in Section 5.3.2, was used in this investigation although these aspects could also be manipulated. A baseline configuration was selected for convenient comparison with parameters set as $d_v = 2mm, d_h = 0mm, \alpha = 0°, w = 8mm$ (the distance between coil centres).

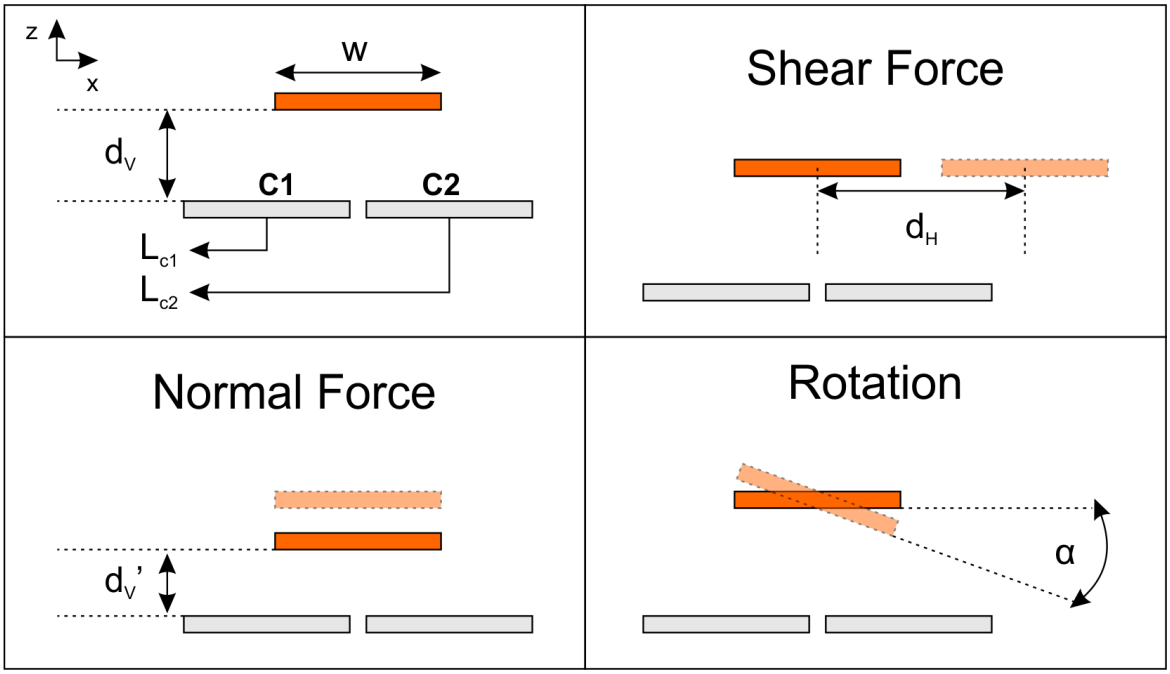

Fig. 5.5 Indication of the parameters of target movement in a two axis soft inductive tactile sensor (indicated in Figure 5.1). Parameters: d_v = vertical target displacement; d_h = horizontal target displacement; α; w = target width; $C1,2$ = Coil 1 & Coil 2; $L_{c1,2}$ = Inductance C1 & C2

5.3.3.1 Vertical Displacement

A vertical movement of the target occurs in the sensor under pure normal loading. In the physical experiment, the target was moved at 0.1 mm intervals relative to the stationary coil pair using the micropositioning stage, over a range of 5mm. This was selected based on the calculated inductance drop of Texas Instrument's coil design tool [134], defined at the

point where inductance was within 1% of the inductance of a coil with no target. At each interval (when the target was static) the coil inductances were measured at a sampling rate of 100Hz for 1s and these data points were averaged to provide inductances L_{c1} and L_{c2}. Each test was repeated three times. This configuration was emulated in the simulation with the target moved at 0.1 mm intervals and coil inductance was obtained from the simulation as an output parameter. A combined inductance parameter to represent vertical displacement is then determined as:

$$L_z = L_{c1} + L_{c2} \tag{5.3}$$

5.3.3.2 Horizontal Displacement

A horizontal movement of the target occurs in the sensor under pure shear loading. A process similar to that described for Vertical Displacement was used for both physical experiment and simulation. Assuming symmetry, the target's horizontal position was varied between 0 and 5 mm from the baseline position in the positive X direction (Figure 5.5). This was the point where the trailing edge of the coil passed the horizontal bound of the second coil. A combined inductance parameter for horizontal displacement was defined as:

$$L_x = L_{c1} - L_{c2} \tag{5.4}$$

5.3.3.3 Target Rotation

Target rotation represents an undesired disturbance for this sensor which cannot be differentiated from horizontal displacement of the target. This occurs when loading results in rotation of the target relative to the coils so they are not parallel. This was investigated by positioning the target centrally above the coil pair and rotating the target clockwise between 0 and 20 degrees, at 2 degree intervals, using a rotation micropositioning stage. This range was selected as the maximum rotation that may occur in the baseline configuration (d_v =

2 mm, w = 8 mm). The resultant inductance pairs were then processed to determine the effective horizontal inductance (L_h) measures.

5.3.3.4 Target Size Optimisation

The width of the target relative to the coil pair will affect the characteristics of both the vertical and horizontal measures detailed above. This aspect was used to explore the use of the computational model to inform and optimise sensor design, in which the objective was to maximise the combined sensitivity of the sensor in both vertical (normal force) and horizontal (shear force) measurement. The simulation was therefore used to investigate these attributes of target sizes 8 mm (distance between coil centres), 15 mm (complete coverage of the two coils), and 22 mm (target overhanging both coils).

5.4 Results

5.4.1 Simulation Data

Figure 5.6 presents indications of the changing magnetic field under each movement parameter. Under the initial conditions, the field can be seen to be disturbed by two factors: the target and the unpowered coil. Under the three movements applied, the target caused deformation in the field by the changing strength and position of the eddy currents within. This serves to change the areas of highest flux density, at which sensitivity will be increased. This may not be accurately predicted by the standard equations, giving credence to the use of FE simulation in this investigation. The unpowered coil does not move in relation to the powered coil between movements and therefore will not affect the measurements directly. The deformation it causes 'squashes' the field between the coils compared to the shape on the opposite edge of the coil. While the resultant effect on inductance is not known, this

serves to reduce the field strength above the unpowered coil, creating a more focused area of sensitivity for the measurement.

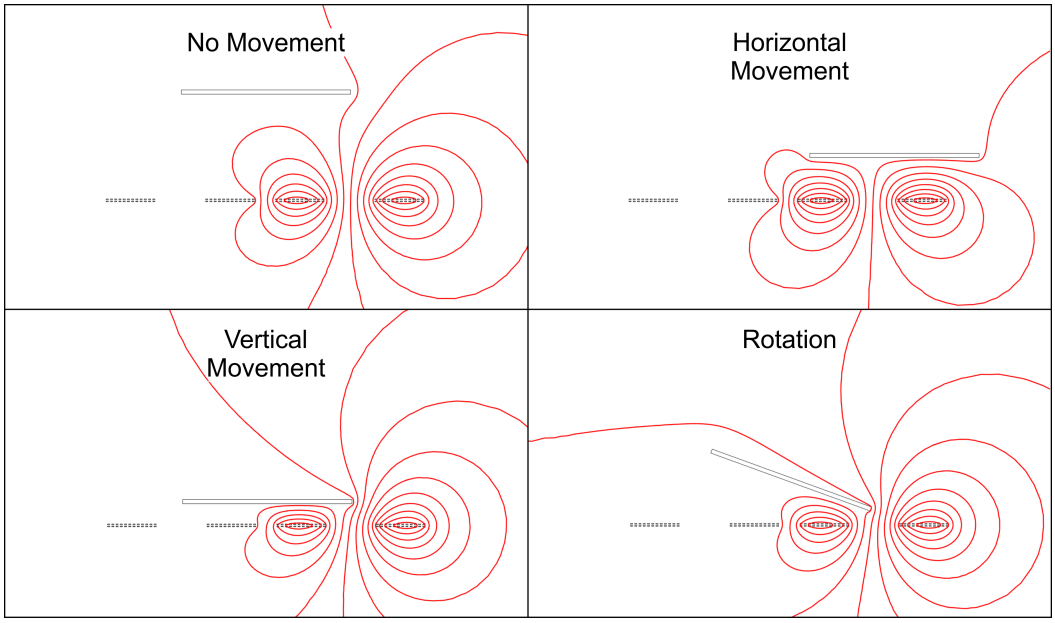

Fig. 5.6 The magnetic field generated by coil 2 during sequential activation under the test conditions shown in Fig. 5.5. The magnetic field is morphed dependent on the displacement and rotation of the target. Gradient lines indicate magnetic vector potential perpendicular to the plane (Wb/m)5.5.

5.4.2 Experimental Validation

Figure 5.7 presents the compared results from the simulation and validation study. Overall the model responded well, replicating the correct trend of inductance change across all parameters. The model showed variation from the validation study in the horizontal and rotational movements, discussed in further detail below.

Under normal displacement the inductance of the simulated coil dropped on both coils when target separation was reduced. The curves of the reduction both showed similar profiles (Figure 5.7a) across the full range of data, however the model predicted a greater drop in inductance than the validation proved. This may be explained by the presence of additional

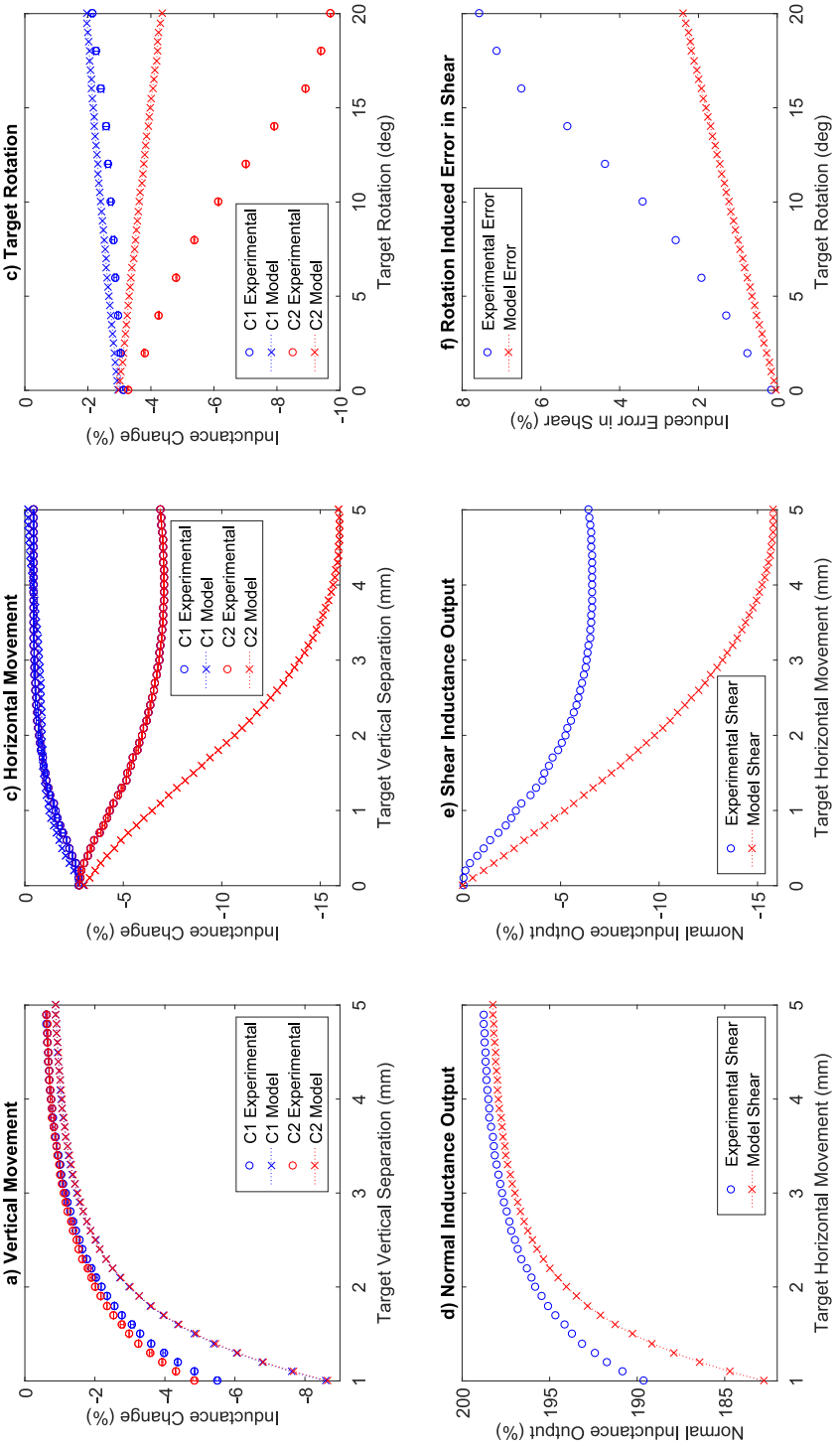

Fig. 5.7 Percentage change of inductance ($\Delta L/L_0$) for a) Vertical Movement, b) Horizontal Movement, and c) target rotation. Overall outputs for d) Vertical Movement (Eq.5.2) and e) Horizontal Movement (Eq.5.1). f) The error in shear induced by the rotation.

wiring in series with the validation coils to connect the measurement electronics. This would raise the overall inductance, and reduce the normalised inductance change.

Under horizontal displacement the inductance of coil 1 was increased as the target moved horizontally away, while the inductance in coil 2 decreased as the target moved toward it (5.7b). For coil 1, the trends between simulation and validation are closely matched, whereas for coil 2 the inductance change is nearly doubled.

Under rotation, the inductance change reflected that of the horizontal displacement, with coil 1 increasing and coil 2 decreasing. Once again coil 1 follows closely to the trend, but the main variation between the two responses as coil 2. In this, the simulated response shows an equal and opposite change to coil 1, whereas the validated coil 2 response was much greater showing a similar profile to that of the horizontal movement. This may be explained by the 'dead zone' in the coil centre described as a limitation of the model.

5.4.3 Target Size Optimisation

The investigation of target width's effect on resolution showed differences in resolution in both shear and normal displacement (Figure 5.8). The maximum shear and normal ranges are presented in table 5.1. In the shear case, the two smaller targets showed a similar trend, rising almost linearly before peaking at the larger horizontal movement. The 22 mm target has a lower range, and follows a different trend to the smaller targets, initially slowly increasing before a faster increase in the larger displacement. This may be explained by the varying change of sensor coverage with each size. The large sensor must travel a greater distance before the edge of the target is above the coil, and further movement causes inductance change. The smaller coils do not exhibit this, ans any small movement will change the inductances.

For normal movement, all targets follow the same trend, but exhibit different ranges. In particular, the 8mm target covered a lower percentage of the coils, and so showed a lower difference in inductance. For both movements, the 15 mm target showed the greatest range

and therefore resolution. This showed that the optimum width of the modelled sensor was 15 mm, or the distance between the outer edges of the two coils.

Table 5.1 Maximum ranges for the width exploration

Width	Maximum vertical output	Maximum horizontal output
8mm	29.6%	24.2%
15 mm	31.4%	71.0%
22 mm	12.8%	69.1%

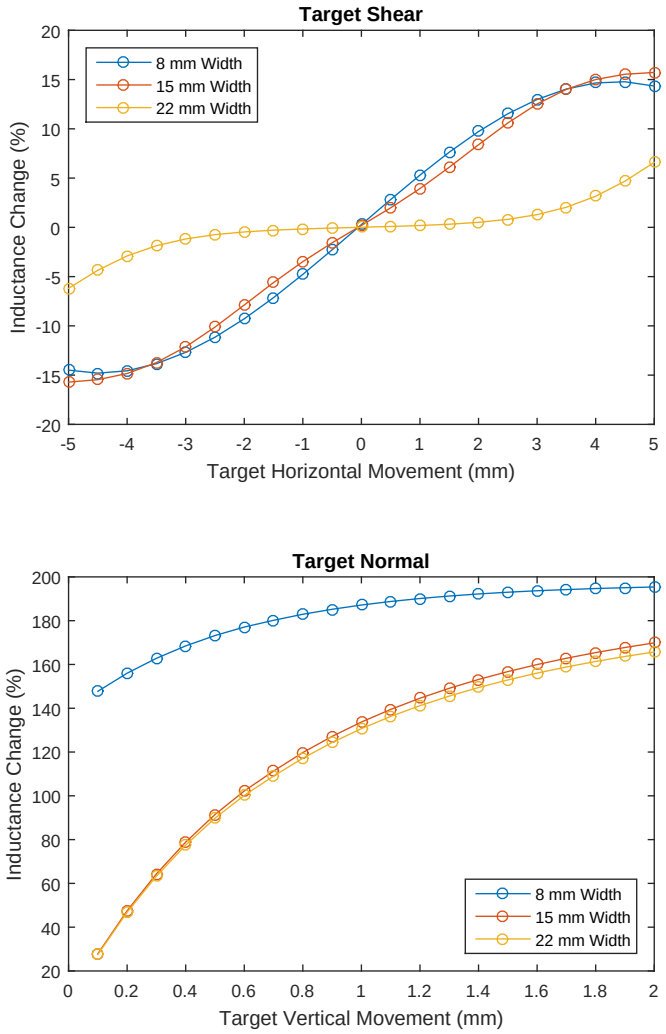

Fig. 5.8 Inductance change ($(L_{c1}-L_{c2})/L_0$, and $(L_{c1}+L_{c2})/L_0$) with varying horizontal and vertical target placements

5.5 Discussion

This section presents a simulated and validated analysis of different target parameters of an inductive tactile sensor. The simulations were built based on an existing sensor, presented in [99]. The ultimate aim was to use these validated simulations as an investigative tool to identify the key design parameters of soft inductive tactile sensors.

The validations of the simulation showed consistent trends in inductance change throughout all motions. While the absolute values varied in magnitude between the experimental and modeled results, this was a known limitation of the model. A more useful output was to consider the percentage change in inductance for different configurations and scenarios, a common approach in sensor design and analysis. Instead, the percentage change in inductance was calculated to normalise the changes in inductance. This value was then used to validate the model response to the four applied parameters.

The 2D planar simulation agreed closely with the validation, replicating the inductance trends over all of the tested parameters. The model can simulate variation in both geometric parameters and design aspects of the sensor. The changes in target position and rotation have been validated, and define the movement of the target under applied force. Currently, the width of target is the only design parameter to be evaluated with the simulation. While this evaluation showed promise, there are further parameters which can be evaluated. The target thickness and varying numbers of coil layers are of particular interest, as well as the influence of external conductors causing noise in the system. The simulated environment will also allow complex substrate geometries, such as a curved coil substrates, to be investigated

A limitation with this model was the inability to model certain geometric features. As the coils were modelled as sets of parallel wires, there was no generation of magnetic field between them, leading to an uncharacteristic plateau in the shear analysis. The differences this caused in the overall field also led to errors in the initial width analysis, causing a higher relative inductance change as the width increased. While the simulation cannot accurately predict the inductance change across all parameters, the conforming trends confirm its viability as a design tool.

Currently the design tool is limited to a 2D plane. While this reduces the computation cost and allows simple geometric analysis to be performed on the target, the simulation is unable to compute more complex targets. For this a 3D simulation will be required. The 3D simulation would offer further detail in the simulation, allowing larger arrays of coils and varying coil shapes to be analysed by the simulation. It would also offer a closer response

to the true inductance of the system, and could therefore be validated against an absolute measure of inductance rather than inductance change.

From the errors mentioned above, it is evident that a more complex simulation is required to model a SITS. While not fully representative of the true values of inductance, the 2D planar model has highlighted several design parameters which must be considered in the optimisation of the sensor. The parameters are as follows:

- Displacement - d_{xyz}
- Rotation - R_{xyz}
- Target Size - Length and Width

A further parameter which may affect the sensor output is the target shape. Different coverages of the coil have been shown to affect the sensor reading, which in a 3D environment will be affected by shape as well. The above parameters are all target focused, and may be investigated with a 3D lumped model to simplify the coils.

The next focus of investigation should be on the coils. The unpowered coil has shown to affect the magnetic field propagated, and so their separation should be investigated to deduce it's full effects on the sensor. Further to this, different shapes of coil will likely exhibit different inductances and interferences due to the wiring pattern and area of the coils which run close to one another. For these two parameters, a higher fidelity 3D model to represent the full wiring structure will be required.

5.6 Chapter Summary

In this chapter a 2D planar FE model was used to assess the design parameters present in the 2 axis SITS. The simulation was validated experimentally for a sensor operating to measure two components of movement. While the model showed some deviation in the absolute

values of the sensor output, it correctly predicted the general trends observed under three parameters, two displacements and one rotation. Because of this, it is clear that the 2D model is insufficient for use in the SITS optimisation. It has, however, identified several key parameters which may be applied to higher fidelity models to assist in a full optimisation of both the coil and target components.

Chapter 6

Computational Optimisation of Inductive Tactile Sensors in 3D

This section presents a detailed analysis into the design parameters of the SITS. Due to limitations in the 2D simulation, 3D models were required to fully understand the interaction between coils and target. First, a lumped coil model was developed to analyse the target geometric parameters. Two shapes, three sizes, three displacements and two rotations were assessed to produce an optimised target. Second, a full 3D representation of the coil was generated to assess variations in the coil geometry and interferences between the coils.

6.1 Introduction

The computational model presented in Chapter 5 presented several design parameters which will assist in the optimisation of a 2D SITS. While the simulation was able to replicate general trends in the inductance change of the sensor, however had limitations in both the magnitude of response and the lack of certain geometric features in the coils. To rectify these limitations, two further models were developed to assess design parameters of the sensor in more detail.

6.1.1 Chapter Objectives

In order to produce a higher fidelity model of the 2-axis SITS, further investigation into the finite element design tool was proposed. This section details the investigation, and aims to fulfil the following objectives:

Objective 6.1 To produce and validate a simplified 3D model of the SITS to assess further target parameters.

Objective 6.2 To produce and validate a fully representative 3D model of the SITS to assess the design parameters relating to the coils.

Objective 6.3 To assess a variety of target parameters to discern their effects on the SITS measurement range.

Objective 6.4 To recommend a series of target parameters which generate an optimal SITS.

6.2 Methods

The 2D planar model presented in Chapter 5 exhibited several limitations in the initial investigation into design parameters. In particular, the inability to simulate out of plane

geometries resulted in discrepancies between simulation and validation in the shear and rotation cases. These limitations may be rectified by a 3D model, either representative or simplified, allowing the field to be generated around the full circumference of the circular spiral. The more advanced models will also allow further geometric parameters to be investigated, such as three axis displacement and target shape. New 3D computational models were developed for this chapter using multi-physics FEA software (COMSOL Multiphysics [137]). The existing validation dataset presented in Chapter 5 was used to validate both simulations. Once again a 7mm diameter, 2 layer coil with 12 turns per layer was used to keep the simulations consistent with the previous work.

6.2.1 Lumped 3D Model

The lumped 3D model of the 2-axis SITS was developed first to reduce the computation time needed to assess the 3D design tool. Rather than producing a full representation of the individual wires within the coil, they were simplified to a lumped annulus of the same outer dimensions of the coil (Figure 6.1). The annulus was set as a 24-turn coil, with turn length equal to the mean turn length of the spiral.

The lumped model allowed further investigation of the target movements investigated in Chapter 5. The parametric study of target displacement performed previously was expanded to three displacements ($d_{x,y,z}$) and two rotations (($r_{x,y}$). Each of these movements had the potential to occur under applied force, and so were of interest in the investigation to explore their effects of sensor response. Ranges of 2 mm were selected in each dimension where the inductance change would reach 60% of the maximum change, selected based on results of the experimental study in Chapter 5. After this point decreasing sensitivity was observed and would be detrimental to an optimised sensor.

Variations in the target geometry were also enabled by the lumped model. To explore the effects of target shape on sensitivity two shapes, an 8 mm square and 8 mm diameter circle, were investigated under variations in x, y and z. The square target was also varied in

length and width to deduce the best size of target in both dimensions. These parameters were selected based on the coil geometry. Width was selected as equal to the coil diameter, as well as 2 mm above and below (equal to the displacement limit). Length was selected to be equal to the total of both coils, length between coil centres, and 2 mm wider than the the coil separation gap. The values for the movement and geometry studies are presented in Table 6.1.

A limitation for the lumped model was the inability to model coil interactions. Only a single coil was able to be analysed at once, that is if a second lumped coil was present and un-powered it would be treated as a solid mass of copper. Therefore interaction effects between the coils were not able to be modelled and would require a more complex system. To determine the inductances of two coils, all displacements and rotations applied were performed in both directions due to symmetry within the model. The responses may be calculated by:

$$L_{c1}(d_z, d_y) = L_{C2}(d_z, -d_y) \tag{6.1}$$

Table 6.1 Parameter values for the lumped coil simulation

Parameter	Values
d_x	-2:0.5:2 mm
d_y	-2:0.5:2 mm
d_z	0.1:0.1:2 mm
r_x	-5:1:5°
r_y	-5:1:5°
W	5, 7, 9 mm
D	3, 9, 15 mm

6.2.2 Full 3D Model

After the limitations of the lumped 3D model were observed, a full 3D representation of the coils was produced. This allowed both the effects of coil shape as well as their planar

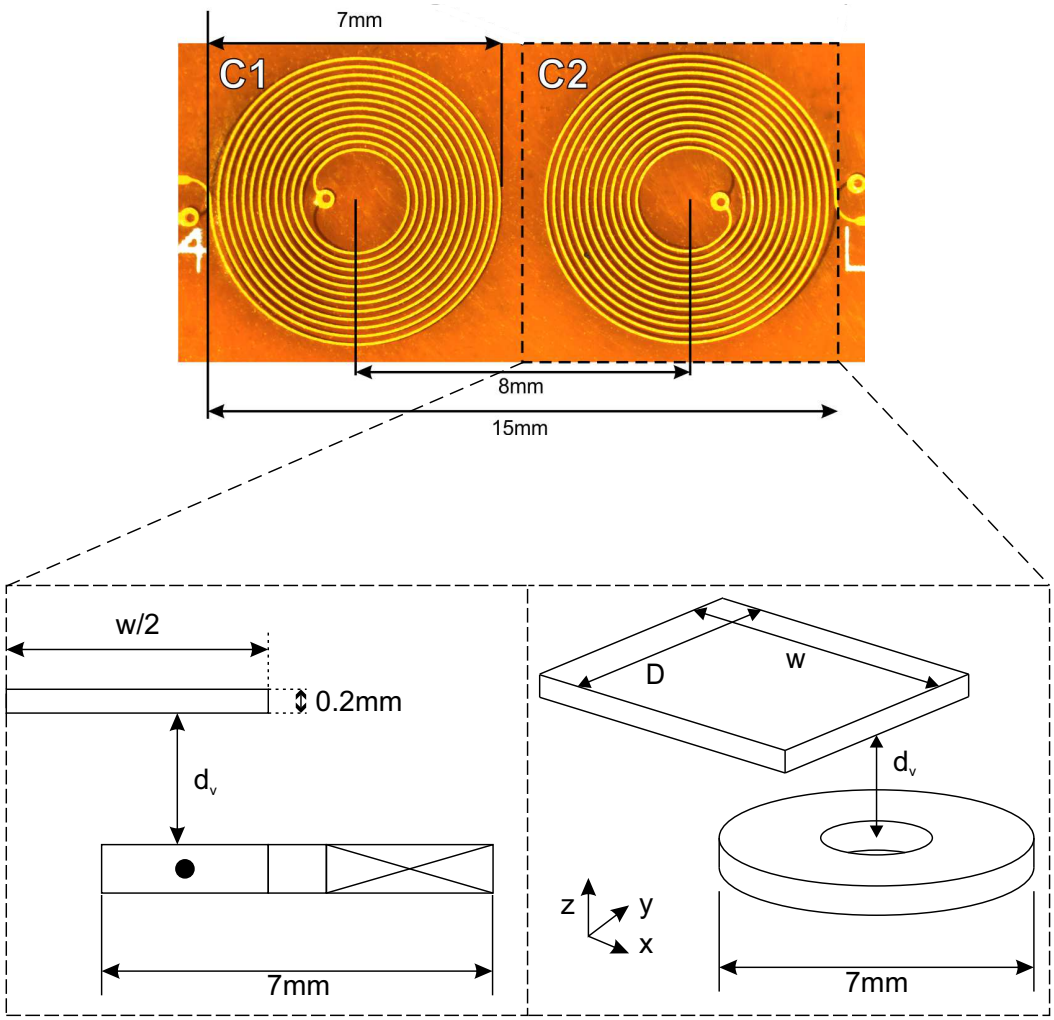

Fig. 6.1 Schematic of the lumped model simulation, where w = Target Width, mm; D = Target Depth, mm; $d_{x,y,z}$ = Target Displacement, mm; $r_{x,y,z}$ = Target Rotation, deg

separation to be observed. 3D representations of the coils were produced in Solidworks [138] and imported into COMSOL [137]. An 8 mm square target was placed 2mm above the centre-point of the coils (Fig 6.2c) in order to simulate a completed sensor. Two coil geometries, 7mm square and circular spirals, were produced based on the existing validation model. Both were then simulated at different planar separations (C_{sep}, table 6.2) to determine interaction effects.

The 3D models required an extremely fine mesh to precisely map the geometries of these coils. The model consisted of 3,000,000 elements with a minimum element size of 0.1 mm,

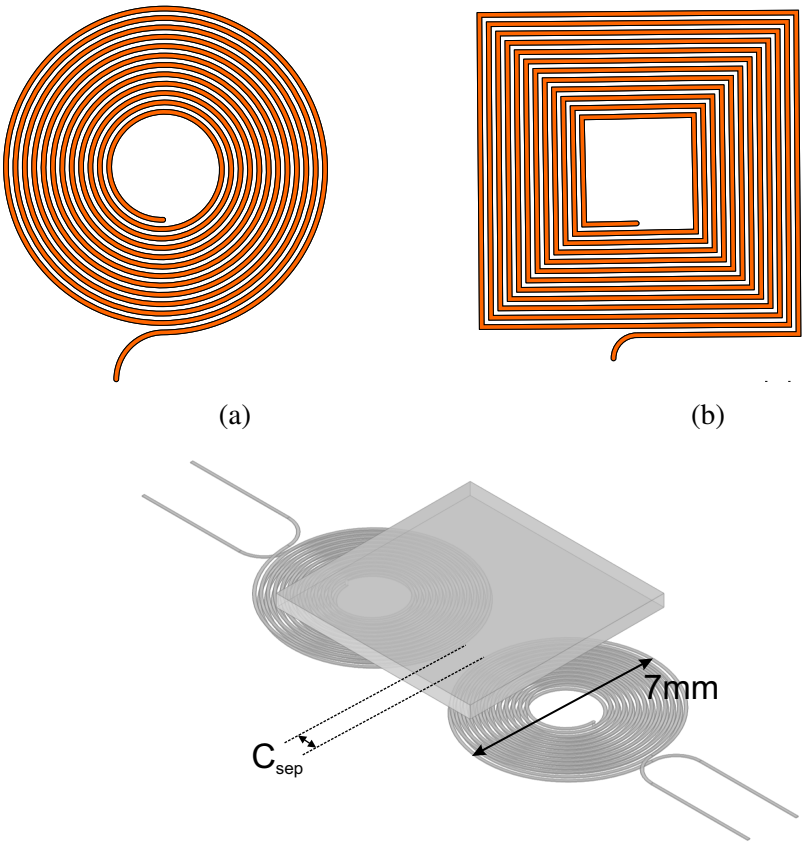

Fig. 6.2 Diagram of the (a) Circular and (b) square spiral coils. (c) The 3D model simulation of the circular planar spiral coils, where C_{sep} = Planar Separation, mm

the maximum size an element must be to accurately map the traces (the size of trace width and separation). The size of the model had exceeded the limits of a standard workstation PC, requiring roughly 60 Gb of memory to compute. Therefore the model was migrated to a High Powered Computing (HPC) node. This allowed the more complex models to be completed with less computing time.

Table 6.2 Parameter values for the 3D coil simulation

Parameter	Values
C_{sep}	0.1, 1, 3 mm
Shape	7 mm Square and Circle

6.3 Results

As the coils were now adequately represented in the simulations, the following results are presented in uH. To validate the study, the results of the simulations were compared to both the previous validation study involving a 7 mm diameter 24 turn coil (Chapter 5), and the spiral coil design tool provided by Texas Instruments [134]. The variances in inductance are shown in Figure 6.3. Unlike the 2D model of the system, both models resulted in inductances of the same magnitude as both the validation system and design tool. Results from the simulations were within 5% of the design tools, owing to the systems being equation-based. The validation system was around 35% higher inductance, which may be explained by the increased circuit complexity in the measurement system.

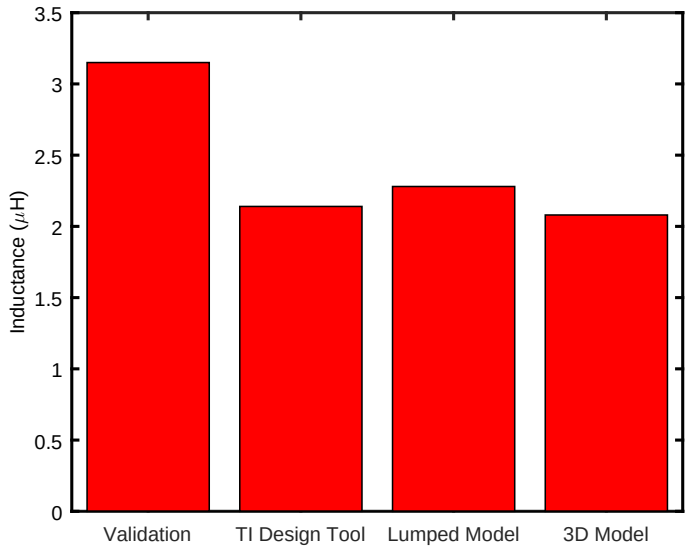

Fig. 6.3 Comparison of the simulations to an experimentally validated inductance, indicating higher inductance in the validation coil

6.3.1 Lumped Simulations

Results of the lumped simulation are presented in terms of the dimensional inductance (Equations 5.4 & 5.3). Only changes in d_x and R_y caused changes in resultant shear, therefore other parameters do not have associated shear results.

The sensor range for each displacement was observed for both square and circular 8mm targets (Fig. 6.4). For the below results, larger ranges in the Normal output for z displacement and shear output for x displacement will give an increased range for the sensor. For shear, the square target achieved a range of 1.14 μH compared to the circular target's range of 0.95 μH. For normal output, the square target was once again higher with 0.60 μH to the circle 0.48μH. Both results (Fig. 6.4 b & d) indicate the square target as the highest range. Changes in d_x, y varied the normal output by up to -0.17, 0.06 μH for square and -0.19, 0.12 μH. In both cases (Fig. 6.4 a & c) the movements of the square targets induced less error in the normal force reading.

Figure 6.5 presents the results of the target length variation study. The study used a rectangular target of width 7 mm and thickness 0.2mm, with lengths of 3, 9 and 15 mm. The ranges for each dimension change are presented in Table 6.3. For shear, a length of 9 mm gives a resolution 4x greater than that of the long and short targets. This is likely because of the different coverages of the coils caused by the targets. Long and short targets offer a lower change in coverage of each coil throughout d_x, thereby causing a lower change in inductance. For d_z, the longest coil offers by far the greatest range, owing to a greater coverage of the coils. For the d_x error in normal reading, the smallest coil offers almost zero effect on the output, while for d_y the ranges of all targets are comparable. Coupling this with the other results, 9 mm can be seen as the best target size tested.

Table 6.3 Parameter ranges from the target length study

Target Length	d_x Normal μH	d_x Shear μH	d_y Normal μH	d_z Normal μH
3mm	0.112	0.248	0.002	0.077
9mm	0.058	1.212	0.122	1.200
15mm	0.163	0.350	0.334	2.563

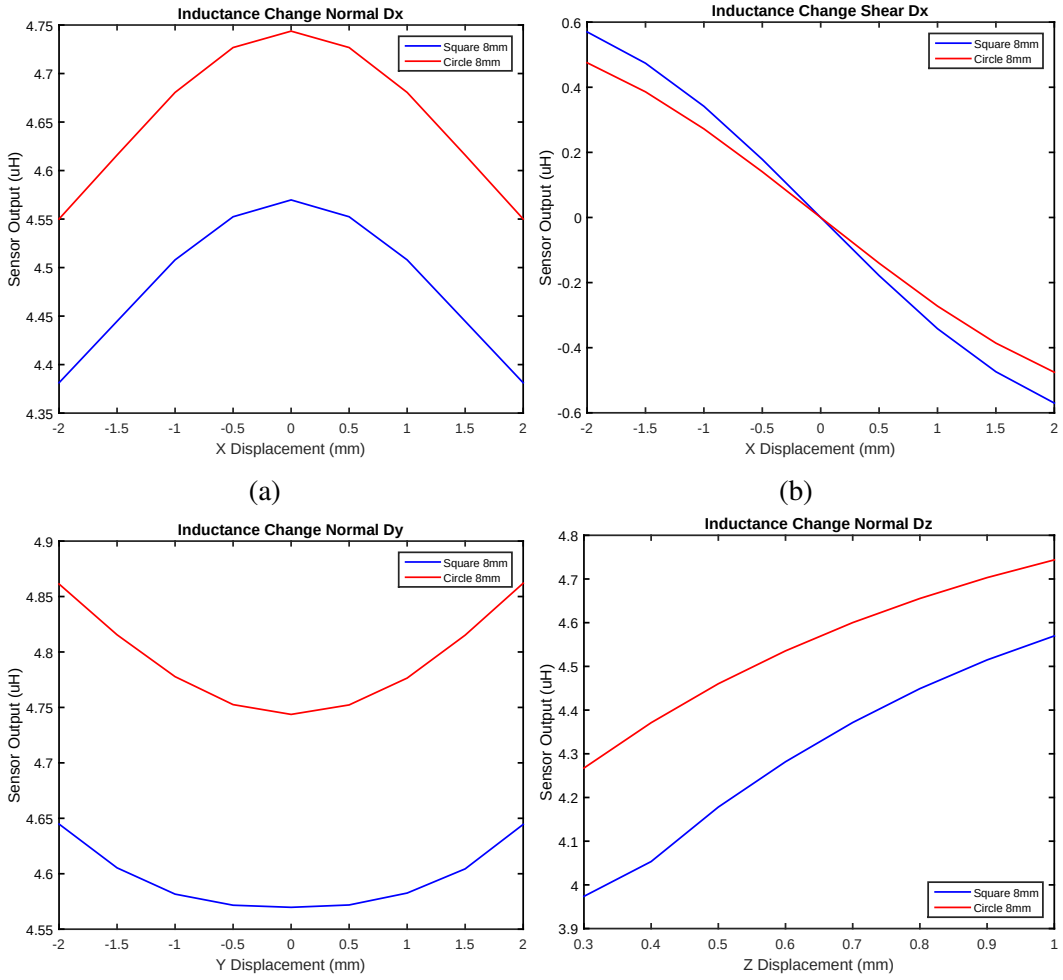

Fig. 6.4 Results of the shape variation study: d_x Normal (a) and Shear (b), d_y Normal (c), and d_z Normal (d)

Figure 6.6 presents the results of the target length variation study. The study used a rectangular target of width 7 mm and thickness 0.2mm. For both shear and normal measurement (Figure 6.6b & d), targets of width greater than or equal to the coil diameter give a greater resolution. This is once again likely due to the greater coverage of the coils. In d_x and d_y normal output, the larger target will offer less error in d_y however more error in d_x, with the opposite being seen for the small target. Therefore the medium width can be seen as more optimal, with relatively high resolutions and lower error. The ranges for each dimension change are presented in Table 6.4.

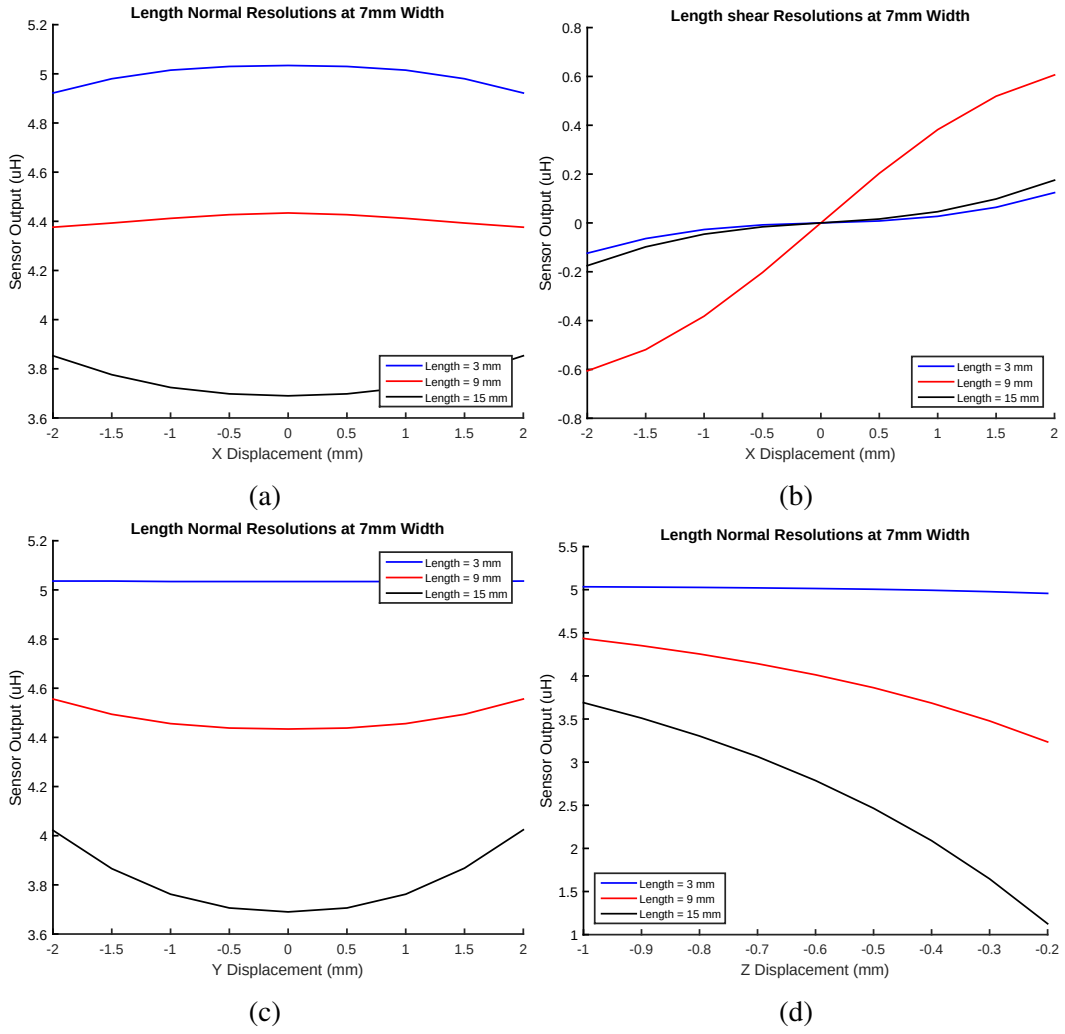

Fig. 6.5 Results of the Length variation study: d_x Normal (a) and Shear (b), d_y Normal (c), and d_z Normal (d)

Table 6.4 Parameter ranges from the target width study

Target Length	d_x Normal μH	d_x Shear μH	d_y Normal μH	d_z Normal μH
5mm	0.031	1.074	0.254	1.147
7mm	0.058	1.212	0.122	1.200
9mm	0.065	1.226	0.026	1.201

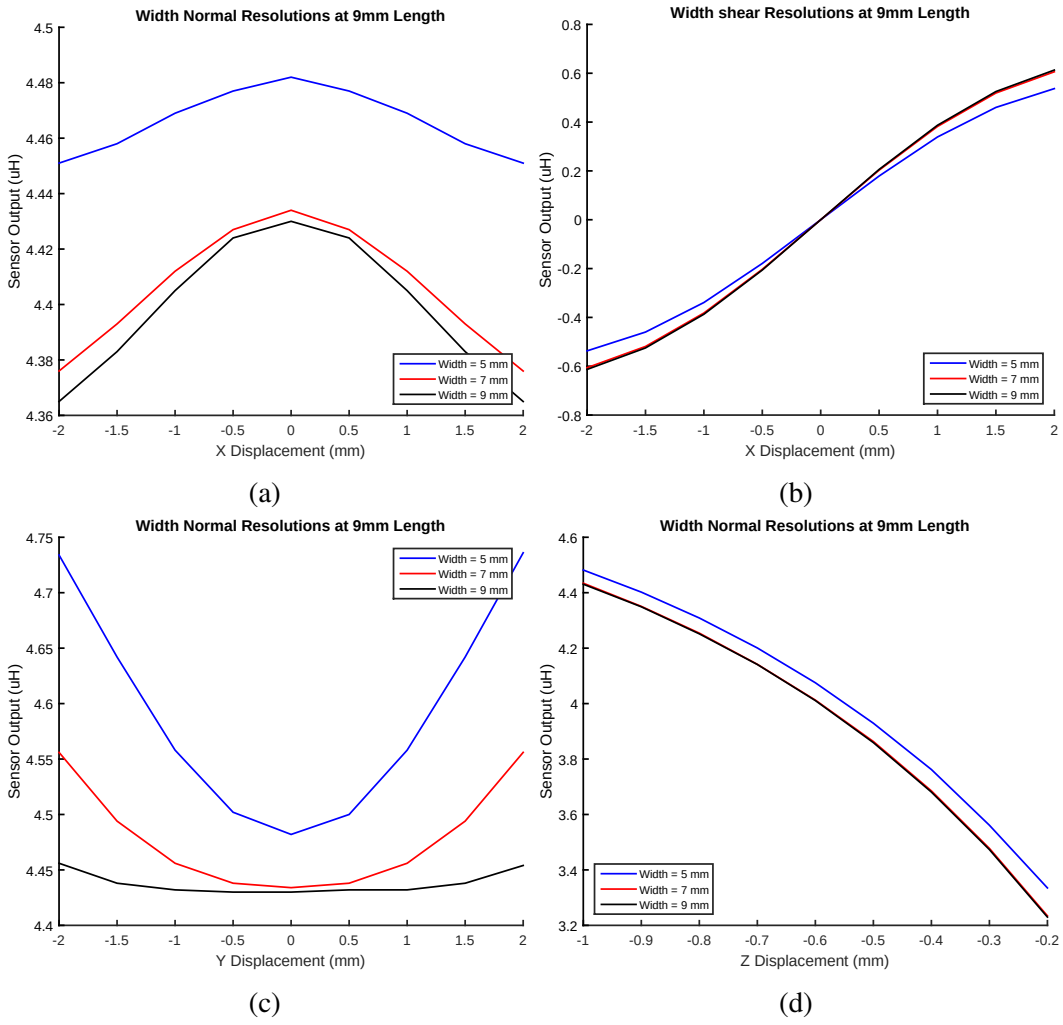

Fig. 6.6 Results of the Width variation study: d_x Normal (a) and Shear (b), d_y Normal (c), and d_z Normal (d)

The effects of target rotation in both R_x and R_y are presented in Figure 6.7. Rotation R_z is not presented, as the symmetric response yielded no change in sensor output. R_x presented identical responses for equally positive and negative values, therefore only the positive values are presented. For both normal and shear output, a change in R_x offers minimal change in the resultant outputs, with a maximum of 0.012 μH in normal and 0.008 μH in shear. For R_y, the effect is stronger, causing a 0.030 μH variance in normal, and a 0.185 μH variance in shear output.

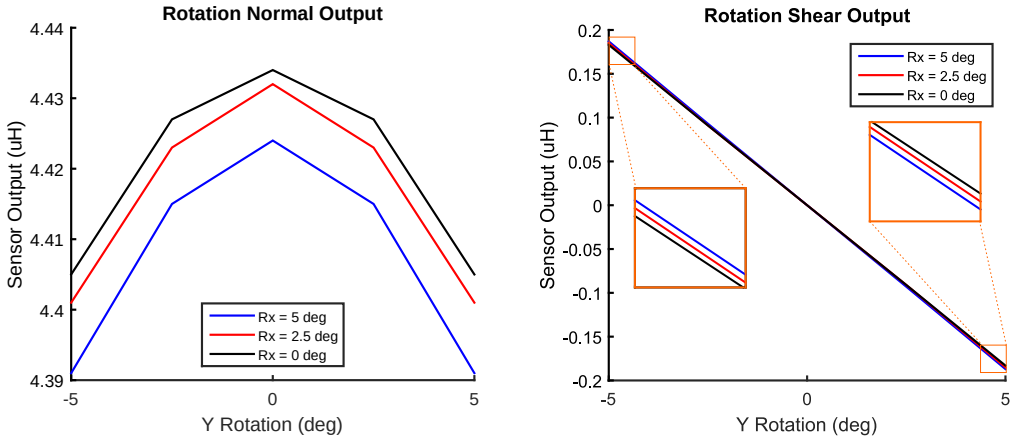

(a) (b)

Fig. 6.7 Results of the Rotation study: d_x Normal (a) and Shear (b), d_y Normal (c), and d_z Normal (d)

6.3.2 Full 3D Model

For the full 3D model, two parameters were assessed: The coil shape and separation. The results are presented in Figure 6.8a. The square coils have on average an inductance 12% higher overall than that of the circular coils. This is supported by inductor theory [139] and therefore representative of the inductor values.

Between separations, the inductances of the square and circle coils dropped by 1.7% and 1.6% respectively as separation was reduced from 1 mm to 0.1 mm, while both increased by 2.3% and 2.6% when the separation was increased from 1 mm to 3 mm. This shows that the

coils may be brought closer together with a small loss in inductance and therefore sensitivity. The effects of coil separation are more prevalent in the square coils than the circle. This is likely because of the increased area of the two coils in close proximity, with the wiring of the two coils being adjacent for the full.

Figure 6.8b shows the variance in the distribution of magnetic field strength between the two coils. As the square coil has a higher level of inductance it would be expected that it's resolution is also higher. This may not be the case, as the magnetic field is not evenly distributed around the coil. Eddy current density increases under a stronger field [140], so therefore an uneven field will change the areas of high sensitivity in the SITS. In the circular coil, which displays an even field, the area of highest sensitivity is located at the centre of the coil. In the square coil, the strongest field is located at the corners of the spiral, showing an extended area of high sensitivity. The effects of this on the overall sensitivity are as yet unknown.

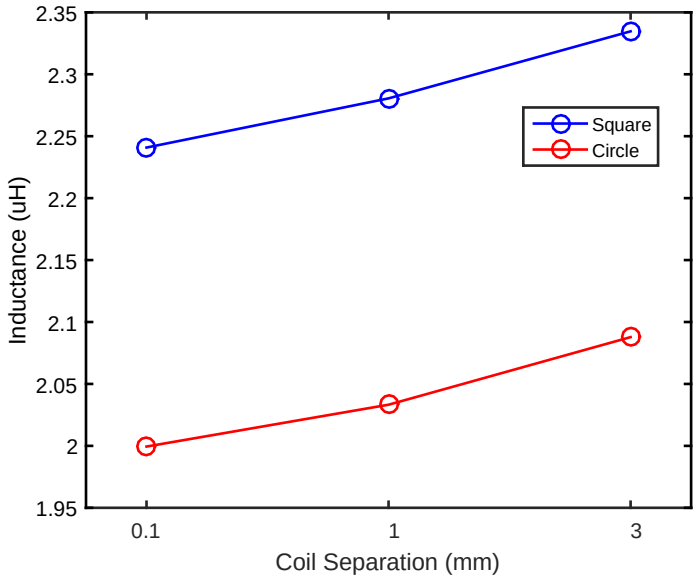

(a)

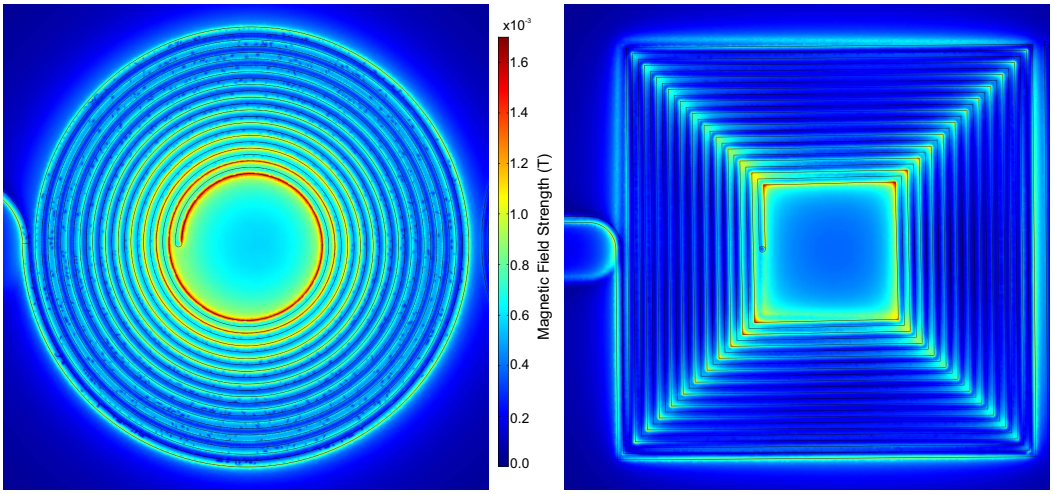

(b)

Fig. 6.8 (a) Comparison of the inductance change between square and circular 7mm coils, spaced at 0.1, 1, and 3 mm; and (b) The magnetic Field Strength (Tesla)

6.4 Discussion

This chapter presents advancements made to the model developed in Chapter 5 in order to further analyse the design parameters of an inductive tactile sensor. The two 3D models were validated against a sample coils and a coil design tool provided by Texas Instruments [134].

Both models produced a result similar to that of the design tool, however were both lower the validation study. This may be explained by the additional circuitry required for the LDC connection raising the overall inductance. This however should not affect the range of the sensor as the magnitude of inductance change is the same, owing to the additive nature of series inductors [141].

The lumped simulation performed well overall in the study, giving relevant profiles for inductance change across all parameters. For the shape study, both the circular and square targets performed similarly, each presenting the same trends in inductance change for both normal and shear output. In terms of range, the square target gave a larger range in both intended outputs and caused less error in the others. This shows the square target as the optimum shape for a 2-axis SITS, however the small differences in range present the target shape as a less important factor in comparison to the target sizes.

The geometry study further assessed the square target to find the effects of both length (l_x) and width (l_y) on the range of inductance output. For a 2 axis SITS, the results present the target width as a less important factor in the sensor range, rather the parameter serves to reduce the errors caused by target displacement in non-ideal conditions. While a wider target will reduce errors in the normal output, errors in the shear are increased. Coupling this with the range results presenting limited returns for targets wider than 7mm, the optimal value of width for the current coils is 7 mm, or the diameter of a single coil.

The target length results presented similar findings. A longer target would give additional range for the normal output of the sensor, however would also increase the resulting error from the non-ideal displacements. Furthermore the range of shear output would be severely limited. Therefore once again a mid range size is selected, offering a compromise between sensor resolution and error in both dimensions.

Rotation about the y axis had the greatest effect on the sensor outputs in both normal and shear. The error induced in the reading was equal to around 0.05 mm difference in the normal output, and a 0.5 mm error in the shear value. From this it is clear that the prevention of target rotation is key factor in the optimisation of the sensor. A potential solution would be

to keep the ratio between the thickness and width (T_{ela}/W_{ela}, Figure 6.9) as low as possible, preventing large moments being created from applied shear forces. This however would reduce the range of the normal output, and would be highly dependent the material properties of the elastomer used as a substrate. Advancements to the simulation to include a mechanical analysis of the elastomer would allow the sensor to be further optimised to prevent target rotation.

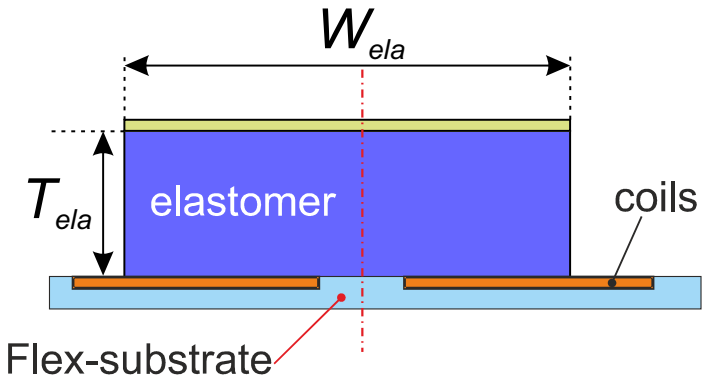

Fig. 6.9 Schematic indicating the geometric parameters of the elastomer which may help prevent rotation: Elastomer Width (W_{ela}) and Thickness (T_{ela})

The full 3D simulation focused on the variance of coil parameters to identify their effects on sensitivity. In terms of raw inductance the square coil offers 12% more sensor range than the circular coils, but noes not necessarily mean a higher sensitivity in both dimensions because of the different distributions of the magnetic fields produced (Figure 6.8). Because of the nature of eddy currents increasing in a stronger field, the areas of highest sensitivity will be found at the areas of high field strength. In the circular coil, the field is focused on the inner edge of the coil, and so a greater shear sensitivity will be observed as he edges of the target pass this area, in particular at low shear forces. The square coil has the field focused on the corners of the coil, and would likely observe a consistent sensitivity across the full shear range while presenting a lower normal sensitivity.

The changes in coil separation were assessed to deduce the interaction between the powered an un-powered coil. As the un-powered coil is present in the generated field, eddy currents are induced in the same manner as the target. In a similar manner to the target vertical displacement, smaller separation between the coils caused a drop in the inductance.

While this reduces the sensor's sensitivity, the relatively small drop of 1.6% can be deemed acceptable to reduce the size of the sensor.

From the above investigation, parameters may be drawn to produce a more optimal 2D SITS. A square target has been shown to offer higher sensitivity with lower error compared to a circular target. For sizing, the square target should have a length equal to the distance between the coil centres, offering the best combination of normal and shear resolution. Target width should greater or equal to the coil diameter to reduce the effects of y-axis shear, while keeping sufficient resolution in x-axis shear and z-axis normal movements. The coil size may be reduced to fit smaller size requirements, however this will also reduce sensor resolution in all axes.

6.5 Chapter Summary

This chapter presents advancements to the design tool proposed in Chapter 5. Two different 3D models are presented, a less complex version to investigate target parameters and a full geometric representation to investigate coil interactions and shape. The optimum target is deduced to be a square of equal dimensions to the distance between coil centres. The optimum coil geometry was deduced to be a length equal to the distance between coil centres, and a width slightly greater than coil diameter. The complex simulated showed that coil separation may be reduced to the minimum that manufacturing tolerances will allow, and indicated some interesting relationships between coil shape and sensor resolution. These parameters will be applied in future research to develop an optimised version of the SITS.

Chapter 7

A Sensor for Slip Detection within a Grasper Jaw

Chapters 5 and 6 presented a method of target optimisation for a two-axis SITS. With optimum parameters for the target deduced, a two-axis SITS is built, calibrated, and used to detect slip on a soft tissue simulant.

7.1 Chapter Objectives

The primary aim of the two-axis SITS is to reduce errors in surgical tissue manipulation tasks through the identification and thus prevention of slip (Chapter 4). This work involved fabrication and evaluation of a 2:1 scale fully functional prototype for detailed investigation, followed by fabrication of a 1:1 scale prototype to assemble a proof-of-concept instrumented grasper system.

Objective 7.1 To fabricate and characterise a scaled prototype of the proposed two-axis SITS

Objective 7.2 To assess the performance of the sensor in the detection of slip on soft tissue analogues.

Objective 7.3 To fabricate and evaluate the efficacy of a 1:1 (miniature size) two-axis SITS.

7.2 Sensor Fabrication

A two-axis SITS was produced using the optimised target parameters from Chapter 6, with parameter presented in Table 7.1. A pair of 7 mm diameter coils with the same specification as Section 5.3.2 were used to measure the inductance drop. The coils were fabricated on polyimide film by a standard FPC process (FS Technologies, co., ltd.; Shenzhen,China). The elastomer layer was laser cut (VLS3.50, Universal Laser Systems; AZ, USA) into squares of 8 mm size. The conductive targets were cut from copper sheet, and then the three layers were attached using cyanoacrylate glue. The sensor was then affixed to an acrylic mount with double sided tape (3M; MN, USA) for insertion into the calibration system. The assembled prototype is shown in Figure [FIG] The calibration method is presented in Section 7.3.1.

Table 7.1 Target parameters for the sample SITS

Thickness	0.2 mm
Width (x)	8 mm
Length (y)	8 mm
Target separation (z)	2 mm

7.3 Sensor Characterisation

The SITS has been build to the optimum specifications, the response under loading has not been explored. Therefore an analysis was planned to characterise the sensor across a two-axis range of allied forces.

7.3.1 Experimental Configuration

To characterise and evaluate the SITS, a similar experimental configuration to Section 5.3.2 was used. Two linear micro-positioning stages were arranged to allow horizontal and vertical movement (Figure 7.1a). The horizontal stage was fitted with a 6 axis Force/Torque sensor (Nano17-E, ATI Industrial Automation, NC, USA) to monitor the applied forces. A custom LabVIEW (National Istruments, TX, USA) program was used to control the stages and to acquire data from the F/T sensor and SITS. The sensors were calibrated with a quasistatic scanning process with 1mm in the z axis, and $\pm$ 2mm in the x axis, with step sizes of 50 μm (Figure 7.1b). A Genetic Programming (GP) algorithm [142] was used to generate calibration equations from $L_{x,z}$ to $F_{x,z}$.

7.3.2 Sensor Performance Evaluation

The hysteresis and repeatability of the two-axis SITS was assessed using the same experimental configuration as the calibration (Figure7.1a). First the sensor was indented over 100 cycles in the Z axis to a displacement of 1 mm at 0.2 mm/s. The shear output was assessed by preloading the sensor to 10N and applying a 1mm shear to the copper target at 0.2 mm/s.

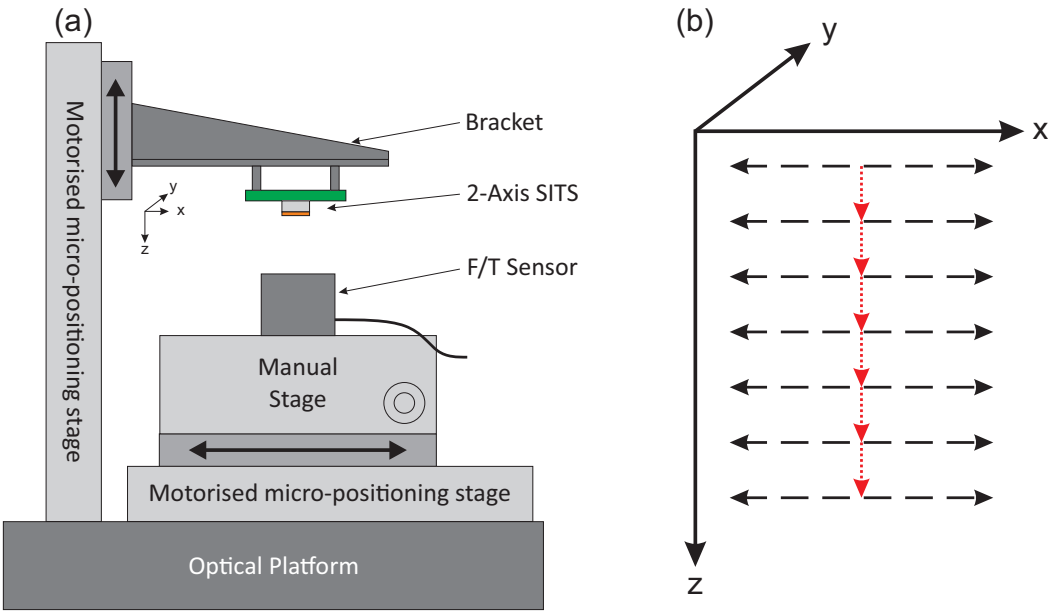

Fig. 7.1 a) The experimental test platform used to calibrate and characterise the 2-axis SITS; and (b) Scanning method of the calibration

Fig 7.2 a & b show the first five cycles for both compression and shear, indicating the sensor output closely matches that of the Nano17. The hysteresis of the sensor in both shear and compression were assessed by recording the output of the two-axis SITS over a loading and unloading cycle under the same conditions as above. The maximum hysteresis errors were 8.77 & 9.71% (0.09 & 1.55 N) of the maximum applied shear and normal force (0.03 & 16 N) (Figure 7.2 (c) & (d)).

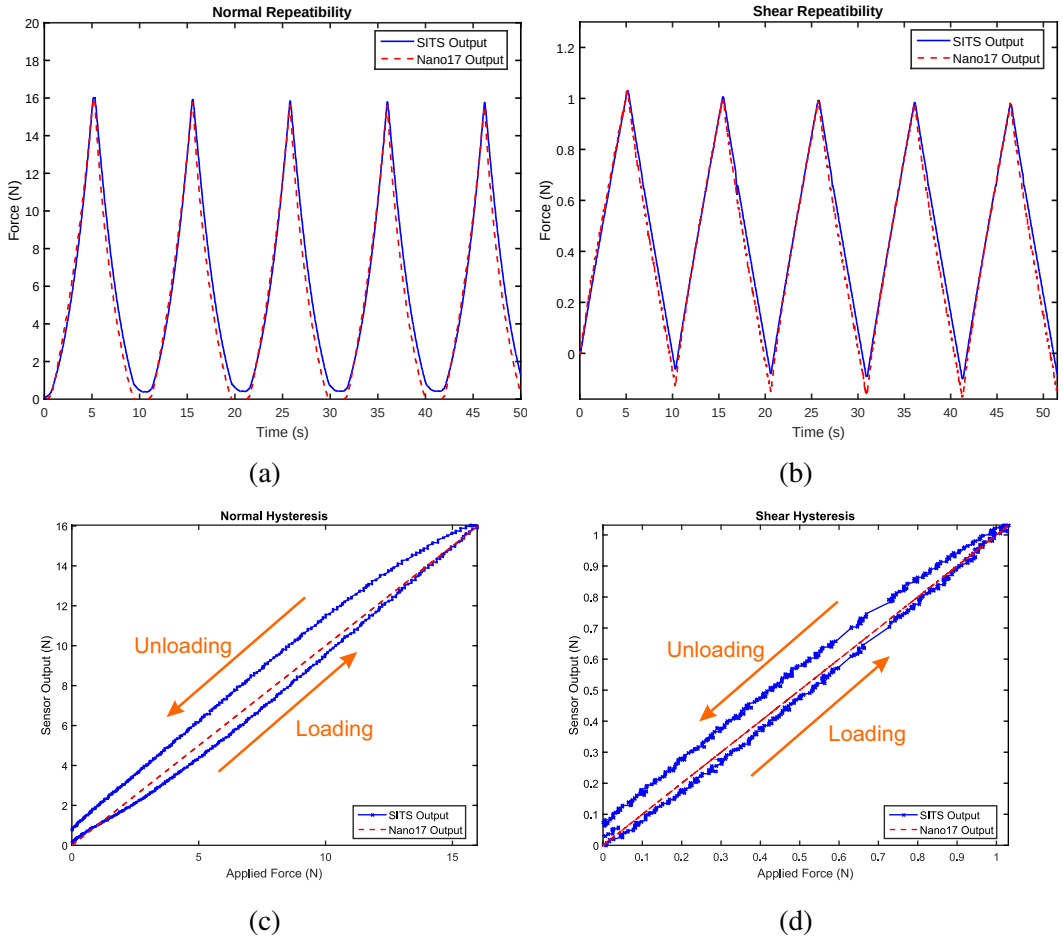

Fig. 7.2 Five cycles of the Normal (a) and Shear (b) loading repeatibility test; and Hysteresis in Normal (c) and Shear (d) axes of the sensor

7.4 Slip Evaluation

Tests were conducted to evaluate the sensitivity of the sensor for the identification and quantification of slip. The system was used to probe a tissue simulant (Adult Skin, SynDaver Labs, FL, USA [143]) placed under a slip regime. The simulant was selected as an alternative to the porcine model used in 4, owing to it's similar frictional properties [144] and the removal of specific disposal requirements for animal models.

7.4.1 Experimental Methods

The test system used in section 7.3.1 was modified to fix the hydrogel sample on the horizontal stage (Figure 7.3). Applied stress and shear speed were identified as key variables within the grasping environment (based on findings from section 4.3.2) and were accordingly varied to replicate different conditions related to surgical grasping. Compressive forces were applied by lowering the sensor to varying displacements from 0.25 to 1.00 mm. The sensor was then moved 20mm horizontally at three speeds between 2 and 6 mm/s to replicate the conditions of section 4.3.2. A total of twelve conditions (three speeds x four displacements) were repeated six times, totalling 72 tests. The displacement was controlled and forces were recorded at 100 Hz through a custom LabVIEW VI.

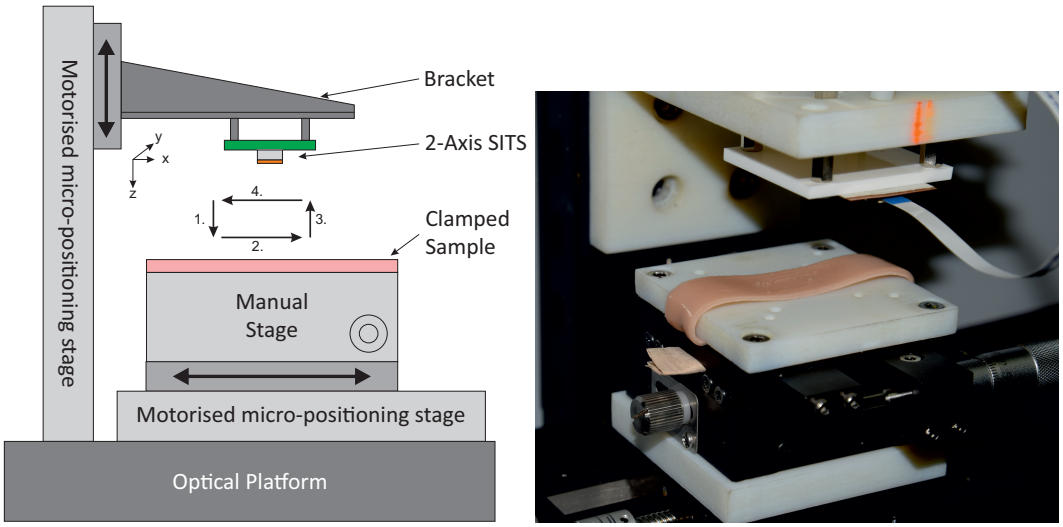

(a) (b)

Fig. 7.3 (a) Schematic of the friction testing setup, indicating the actuation cycle (1. Loading, 2. Shear, 3. Unloading, 4. Return to starting position); and (b) Photo of the clamped hydrogel sample

The output data was post processed using MATLAB (Mathworks, MA, USA) to generate the coefficient of friction (μ) at all points along each test (Figure 7.4). The point at which slip occurred was defined as the first peak, or the point at which the differential ($d\mu/dt$) first became negative, as in Chapter 4. At this point, the current frictional forces ($F_{XZ,slip}$) and coefficient of friction (μ_{slip}) were recorded. Each loading case was repeated 6 times. The

point of slip was identified on each individual response, with the six repeats for each condition then being averaged to give an overview of each metric. Results were then correlated and compared against existing data on hydrogel friction.

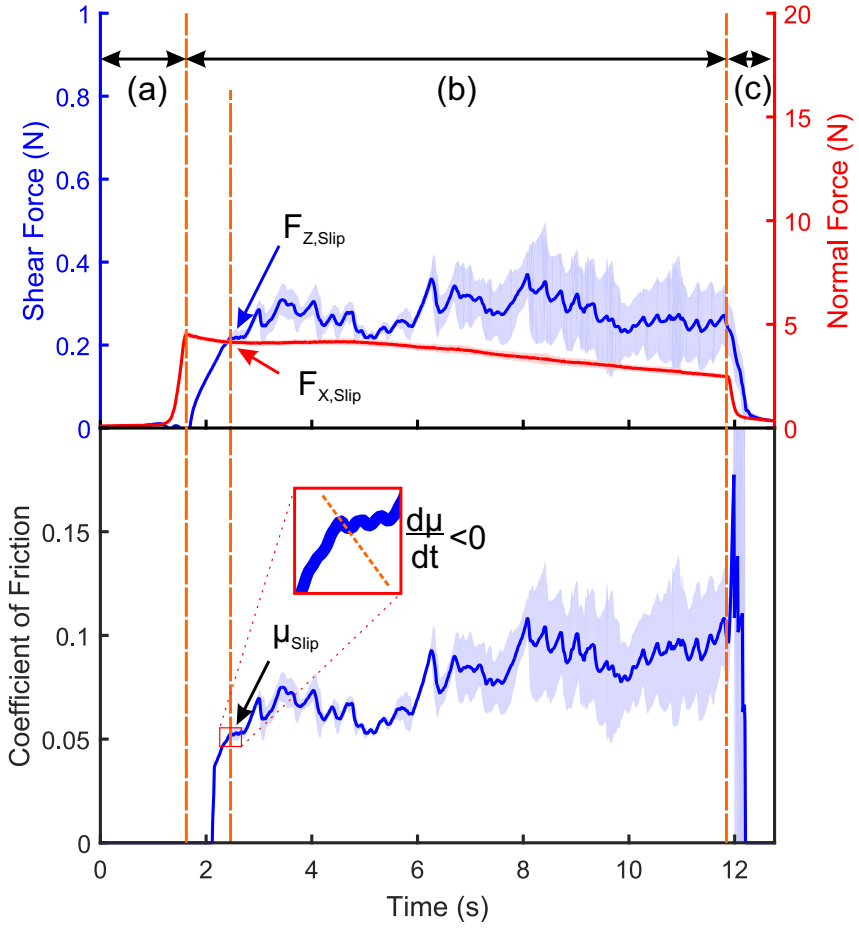

Fig. 7.4 Example plots of the force and Coefficient of Friction (Mean ± SD) (a) Loading Phase, (b) Shear Phase, (c) Unloading Phase. The slip point ($d\mu/dt < 0$), Forces at Slip ($F_{XZ,slip}$) and Friction at Slip (μ_{slip}) are indicated.

7.4.2 Results

The mean force profiles for each grasping condition are presented in Figure 7.5. It can be seen that across all conditions the normal force increases under initial loading, and then

reduces under shearing. This reduction could be explained by the varying resultant force on the target, as shear force is applied the target it deforms laterally and tilts slightly. During the unloading phase, the normal force reduces to zero faster than the shear force, indicating a slight difference in the recovery period between normal and shear.

The mean profiles of the coefficient of friction are presented in Figure 7.6. Many conditions show an initial increase to a peak before showing a trough. The unloading phase for the higher load cases shows a sharp peak in the coefficient of friction. This is an artefact of the different rates of recovery between the sensor dimensions. As the force approaches zero, the resultant CoF increases exponentially.

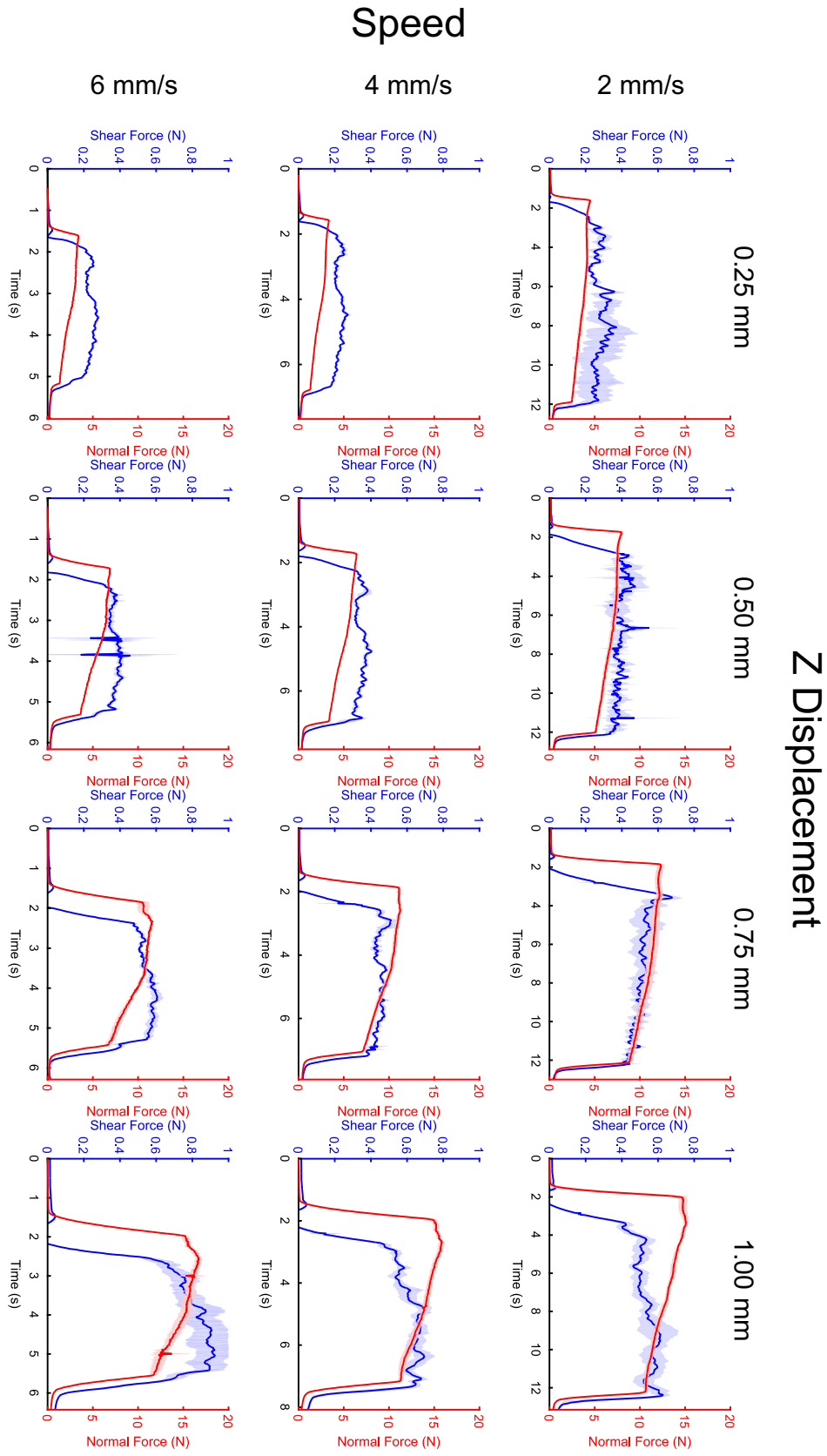

Fig. 7.5 Mean shear ($F_{X,slip}$,blue) and ($F_{Z,slip}$,red) force profile ±SD, separated by condition.

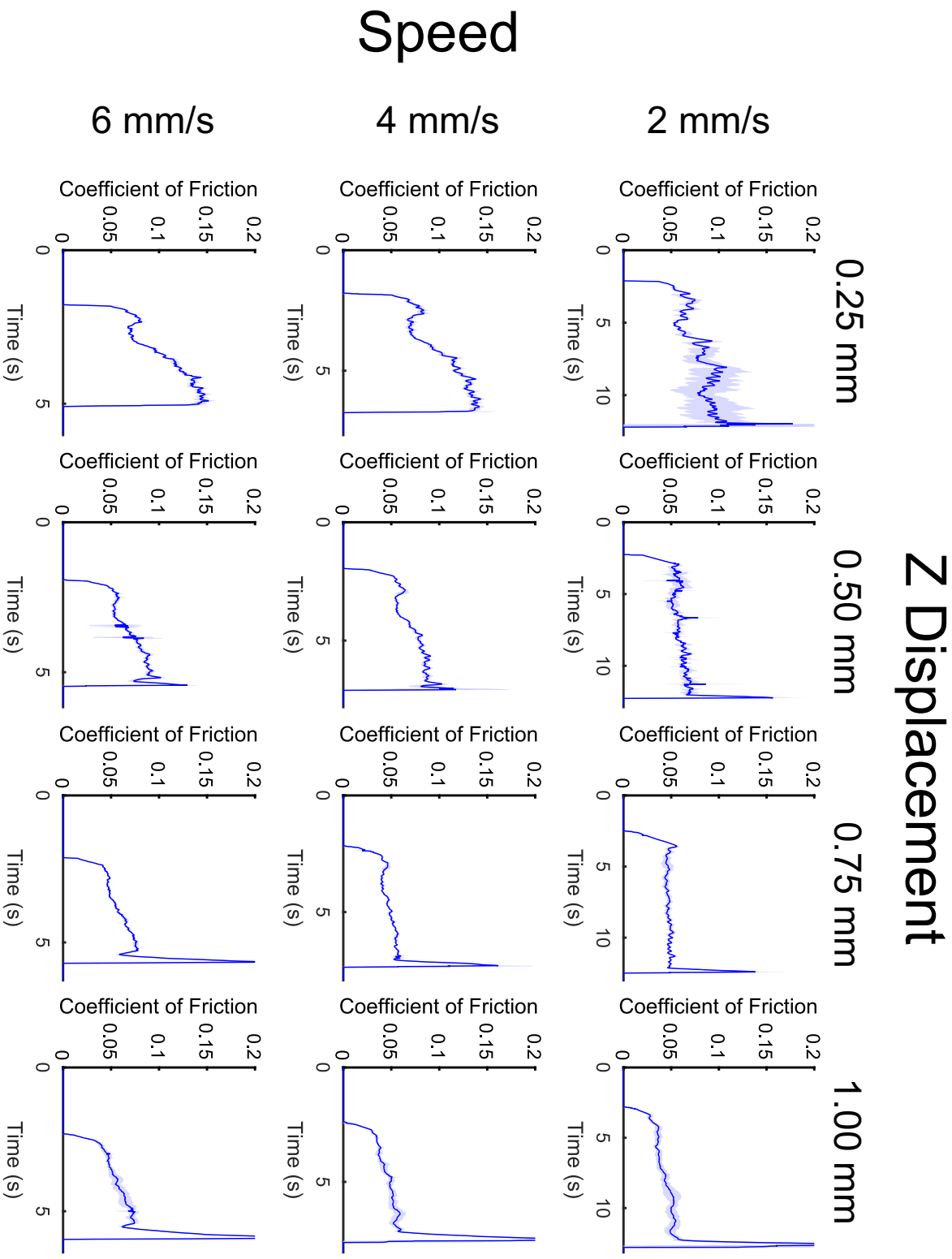

Fig. 7.6 Mean Friction Coefficient ($\mu_{X,slip}$) profile ±SD, separated by condition.

For each of the cases, the normal and shear forces ($F_{X,Z}$) and the friction coefficient (μ) were recorded at the point of slip. The consistency of the repetitions was assessed using a One Way ANOVA for each metric, all of which achieved p>0.99 indicating no significant differences between repeats.

It is evident from Figures 7.7a & b that different loading cases cause variances in both normal and shear force, increases in all cases but one. Different speed cases also vary the measured forces in both shear and normal force. In normal force (Figure 7.7b) an increase in speed causes a decrease in force for the three lower load, however at the higher loading case an increase is observed. For shear force (Figure 7.7a), the speed affected change in force varies dependant on applied load, with some cases increasing and others decreasing. Due to this variance, it is needed to assess not only the raw measured forces but the coefficient of friction calculated from them. Two way ANOVAs gave p<0.0005 in all cases, indicating significant differences in both shear and normal forces between all loading cases and speeds.

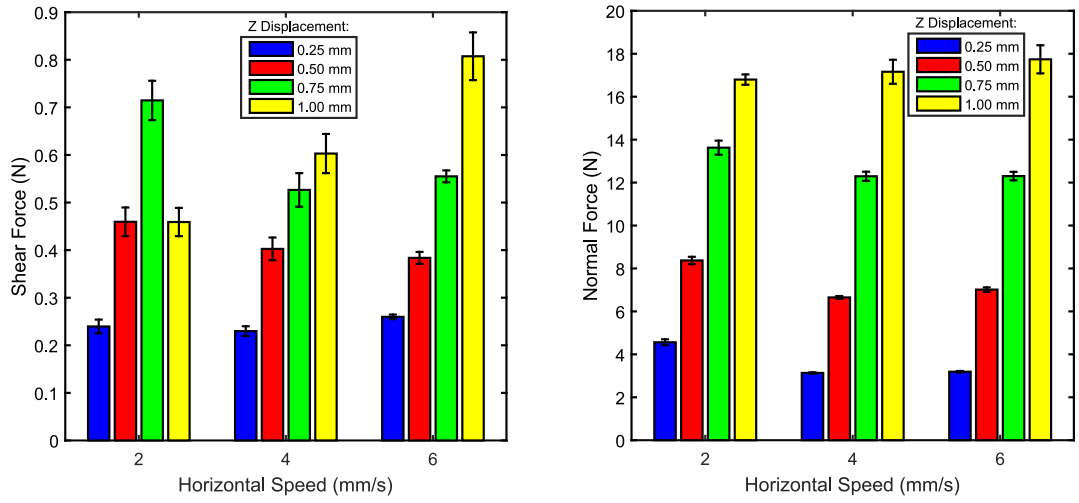

(a) (b)

Fig. 7.7 (a) Mean values of $F_{X,slip} \pm 95\%CI$; and (b) Mean values of $F_{Z,slip} \pm 95\%CI$

Figure 7.8 presents the change in coefficient of friction with varied load and speed. The mean value of μ_{slip} across all cases was 0.052 ($\pm$0.015 SD). An increase in vertical displacement and normal load causes a decrease in μ_{slip} whereas an increase in horizontal

speed causes a decrease. This is consistent with previous studies on the frictional properties of hydrogels [145, 146].

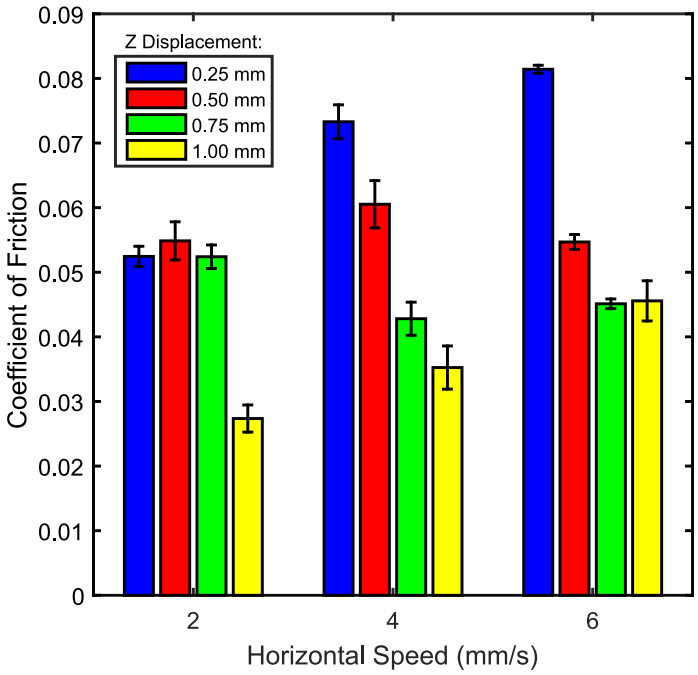

Fig. 7.8 Mean values of $\mu_{slip} \pm 95\%CI$

7.5 Grasping Sensor Prototype

For the SITS to be used within a grasper face the sensor needed first to be miniaturised to less than 5 mm width, as specified by the design requirements in Chapter 2.5.

As magnetic fields have a predictable spread around specific coil geometries [147] the sensor may be miniaturised according to the existing trends in target geometry, keeping the target geometries to the same ratio as the coil geometry. The miniaturisation of the coil will cause a significant drop in the inductance and resolution of the sensor. This presented a key design challenge based on the LDC chips used to measure the coil inductances. The

LDC1614 was limited to a maximum 10 MHz coil resonant frequency and minimum 0.25 kΩ resonant impedence, resulting in a minimum measurable inductance of around 0.2 μH.

New coils were produced to conform to the design requirements, shown in Figure 7.9a. Two-layer coils of 3.5 mm diameter were produced with 6.5 turns per layer with 100 μm trace width and spacing, totalling 13 turns. The coils were more densely packed than the previous coils used in Chapters 5 & 6 having a smaller spacing in the centre of the coil. A 4 mm square target was suspended above a 4 x 4 x 2 mm section of EcoFlex 00-30 silicone, and arranged between the coil centres. The sensor was calibrated according to the procedure in section 7.3.1 up to a maximum of 4.8 N (300 kPa) normal and 1.0 N shear.

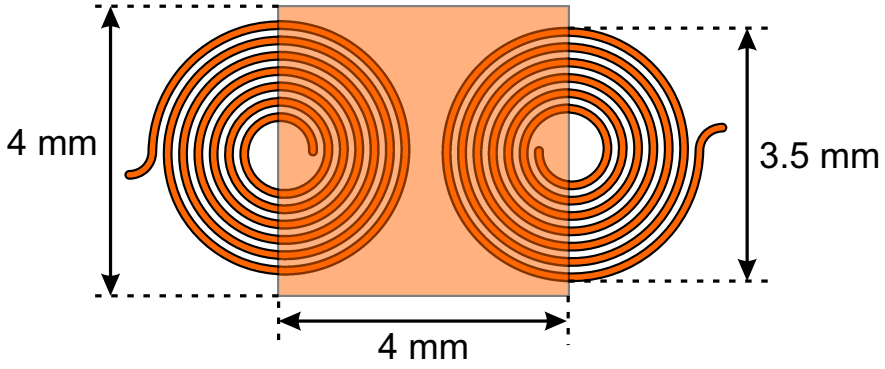

(a)

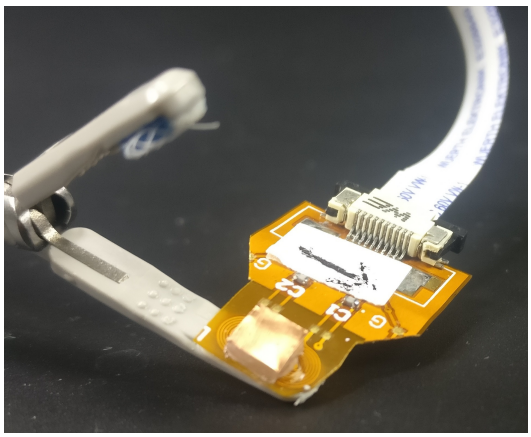

(b)

Fig. 7.9 (a) Schematic of the miniaturised coil, indicating coil and target sizes; and (b) The manufactured prototype, with the sensor mounted on a toothless 5 mm laparoscopic grasper (Epix, Applied Medical)

The sensor was affixed to the face of a pair of representative 5mm atraumatic surgical graspers (Epix, Applied Medical, CA, USA) with cyanoacrylate glue (Loctite 401, Henkel, Germany). Because of the size of the connector used to connect to the sensing electronics, a section of the FPC was left overhanging the side of the grasper. The sensor replaced one of the two silicone pads on the face of the Epix graspers, allowing the sensor to directly contact any grasped sample to directly measure the tissue tool interface.

7.5.1 Performance Evaluation

To evaluate the performance of the prototype graspers, a consultant urologist performed two grasping tasks to assess the performance in the angular face of the grasper. The tasks were performed in an EOSim portable laparoscopic training platform (eoSurgical Ltd., Edinburgh, UK) used in Chapter 3. The tissue simulant used for slip analysis (Adult Skin, SynDaver Labs, FL, USA [143]) was used to replace ex-vivo tissue for the grasping task. The setup is shown in figure 7.10.

The first task involved ten compressions on the tissue simulant. Two typical grasps are presented in Figure 7.11a. For both grasps, the normal (compressive) force rises to just over 1N, before quickly reducing after pressure is released. This equated to just over 50 kPa, reflecting the average pressure for a consultant grasp deduced in chapter 3. The main problem with the dataset is the presence of shear force on the compression test. A small amount of shear would be expected, however in this case the shear value is at the maximum range of the calibration. This may be explained by the rotation of the sensor under compression.

As the scissor action faces close around the sample, the proximal end of the target makes first contact, causing a rotation of the target to roughly 10° (Figure 7.12). Because of this effect, when fully closed the target will be rotated around 10°. Owing to the linear relationship between rotation and shear measurement error presented in section 6.3.1, the scaled displacement error was 0.5 mm. This was equal to the displacement at which 1N force was achieved in the shear axis.

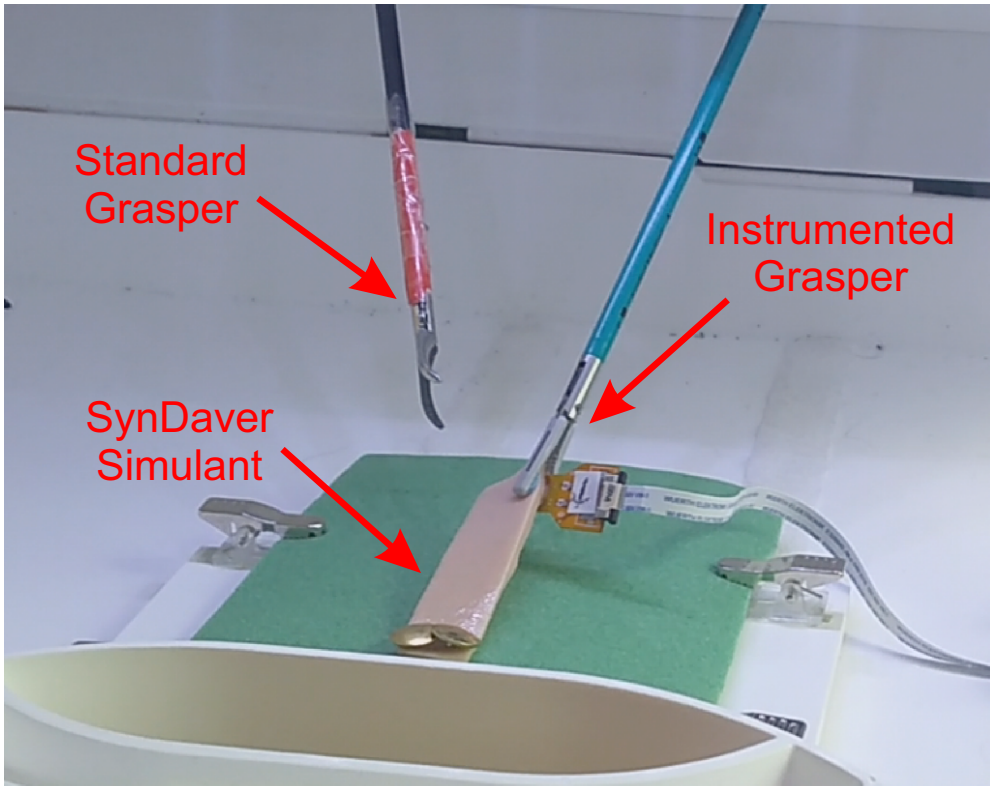

Fig. 7.10 Test equipment for the performance evaluation of the prototype sensor

After the consultant test was complete, an attempt was made to reduce the effect of rotation on the grasping sensor by reducing the thickness of the elastomer layer from 2 mm to 1 mm. The change in sensor resolution in both inductance and force was measured to quantify the effects. For both normal and shear force, inductance change was increased when the elastomer layer was reduced (Figure 7.13 a & c). For force, the normal force range was increased nearly tenfold (Figure 7.13 b) while little difference in range was observed in the shear measurement (Figure 7.13 d). This increase in resolution with a thinner elastomer layer is a result of the target being present in a sronger field close to the coils, causing a sharper change in inductance. Because of this, the thinner elastomer may be advised for future iterations of the sensor.

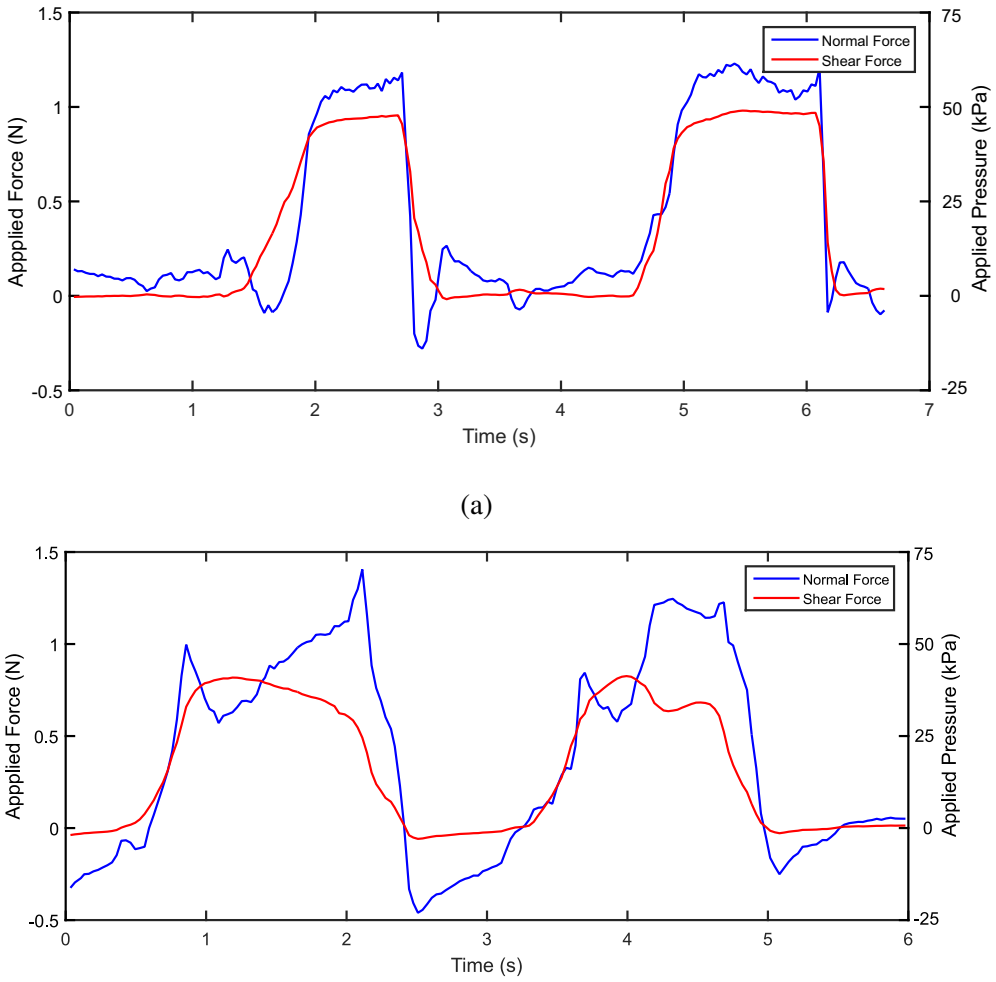

Fig. 7.11 Force data from two typical grasps from the (a) Compression and (b) Pull tests

7.6 Discussion

This chapter presents an optimised two axis SITS as a demonstrator of the technology's capabilities. The SITS was build according to the target geometries suggested by the design tool in Chapter 6, and used the same coils used in the validation of the models. The sensor was calibrated using a commercial six axis load cell and a genetic algorithm to generate calibration equations.

The hysteresis of the sensor in normal and shear response was 9.71 and 8.77%, respectively. While this initially seems large, further inspection of the response shows that the

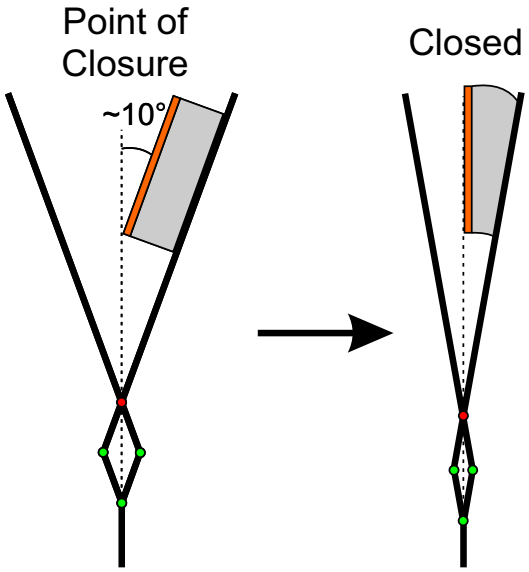

Fig. 7.12 Indicaton of the target rotation under compression in the grasper face

highest error is observed in the unloading portion of the cycle. This would be more significant in cyclic testing, however the tissue slip metric focuses on the loading curve in both dimensions. As the sensors are more accurate in this case, the hysteresis error can be seen as acceptable.

Coefficient of friction calculated from the slip testing was reported as 0.052 ± 0.015. While this is consistent with the static coefficient of friction of hydrogels [145, 146] it is much lower than that observed in Chapter 4. The surface of the SITS was a flat copper surface compared to the triangular teeth of the simulated grasping environment, explaining the variance in friction. This can be seen as a benefit however, as the sensor can detect slip in low friction environments.

While the normal forces measured by the miniaturised sensor were of the same magnitude as previous experimentation(Chapter 3) [25, 110], the shear readings were the same across both the compression and pull tasks. This indicates a significant problem with the measurement, likely caused by an un-optimal elastomer geometry. This effect could be reduced using a thinner elastomer layer, however this would cause the range and resolution of the normal reading to be reduced. To fully optimise a miniaturised sensor, further investigation

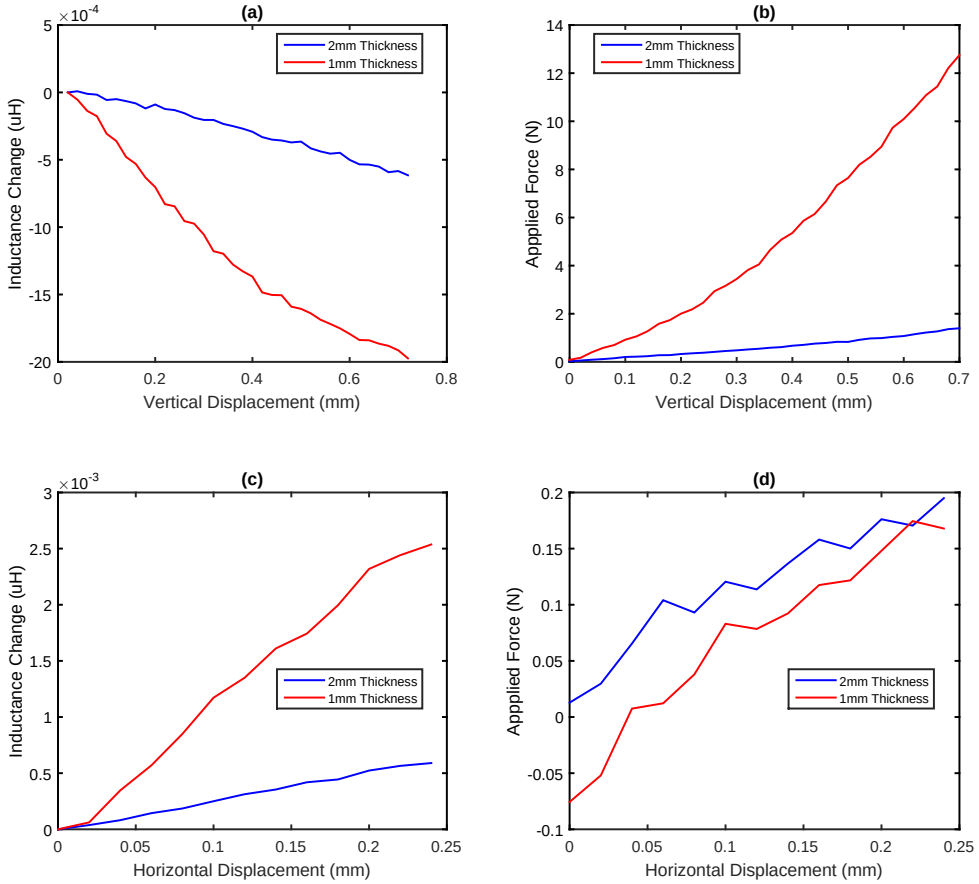

Fig. 7.13 Normal force and inductance range variations over a 0.7 mm target displacement, showing differences between the 1 and 2 mm elastomer thicknesses

is required on the elastomer layer to fully understand it's response under abnormal loading cases such as the grasper jaw.

The inductance magnitude of the miniaturised sensor was much lower than that of the initial prototype, with a coil inductance of 0.5 μH compared to 3.2 μH. This will cause a large decrease in the range and resolution of the sensor, as the raw inductance change will be lower under the same target displacement. Therefore this will need to be raised to allow sufficient resolution of the sensor. To do this the number of turns in each coil must be increased. With current techniques, this may be achieved by:

- **Increasing Winding Density**

  By reducing the wire width and spacing within the coil, the number of turns in the same area of each layer may be increased. This will boost the inductance at the cost of a more complex coil, requiring more advanced manufacturing techniques.

- **Increasing Layer Count**

  An increase in layer count will increase the total number of turns in the coil. An increase of layers from 2 to 4 will increase the overall inductance by 330% [134]. This will require a more complex manufacturing technique, and will increase the thickness of the FPC. This is acceptable, as the extra layers will add less than $200\mu m$ to the overall thickness.

Finally, the inductance ranges of the thinner miniaturised prototype seem to indicate a higher range and resolution for the observed force and inductance changes. While this shows promise the response of the sensor is not fully understood, particularly the mechanical response of the elastomer in relation to multiaxial forces. Therefore future investigation will be required to gain further insight into a truly optimised SITS.

7.7 Chapter Summary

In this Chapter an optimised two axis SITS is manufactured calibrated and characterised as a demonstrator of the technology, showing low hysteresis and high repeatability. The sensor is successfully used to measure the coefficient of friction at slip on a low friction surface, indicating it's potential in the assessment of slip in a grasper jaw. A miniaturised prototype of the sensor is produced to fit within the geometric constraints of the grasper face. The sensor performed well in the normal measurement, however shear measurements showed significant errors. A thinner version of the miniaturised sensor was tested, showing a higher resolution than the previous version. These results are very promising, indicating the potential of a miniaturised SITS for use within a surgical grasper.

Chapter 8

General Discussion and Conclusions

In this section, relevant results from all chapters will be discussed to encompass the research topic as a whole. The methods of grasping task optimisation will be discussed, as well as how the simulated investigation could benefit SITS optimisation as a whole.

8.1 Assessment of Research Objectives

Section 1.1.1 presented several objectives for the research project. This section details the manner in which the objectives have been fulfilled.

1. To identify appropriate sensing technologies which may be integrated into a surgical grasper.

Tactile sensing was identified in Chapter 2 as a key mode of sensing for the optimisation of grasping tasks. A range of relevant tactile sensors were assessed for their potential for integration, with a wide range of tranducer technologies.

2. To characterise the forces applied by surgeons to tissue through laparoscopic graspers.

Chapter 3 details the investigation into the forces applied by surgeons in a simple grasping task. Characteristics of the forces applied were realised between different skill levels of surgeon, with relevant applied forces carried through to later chapters for further analysis.

3. To select an appropriate sensing approach for the improvements of grasping tasks.

Two methods of grasping optimisation were presented in Chapter 4 two prevent errors cause by the incorrect application of force. Tissue slip prevention was identified as the superior metric as the detection of slip can be seen as independent of tissue type, as it searches for the pint where $d\mu/dt < 0$. Also, it allowed the compressive force to be reduced to it's minimum, as such the upper bound of safe grasping would not be reached, nullifying the effectiveness of the NSRc.

4. To investigate the design parameters needed to optimise the chosen sensing method for the optimisation of the grasping action.

Chapters 5 & 6 present modelling methods of the SITS intended to investigate the design parameters of the sensor. A variety of target configurations and coil parameters were assessed, and concluded in specific target-coil geometric coupling that would give the optimum sensitivity from a two axis SITS.

5. To produce and evaluate a demonstrator of the sensing technology in laboratory conditions.

Chapter 7 details the production of an optimised two axis SITS. The sensor is evaluated for it's hysteresis and repeatability, showing a good response in both manners. The SITS was then used to detect slip on a tissue simulant showing it's ability to be used in conjunction with the optimisation method presented in Chapter 4.

8.2 General Discussion

Surgical graspers have been identified as the most prevalent cause of error within MIS, having been associated with over 1/3 of all errors [114]. Of these 4/5 were attributed to incorrect force application on the grasped tissue causing either crush trauma or abrasions from slippage. This presents a clinical need for the improvement of grasp force control to improve the grasping change and Therefore they present a potential area of improvement. In particular, a lack of force sensing on the grasping surfaces has been shown to increase the chances of error, owing to the lack of kinaesthetic and tactile feedback masking the applied forces from the surgeon [25, 110, 111]. This lack of feedback is present in manual laparoscopic tools, and in completely removed in current master-slave robotic assisted systems.

To mitigate the chances of error, and so improve the action of grasping, various feedback techniques have been proposed, however the levels of efficacy are mixed [148–150]. As robotic surgery becomes used in more complex and delicate surgeries, the increase in tissue fragility will reduce the margin of error for force application [23]. As such the need for intelligent surgical tools will only increase in the coming years.

To measure the applied forces within the surgical environment many have proposed miniaturised force sensors to be integrated within the grasper face. Each of these modes, however, present limitations that offer a non-optimal response (Chapter 2.4). One mode in particular, the soft inductive tactile sensor, was identified as a sensing mode with high potential, but further understanding was required to fully understand the design requirements for surgical grasping.

Some previous studies had been performed to quantify the forces applied to objects by surgeons through graspers [49], however data on the forces applied to tissue was limited [25, 54]. The results of Chapter 3 and it's resultant paper agreed with the previous studies in the upper bound of pressures applied by surgeons, and also revealed a link between a surgeon's skill and their mean applied force in the tissue. While this chapter served as a

method of defining the bounds of compressive forces, the results may be used to inform the wider field of grasping to assist different improvements to the tools.

The primary requirement for the SITS was to provide a measurement range of up to 300kPa in normal force. An analysis of relevant literature revealed a distinct lack of data regarding the pressure applied to tissues by manual graspers, focusing mainly the application of specific pressures directly to tissues. Because of this paucity of information, many existing sensors are calibrated to either an arbitrary value of force based on the design configuration [151], or simply report an uncalibrated sensor output [10]. The pressure is seen as more significant than force in the optimisation of a grasping task [25, 27], and so it's calculation is key for a grasping force sensor. The SITS presents an immediate solution to this. As the sensor protrudes slightly from the grasper face, the contact area can be defined as the surface area of the upper face of the sensor. Other sensing methods in line with the grasping face would require further sensors to detect the area of tissue grasped to gain the ability to directly calculate pressure.

Chapter 4 indicated that to assess the tissue tool interface for grasper optimisation, a minimum of two degrees of freedom are required. This is echoed by other research across various sensing methods within the grasper face [49, 92, 117]. The current scaled SITS prototype measures in two degrees of freedom, with hysteresis errors of around 8%. While this is higher than comparable 'hard' sensing methods such as optical fibres [92, 152] and capacitive sensors [151], they hysteresis levels were consistent with other elastomer-based tactile sensors [16, 153]. Others sensing methods have been used to create 3 DoF tactile sensors to measure the lateral shear [154] of the grasper in addition to the compression and axial shear of the current prototype. While this surpasses the current capabilities of the sensor, three axis versions of the SITS have been proposed [99]. This will however require further efforts to the miniaturisation to fit within the standard 5mm grasper face.

Owing to the small size constraints of the surgical grasper face, the repeatability of manufacturing becomes a significant problem. The FPC, silicone and target were produced using precision techniques, however the final assembly of the prototype sensor was performed

manually. This caused variance in the inductances between sensors under zero load, meaning individual calibrations were required for each prototype. This is a significant disadvantage compared to piezoresistive sensors [8, 10] which show excellent repeatability between prototypes. Some potential solutions to the manufacturing precision exist, such as the use of conductive polymers as both target material and elastomer substrate. Carbon nanotube doped silicone has been proven to be an adequate replacement for metallic targets in eddy current sensors [155]. Using a single continuous layer would reduce the chances of manufacturing errors, but would increase the complexity of the coil interactions.

While increased forces had previously been liked to higher tissue trauma [25], little existed on the detection of slip through force analysis. This was central to the research to define the lower bound of forces needed to maintain an optimal grip, thereby minimising grasping forces and ensuring that they were kept far below the upper bound. Other methods of slip detection exist for tissue, however relied on different transducer mechanisms such as vibration [156] and temperature measurement [116]. These other methods are limited as there is no potential for slip detection within the sensor; it can only detect the moment that slip occurs. Using forces within the calculation, however, will allow a threshold friction to be established to be used as a preventative measure. Through analysis on tissue (Chapter 4) a method to detect the point at which tissue slips was established. While this has not been used in a grasping interface, the searching for a local maxima is used in tribology to detect the point of slip is a standard process [146, 157, 158]. The measure was successful for detecting slip both in the simulated grasping environment as well as the prototype sensor. Such a measure has the potential to be used as a closed loop control method for a robotic grasper by minimising the compressive forces to ensure a secure grip on the grasped tissue while also reducing the chance of crush damage. This would prevent the two main causes of damage caused by graspers [114] with a single implementation of sensing.

Finally, a decision must be made on the suitability of the sensor to be used within a commercial clinical environment, and the advancements required for the sensor to be fully suitable. The grasper mounted prototype has shown that the sensor in it's current state may

be deployed on an existing grasper, however the quality of the sensor response was reduced. TO rectify this, the inductance range of the smaller coils must be increased and further optimisations must be investigated based on the size and geometry of the elastomer layer. The biocompatibility of the device must also be investigated. Because of the intention for the sensor to directly contact the grasped tissues, all materials on the outer face must cause minimum immune response from the body. Copper has been shown to cause an extensive immune response from the body [159], and so the open-metal face of the sensor must be encapsulated to prevent contact. PDMS presents an ideal candidate for this encapsulation, offering a inert, biocompatible surface to contact the tissue [160] while remaining moderately flexible to allow deformation of the sensor.

The measurement signals from the SITS coupled with the slip detection method have the potential to be deployed in both manual and robotic surgical graspers in two different ways. In manual graspers, the metric may only be used to present haptic or visual feedback to the surgeon as a warning. Robotic systems present a more interesting use of the metric. While still allowing the use of feedback, a closed loop control of the grasper could be implemented to minimise the compressive force while maintaining a secure grip on the tissue.

While the current state of the sensor is not fully suitable for use in a grasper, without the restrictive size constraints it had been shown to respond precisely to applied forces. Because of this the sensor lends itself to deployment in various robotic technologies where robust multi-axis sensing is required, where less modifications must be made for the sensor to be fully functional. In particular, as the sensor has been proven for use in gripping tasks it may be directly applicable general robotic manipulation tasks. Further to this, the scalability of the sensor range based on the elastomer stiffness would allow deployment to both low and high force applications.

8.3 Future Work

This research has given an insight into the requirements and design characteristics of a multi axis tactile sensor used for surgical grasping. This section looks towards future works which may be conducted to further optimise the designs of such sensors.

8.3.1 Grasping Task Optimisation

The two presented methods of grasping optimisation showed promise, however further research is required to ensure the efficacy of both metrics.

- **Tissue Slip**

  Slip has been evaluated with the prototype sensor, however this was under specific conditions of parallel grasping faces. Under the scissor-jaw mechanism used in most graspers, thicker grasped samples would exhibit extremely different reactions forces, and the frictional interaction would be different to that of the ex vivo equipment. Further investigation using *in vivo* conditions can be performed with the sensor deployed on the face of a scissor jaw grasper to apply the forces, as this more accurately represents the surgical environment.

- **Closed Loop Control**

  The outputs of the SITS could be used as the input into a closed loop control system to be be implemented into a robotic system. This would use a combination of the two methods to both minimise grasping forces while ensuring a secure contact with the grasped samples. The control system would both reduce trauma from current robotic systems, and pave the route towards the fully autonomous grasping of tissues in surgery.

8.3.2 Simulation Advancements

While the SITS simulation performed well overall, further advancements may be made to more accurately simulate the properties of the SITS.

- **Coil Size Variation**

  In the current model, a single size of coil is investigated. This allowed the validation of the model with and existing set of coils without the need for time expensive design and manufacture of new, varied coil sizes. Future models could use variable coil sizes to assist in an optimised miniaturisation of the sensor. This could potentially offer a more optimal sensor than the existing grasper prototype, with enhanced range in the same geometric constraint.

- **Elastomer Analysis**

  Currently the simulated environment relies simply on the electromagnetic link between coils and target to optimise the design characteristics of the sensor, and so the simulation outputs only the dimensional inductances. The addition of an elastomer layer in the simulation would allow for applied forces to be simulated rather than the target displacements in the current model. This would allow a full optimisation to occur dependent on factors such as the elastomer stiffness and geometry, and to tailor the sensor to the intended application.

- **Three Axis SITS Simulation**

  The current model simulates a two coil, two axis SITS. While this particular was chosen due to geometric constraints in the grasper jaw, the modelling process may also be applied to SITS with further degrees of freedom. While some characteristics of the models may be carried across, the different target position will cause variation in the optimum parameters for the target. Further investigation will be required to fully optimise such sensors, however the current methods will undoubtedly assist in this.

- **SITS Design Tool**

  Once optimised and simulated across the proposed conditions above the simulations

may be used to create a design tool for all instances in which it may be used. The design tool would allow a user to input their sensing and geometric requirements to generate the optimal SITS design for the scenario. This would be the final step in SITS design, and would be applicable for any application of the sensor.

8.4 Concluding Remarks

While methods of optimising grasper performance exist, they do not fully represent the relationship between the grasper and tissue. The work presented in this thesis details a new approach to grasper optimisation intended to reduce multiple errors during surgery. To assist the validation of the optimisation method, analysis has been performed to define the forces applied in surgery and to assess the improvement method parametrically. Current methods of intraoperative force sensing are insufficient for this approach, therefore a new mode of sensing is applied to the face of a laparoscopic grasper. To remedy this paucity, a soft tactile sensor has been optimised for usage in the grasper jaw, and has been validated to be sufficient for the task of grasping improvement.

Whilst the main theme presented in this thesis has focused on the optimisation of MIS grasper usage, the research within is relevant to multiple fields. The notion of slip detection in soft objects is applicable not only in the surgical field, but may be applied across the whole research area of robotic manipulation. Similarly, the optimisation of the SITS geometries further explores a new sensing technology, which may be applied to a variety of applications in which multi axis force sensing is a requirement.

References

[1] J. Gafford, Y. Ding, A. Harris, T. McKenna, P. Polygerinos, D. Holland, A. Moser, and C. Walsh, "Shape deposition manufacturing of a soft, atraumatic, deployable surgical grasper," *Journal of Medical Devices*, vol. 8, no. 3, p. 030927, 2014.

[2] V. Ottani, M. Raspanti, and A. Ruggeri, "Collagen structure and functional implications," *Micron*, vol. 32, no. 3, pp. 251–260, 2001.

[3] M. Frisen, M. Mägi, L. Sonnerup, and A. Viidik, "Rheological analysis of soft collagenous tissue: Part i: Theoretical considerations," *Journal of Biomechanics*, vol. 2, no. 1, pp. 13–20, 1969.

[4] H. Visser, E. Heijnsdijk, J. Herder, and P. Pistecky, "Forces and displacements in colon surgery," *Surgical Endoscopy And Other Interventional Techniques*, vol. 16, no. 10, pp. 14 263–1430, 2002.

[5] D. Purves, G. Augustine, and D. Fitzpatrick, "Mechanoreceptors specialized to receive tactile information," *Neuroscience,*, 2001.

[6] U. Seibold, B. Kubler, and G. Hirzinger, "Prototype of instrument for minimally invasive surgery with 6-axis force sensing capability," in *Robotics and Automation, 2005. ICRA 2005. Proceedings of the 2005 IEEE International Conference on*. IEEE, 2005, pp. 496–501.

[7] Y. Sun, Y. Liu, T. Zou, M. Jin, and H. Liu, "Design and optimization of a novel six-axis force/torque sensor for space robot," *Measurement*, vol. 65, pp. 135–148, 2015.

[8] H. Takahashi, A. Nakai, N. Thanh-Vinh, K. Matsumoto, and I. Shimoyama, "A triaxial tactile sensor without crosstalk using pairs of piezoresistive beams with sidewall doping," *Sensors and Actuators A: Physical*, vol. 199, pp. 43–48, 2013.

[9] M. Hori, A. Nakai, and I. Shimoyama, "Three-axis ground reaction force distribution during straight walking," *Sensors*, vol. 17, no. 10, p. 2431, 2017.

[10] L. Li, B. Yu, C. Yang, P. Vagdargi, R. A. Srivatsan, and H. Choset, "Development of an inexpensive tri-axial force sensor for minimally invasive surgery," in *Intelligent Robots and Systems (IROS), 2017 IEEE/RSJ International Conference on*. IEEE, 2017, pp. 906–913.

[11] M. Cheng, X. Huang, C. Ma, and Y. Yang, "A flexible capacitive tactile sensing array with floating electrodes," *Journal of Micromechanics and Microengineering*, vol. 19, no. 11, p. 115001, 2009.

[12] H.-K. Lee, J. Chung, S.-I. Chang, and E. Yoon, "Normal and shear force measurement using a flexible polymer tactile sensor with embedded multiple capacitors," *Journal of Microelectromechanical Systems*, vol. 17, no. 4, pp. 934–942, 2008.

[13] B. Ward-Cherrier, N. Pestell, L. Cramphorn, B. Winstone, M. E. Giannaccini, J. Rossiter, and N. F. Lepora, "The tactip family: Soft optical tactile sensors with 3d-printed biomimetic morphologies," *Soft robotics*, vol. 5, no. 2, pp. 216–227, 2018.

[14] W. Yuan, S. Dong, and E. H. Adelson, "Gelsight: High-resolution robot tactile sensors for estimating geometry and force," *Sensors*, vol. 17, no. 12, p. 2762, 2017.

[15] J.-M. Kim, C.-M. Kim, S.-Y. Choi, and B. Y. Lee, "Enhanced strain measurement range of an fbg sensor embedded in seven-wire steel strands," *Sensors*, vol. 17, no. 7, p. 1654, 2017.

[16] H. Wang, G. de Boer, J. Kow, A. Alazmani, M. Ghajari, R. Hewson, and P. Culmer, "Design methodology for magnetic field-based soft tri-axis tactile sensors," *Sensors*, vol. 16, no. 9, p. 1356, 2016.

[17] A. G. Harrell and B. T. Heniford, "Minimally invasive abdominal surgery: lux et veritas past, present, and future," *The American journal of surgery*, vol. 190, no. 2, pp. 239–243, 2005.

[18] T. W. Kong, K. M. Lee, J. Y. Cheong, W. Y. Kim, S.-J. Chang, S.-C. Yoo, J.-H. Yoon, K.-H. Chang, and H.-S. Ryu, "Comparison of laparoscopic versus conventional open surgical staging procedure for endometrial cancer," *Journal of gynecologic oncology*, vol. 21, no. 2, pp. 106–111, 2010.

[19] B. Jacobson and A. Murray, *Medical devices: use and safety*. Elsevier Health Sciences, 2007.

[20] M. V. Ottermo, M. Øvstedal, T. Langø, Ø. Stavdahl, Y. Yavuz, T. A. Johansen, and R. Mårvik, "The role of tactile feedback in laparoscopic surgery," *Surgical Laparoscopy Endoscopy & Percutaneous Techniques*, vol. 16, no. 6, pp. 390–400, 2006.

[21] O. A. Van der Meijden and M. P. Schijven, "The value of haptic feedback in conventional and robot-assisted minimal invasive surgery and virtual reality training: a current review," *Surgical endoscopy*, vol. 23, no. 6, pp. 1180–1190, 2009.

[22] E. Yiannakopoulou, N. Nikiteas, D. Perrea, and C. Tsigris, "Virtual reality simulators and training in laparoscopic surgery," *International Journal of Surgery*, vol. 13, pp. 60–4, Jan 2015.

[23] M. Diana and J. Marescaux, "Robotic surgery," *British Journal of Surgery*, vol. 102, no. 2, pp. e15–e28, 2015.

[24] E. P. Westebring-van der Putten, J. J. van den Dobbelsteen, R. H. Goossens, J. J. Jakimowicz, and J. Dankelman, "Force feedback requirements for efficient laparoscopic grasp control," *Ergonomics*, vol. 52, no. 9, pp. 1055–1066, 2009.

[25] R. J. De S., A. Dagan, B. Hannaford, P. Swanson, and M. Sinanan, "Assessment of tissue damage due to mechanical stresses," *The International Journal of Robotics Research*, vol. 26, no. 11-12, pp. 1159–1171, 2007.

[26] J. Bos, E. W. Doornebosch, J. G. Engbers, O. Nyhuis, and D. Dodou, "Methods for reducing peak pressure in laparoscopic grasping," *Proceedings of the Institution of Mechanical Engineers, Part H: Journal of Engineering in Medicine*, vol. 227, no. 12, pp. 1292–1300, 2013.

[27] A. Shakeshaft, J. Cartmill, W. Walsh, and C. Martin, "A curved edge moderates high pressure generated by a laparoscopic grasper," *Surgical endoscopy*, vol. 15, no. 10, pp. 1232–1234, 2001.

[28] Y.-c. Fung, *Biomechanics: mechanical properties of living tissues*. Springer Science & Business Media, 2013.

[29] T. Ushiki, "Collagen fibers, reticular fibers and elastic fibers. a comprehensive understanding from a morphological viewpoint," *Archives of histology and cytology*, vol. 65, no. 2, pp. 109–126, 2002.

[30] S. R. Lammers, P. H. Kao, H. J. Qi, K. Hunter, C. Lanning, J. Albietz, S. Hofmeister, R. Mecham, K. R. Stenmark, and R. Shandas, "Changes in the structure-function relationship of elastin and its impact on the proximal pulmonary arterial mechanics of hypertensive calves," *American Journal of Physiology-Heart and Circulatory Physiology*, vol. 295, no. 4, pp. H1451–H1459, 2008.

[31] D. Miklavcic, N. Pavselj, and F. X. Hart, "Electric properties of tissues," 2006.

[32] R. Pethig and D. B. Kell, "The passive electrical properties of biological systems: their significance in physiology, biophysics and biotechnology," *Physics in Medicine & Biology*, vol. 32, no. 8, p. 933, 1987.

[33] M. Noshiro, T. Morimoto, H. Nagao, and H. Matsuda, "Electrical impedance in the lower limbs of patients with duchenne muscular dystrophy: a preliminary study," *Medical and Biological Engineering and Computing*, vol. 31, no. 2, pp. 97–102, 1993.

[34] J.-H. Chen and S. Adelman, "Macroscopic model for solvated ion dynamics," *The Journal of Chemical Physics*, vol. 72, no. 4, pp. 2819–2831, 1980.

[35] L. Campana, M. Cesari, F. Dughiero, M. Forzan, M. Rastrelli, C. R. Rossi, E. Sieni, and A. L. Tosi, "Electrical resistance of human soft tissue sarcomas: an ex vivo study on surgical specimens," *Medical & Biological Engineering & Computing*, vol. 54, no. 5, pp. 773–787, 2016.

[36] R. Baghbani, M. H. Moradi, and M. B. Shadmehr, "Identifying and localizing of the in-depth pulmonary nodules using electrical bio-impedance," *Journal of Investigative Surgery*, pp. 1–10, 2017.

[37] P. J. Peyton and S. W. Chong, "Minimally invasive measurement of cardiac output during surgery and critical carea meta-analysis of accuracy and precision," *Anesthesiology: The Journal of the American Society of Anesthesiologists*, vol. 113, no. 5, pp. 1220–1235, 2010.

[38] J. Wang, *Analytical electrochemistry*. John Wiley & Sons, 2006.

[39] A. Golberg, H. D. Rabinowitch, and B. Rubinsky, "Galvanic apparent internal impedance: an intrinsic tissue property," *Biochemical and biophysical research communications*, vol. 389, no. 1, pp. 168–171, 2009.

[40] J. Chandler, A. Hood, P. Culmer, D. Jayne, and A. Neville, "Technological assessment of the biogalvanic method for tissue characterization," *Physiological measurement*, vol. 35, no. 2, p. 297, 2014.

[41] J. Wang, "Electrochemical glucose biosensors," *Chemical reviews*, vol. 108, no. 2, pp. 814–825, 2008.

[42] F. Wu, P. Yu, and L. Mao, "Bioelectrochemistry for in vivo analysis: Interface engineering toward implantable electrochemical biosensors," *Current Opinion in Electrochemistry*, 2017.

[43] G. A. Holzapfel and R. W. Ogden, *Biomechanics of soft tissue in cardiovascular systems*. Springer, 2014, vol. 441.

[44] G. J. Tortora and M. T. Nielsen, *Principles of human anatomy*. J. Wiley, 2009.

[45] G. Konig, T. N. McAllister, N. Dusserre, S. A. Garrido, C. Iyican, A. Marini, A. Fiorillo, H. Avila, W. Wystrychowski, K. Zagalski *et al.*, "Mechanical properties of completely autologous human tissue engineered blood vessels compared to human saphenous vein and mammary artery," *Biomaterials*, vol. 30, no. 8, pp. 1542–1550, 2009.

[46] R. Minns, P. Soden, and D. Jackson, "The role of the fibrous components and ground substance in the mechanical properties of biological tissues: a preliminary investigation," *Journal of biomechanics*, vol. 6, no. 2, pp. 153–165, 1973.

[47] J. Palacio-Torralba, S. Hammer, D. W. Good, S. A. McNeill, G. D. Stewart, R. L. Reuben, and Y. Chen, "Quantitative diagnostics of soft tissue through viscoelastic characterization using time-based instrumented palpation," *journal of the mechanical behavior of biomedical materials*, vol. 41, pp. 149–160, 2015.

[48] B. Tang, G. Hanna, P. Joice, and A. Cuschieri, "Identification and categorization of technical errors by observational clinical human reliability assessment (ochra) during laparoscopic cholecystectomy," *Archives of surgery*, vol. 139, no. 11, pp. 1215–1220, 2004.

[49] E. Heijnsdijk, H. De Visser, J. Dankelman, and D. Gouma, "Slip and damage properties of jaws of laparoscopic graspers," *Surgical Endoscopy and Other Interventional Techniques*, vol. 18, no. 6, pp. 974–979, 2004.

[50] B. Demi, T. Ortmaier, and U. Seibold, "The touch and feel in minimally invasive surgery," in *Haptic Audio Visual Environments and their Applications, 2005. IEEE International Workshop on*. IEEE, 2005, pp. 6–pp.

[51] P. Puangmali, K. Althoefer, L. D. Seneviratne, D. Murphy, and P. Dasgupta, "State-of-the-art in force and tactile sensing for minimally invasive surgery," *IEEE Sensors Journal*, vol. 8, no. 4, pp. 371–381, 2008.

[52] H. Xin, J. Zelek, and H. Carnahan, "Laparoscopic surgery, perceptual limitations and force: A review," in *First Canadian student conference on biomedical computing*, vol. 144, 2006.

[53] L. Russell, "The design and development of an intelligent atraumatic laparoscopic grasper," Ph.D. dissertation, University of Leeds, 2015.

[54] J. Barrie, D. G. Jayne, A. Neville, L. Hunter, A. J. Hood, and P. R. Culmer, "Real-time measurement of the tool-tissue interaction in minimally invasive abdominal surgery: the first step to developing the next generation of smart laparoscopic instruments," *Surgical innovation*, vol. 23, no. 5, pp. 463–468, 2016.

[55] C. Richards, J. Rosen, B. Hannaford, C. Pellegrini, and M. Sinanan, "Skills evaluation in minimally invasive surgery using force/torque signatures," *Surgical endoscopy*, vol. 14, no. 9, pp. 791–798, 2000.

[56] G. Tholey, A. Pillarisetti, W. Green, and J. P. Desai, "Design, development, and testing of an automated laparoscopic grasper with 3-d force measurement capability," in *Medical Simulation*. Springer, 2004, pp. 38–48.

[57] P. Dubois, Q. Thommen, and A.-C. Jambon, "In vivo measurement of surgical gestures," *IEEE Transactions on Biomedical Engineering*, vol. 49, no. 1, pp. 49–54, 2002.

[58] M. Felinski, A. Purtell, E. B. Wilson, and S. K. Shah, "Robotic conversion and revisional surgery," in *The SAGES Manual of Bariatric Surgery*. Springer, 2018, pp. 535–545.

[59] J. Rosen, J. D. Brown, L. Chang, M. N. Sinanan, and B. Hannaford, "Generalized approach for modeling minimally invasive surgery as a stochastic process using a discrete markov model," *IEEE Transactions on Biomedical engineering*, vol. 53, no. 3, pp. 399–413, 2006.

[60] J. Brown, J. Rosen, L. Chang, M. Sinanan, and B. Hannaford, "Quantifying surgeon grasping mechanics in laparoscopy using the blue dragon system," *Medicine Meets Virtual Reality 12: Building a Better You: the Next Tools for Medical Education, Diagnosis, and Care*, vol. 98, p. 34, 2004.

[61] B. Ahn, Y. Kim, C. K. Oh, and J. Kim, "Robotic palpation and mechanical property characterization for abnormal tissue localization," *Medical & biological engineering & computing*, vol. 50, no. 9, pp. 961–971, 2012.

[62] R. S. Johansson and J. R. Flanagan, "Coding and use of tactile signals from the fingertips in object manipulation tasks," *Nature Reviews Neuroscience*, vol. 10, no. 5, p. 345, 2009.

[63] A. Vallbo, R. S. Johansson *et al.*, "Properties of cutaneous mechanoreceptors in the human hand related to touch sensation," *Hum Neurobiol*, vol. 3, no. 1, pp. 3–14, 1984.

[64] J. Rosen, M. MacFarlane, C. Richards, B. Hannaford, M. Sinanan *et al.*, "Surgeon-tool force/torque signatures-evaluation of surgical skills in minimally invasive surgery," *Studies in health technology and informatics*, pp. 290–296, 1999.

[65] B. Kübler, U. Seibold, and G. Hirzinger, "Development of actuated and sensor integrated forceps for minimally invasive robotic surger," *The International Journal of Medical Robotics and Computer Assisted Surgery*, vol. 1, no. 3, pp. 96–107, 2005.

[66] A. L. Trejos, A. Escoto, D. Hughes, M. D. Naish, and R. V. Patel, "A sterilizable force-sensing instrument for laparoscopic surgery," in *Biomedical Robotics and Biomechatronics (2014 5th IEEE RAS & EMBS International Conference on*. IEEE, 2014, pp. 157–162.

[67] M. Lazeroms, G. Villavicencio, W. Jongkind, and G. Honderd, "Optical fibre force sensor for minimal-invasive-surgery grasping instruments," in *Engineering in Medicine and Biology Society, 1996. Bridging Disciplines for Biomedicine. Proceedings of the 18th Annual International Conference of the IEEE*, vol. 1. IEEE, 1996, pp. 234–235.

[68] T. Okatani, H. Takahashi, K. Noda, T. Takahata, K. Matsumoto, and I. Shimoyama, "A tactile sensor using piezoresistive beams for detection of the coefficient of static friction," *Sensors*, vol. 16, no. 5, p. 718, 2016.

[69] J. C. Doll and B. L. Pruitt, "High-bandwidth piezoresistive force probes with integrated thermal actuation," *Journal of Micromechanics and Microengineering*, vol. 22, no. 9, p. 095012, 2012.

[70] M. Nie and Y. Gao, "The analytical calibration model of temperature effects on a silicon piezoresistive pressure sensor," *AIP Advances*, vol. 7, no. 3, p. 035120, 2017.

[71] V. Mitrakos, P. J. Hands, G. Cummins, L. Macintyre, F. C. Denison, D. Flynn, and M. P. Desmulliez, "Nanocomposite-based microstructured piezoresistive pressure sensors for low-pressure measurement range," *Micromachines*, vol. 9, no. 2, p. 43, 2018.

[72] H. Wang, D. Zhou, and J. Cao, "Development of a skin-like tactile sensor array for curved surface," *Sensors*, vol. 8427, no. 201, p. 1, 2014.

[73] X. Niu, S. Peng, L. Liu, W. Wen, and P. Sheng, "Characterizing and patterning of pdms-based conducting composites," *Advanced Materials*, vol. 19, no. 18, pp. 2682–2686, 2007.

[74] S.-H. Bae, Y. Lee, B. K. Sharma, H.-J. Lee, J.-H. Kim, and J.-H. Ahn, "Graphene-based transparent strain sensor," *Carbon*, vol. 51, pp. 236–242, 2013.

[75] W. J. Peine, J. S. Son, and R. D. Howe, "A palpation system for artery localization in laparoscopic surgery," in *First International Symposium on Medical Robotics and Computer-Assisted Surgery, Pittsburgh*, 1994, pp. 22–24.

[76] L. Zou, C. Ge, Z. J. Wang, E. Cretu, and X. Li, "Novel tactile sensor technology and smart tactile sensing systems: A review," *Sensors*, vol. 17, no. 11, p. 2653, 2017.

[77] S.-J. Woo, J.-H. Kong, D.-G. Kim, and J.-M. Kim, "A thin all-elastomeric capacitive pressure sensor array based on micro-contact printed elastic conductors," *Journal of Materials Chemistry C*, vol. 2, no. 22, pp. 4415–4422, 2014.

[78] Z. Ji, H. Zhu, H. Liu, N. Liu, T. Chen, Z. Yang, and L. Sun, "The design and characterization of a flexible tactile sensing array for robot skin," *Sensors*, vol. 16, no. 12, p. 2001, 2016.

[79] C. A. Jara, J. Pomares, F. A. Candelas, and F. Torres, "Control framework for dexterous manipulation using dynamic visual servoing and tactile sensors' feedback," *Sensors*, vol. 14, no. 1, pp. 1787–1804, 2014.

[80] B. Heyneman and M. R. Cutkosky, "Biologically inspired tactile classification of object-hand and object-world interactions," in *Robotics and Biomimetics (ROBIO), 2012 IEEE International Conference on*. IEEE, 2012, pp. 167–173.

[81] O. H. Paydar, C. R. Wottawa, R. E. Fan, E. P. Dutson, W. S. Grundfest, M. O. Culjat, and R. N. Candler, "Fabrication of a thin-film capacitive force sensor array for tactile feedback in robotic surgery," in *Engineering in Medicine and Biology Society (EMBC), 2012 Annual International Conference of the IEEE*. IEEE, 2012, pp. 2355–2358.

[82] Y. Wang, G. Liang, D. Mei, L. Zhu, and Z. Chen, "A flexible capacitive tactile sensor array with high scanning speed for distributed contact force measurements," in *Micro Electro Mechanical Systems (MEMS), 2016 IEEE 29th International Conference on*. IEEE, 2016, pp. 854–857.

[83] S. Asano, M. Muroyama, T. Nakayama, Y. Hata, Y. Nonomura, and S. Tanaka, "3-axis fully-integrated capacitive tactile sensor with flip-bonded cmos on ltcc interposer," *Sensors*, vol. 17, no. 11, p. 2451, 2017.

[84] B. Ward-Cherrier, N. Rojas, and N. F. Lepora, "Model-free precise in-hand manipulation with a 3d-printed tactile gripper," *IEEE Robotics and Automation Letters*, vol. 2, no. 4, pp. 2056–2063, 2017.

[85] G. Meltz, W. Morey, and W. Glenn, "Formation of bragg gratings in optical fibers by a transverse holographic method," *Optics letters*, vol. 14, no. 15, pp. 823–825, 1989.

[86] A. D. Kersey, M. A. Davis, H. J. Patrick, M. LeBlanc, K. Koo, C. Askins, M. Putnam, and E. J. Friebele, "Fiber grating sensors," *Journal of lightwave technology*, vol. 15, no. 8, pp. 1442–1463, 1997.

[87] F. Taffoni, D. Formica, P. Saccomandi, G. D. Pino, and E. Schena, "Optical fiber-based mr-compatible sensors for medical applications: An overview," *Sensors*, vol. 13, no. 10, pp. 14 105–14 120, 2013.

[88] X. He, J. Handa, P. Gehlbach, R. Taylor, and I. Iordachita, "A submillimetric 3-dof force sensing instrument with integrated fiber bragg grating for retinal microsurgery," *IEEE Transactions on Biomedical Engineering*, vol. 61, no. 2, pp. 522–534, 2014.

[89] B. Dong, D.-P. Zhou, L. Wei, W.-K. Liu, and J. W. Lit, "Temperature-and phase-independent lateral force sensor based on a core-offset multi-mode fiber interferometer," *Optics express*, vol. 16, no. 23, pp. 19 291–19 296, 2008.

[90] P. Kisała and S. Cięszczyk, "Method of simultaneous measurement of two direction force and temperature using fbg sensor head," *Applied Optics*, vol. 54, no. 10, pp. 2677–2687, 2015.

[91] D. Callaghan, M. McGrath, and E. Coyle, "A force measurement evaluation tool for telerobotic cutting applications: development of an effective characterization platform," 2008.

[92] P. S. Zarrin, A. Escoto, R. Xu, R. V. Patel, M. D. Naish, and A. L. Trejos, "Development of a 2-dof sensorized surgical grasper for grasping and axial force measurements," *IEEE Sensors Journal*, vol. 18, no. 7, pp. 2816–2826, 2018.

[93] J. Singh, J. Potgieter, and W. Xu, "Fibre optic force sensor for flexible bevel tip needles in minimally invasive surgeries," *International Journal of Biomechatronics and Biomedical Robotics*, vol. 2, no. 2-4, pp. 135–140, 2013.

[94] E. A. Mendoza, C. Kempen, A. Panahi, and C. Lopatin, "Miniature fiber bragg grating sensor interrogator (fbg-transceiver) system for use in aerospace and automotive health monitoring systems," in *Photonics in the Transportation Industry: Auto to Aerospace*, vol. 6758. International Society for Optics and Photonics, 2007, p. 67580B.

[95] G. d. Boer, N. Raske, H. Wang, J. Kow, A. Alazmani, M. Ghajari, P. Culmer, and R. Hewson, "Design optimisation of a magnetic field based soft tactile sensor," *Sensors*, vol. 17, no. 11, p. 2539, 2017.

[96] N. Lazarus and S. S. Bedair, "Bubble inductors: Pneumatic tuning of a stretchable inductor," *AIP Advances*, vol. 8, no. 5, p. 056601, 2018.

[97] N. Lazarus, C. Meyer, S. Bedair, H. Nochetto, and I. Kierzewski, "Multilayer liquid metal stretchable inductors," *Smart Materials and Structures*, vol. 23, no. 8, p. 085036, 2014.

[98] T. Kawasetsu, T. Horii, H. Ishihara, and M. Asada, "Size dependency in sensor response of a flexible tactile sensor based on inductance measurement," in *2017 IEEE SENSORS*. IEEE, 2017, pp. 1–3.

[99] H. Wang, J. W. Kow, G. Boer, D. Jones, A. Alazmani, and P. Culmer, "A low-cost, high-performance, soft tri-axis tactile sensor based on eddy-current effect," in *IEEE Sensors*, 2017.

[100] H. Wang, J. W. Kow, N. Raske, G. de Boer, M. Ghajari, R. Hewson, A. Alazmani, and P. Culmer, "Robust and high-performance soft inductive tactile sensors based on the eddy-current effect," *Sensors and Actuators A: Physical*, 2017.

[101] S.-K. Yeh, H.-C. Chang, and W. Fang, "A novel polymer filled cmos-mems inductive-type tactile sensor with wireless sensing capability," in *Solid-State Sensors, Actuators and Microsystems (TRANSDUCERS), 2017 19th International Conference on*. IEEE, 2017, pp. 834–837.

[102] L. Du, X. Zhu, and J. Zhe, "An inductive sensor for real time measurement of plantar normal and shear forces distribution," *IEEE Transactions on Biomedical Engineering*, no. 99, 2014.

[103] R. Giesberts, V. Sluiter, and G. Verkerke, "Design and test of a new inductive force sensor," *Sensors*, vol. 18, no. 7, p. 2079, 2018.

[104] A. W. Brown, S. I. Brown, D. Mclean, Z. Wang, and A. Cuschieri, "Impact of fenestrations and surface profiling on the holding of tissue by parallel occlusion laparoscopic graspers," *Surgical endoscopy*, vol. 28, no. 4, pp. 1277–1283, 2014.

[105] R. H. Taylor, A. Menciassi, G. Fichtinger, P. Fiorini, and P. Dario, "Medical robotics and computer-integrated surgery," in *Springer handbook of robotics*. Springer, 2016, pp. 1657–1684.

[106] C. Schürmann, M. Schöpfer, R. Haschke, and H. Ritter, "A high-speed tactile sensor for slip detection," in *Towards service robots for everyday environments*. Springer, 2012, pp. 403–415.

[107] M. Zhou, S. Tse, A. Derevianko, D. B. Jones, S. D. Schwaitzberg, and C. Cgl., "Effect of haptic feedback in laparoscopic surgery skill acquisition," *Surgical Endoscopy*, vol. 26, no. 4, pp. 1128–1134, 2012.

[108] G. Tholey, J. P. Desai, and C. Ae., "Force feedback plays a significant role in minimally invasive surgery: Results and analysis," *Annals of Surgery*, vol. 241, no. 1, pp. 102–109, 2005.

[109] T. Horeman, S. P. Rodrigues, F. W. Jansen, J. Dankelman, and D. Jj., "Force measurement platform for training and assessment of laparoscopic skills," *Surgical Endoscopy*, vol. 24, no. 5, pp. 3102–3108, 2009.

[110] J. Barrie, Z. Ehteshami, P. Culmer, D. G. Jayne, and A. Neville, "Relaxation and recovery of colon after application of a mechanical stress," *Biomedical Engineering*, 2013.

[111] R. L. Klatzky, S. J. Lederman, C. L. Hamilton, M. Grindley, and S. Rh., "Feeling textures through a probe: Effects of probe and surface geometry and exploratory factors," *Percept Psychophys*, vol. 65, pp. 613–631, 2003.

[112] R. Brydges, H. Carnahan, and A. Dubrowski, "Surface exploration using laparoscopic surgical instruments: The perception of surface roughness," *Ergonomics*, vol. 48, pp. 874–894, 2005.

[113] W. K. Susmitha, G. Mathew, S. R. Devasahayam, B. Perakath, and V. Sk., "Factors influencing forces during laparoscopic pinching: Towards the design of virtual simulator," *International Journal of Surgery*, vol. 18, pp. 211–215, 2015.

[114] P. Joice, G. B. Hanna, and A. Cuschieri, "Errors enacted during endoscopic surgery-a human reliability analysis," *Applied Ergonomics*, vol. 29, no. 6, pp. 409–414, Dec 1998.

[115] J. H. Chandler, F. Mushtaq, B. Moxley-Wyles, N. P. West, G. W. Taylor, and P. R. Culmer, "Real-time assessment of mechanical tissue trauma in surgery," *IEEE Transactions on Biomedical Engineering*, vol. 64, no. 10, pp. 2384–2393, 2017.

[116] N. Burkhard, R. Steger, and M. Cutkosky, "Sensing slip of grasped wet, conformable objects," in *Intelligent Robots and Systems (IROS), 2017 IEEE/RSJ International Conference on*. IEEE, 2017, pp. 5744–5749.

[117] D. Accoto, R. Sahai, F. Damiani, D. Campolo, E. Guglielmelli, and P. Dario, "A slip sensor for biorobotic applications using a hot wire anemometry approach," *Sensors and Actuators A: Physical*, vol. 187, pp. 201–208, 2012.

[118] H. Chen, L. Zhang, D. Zhang, P. Zhang, and Z. Han, "Bioinspired surface for surgical graspers based on the strong wet friction of tree frog toe pads," *ACS applied materials & interfaces*, vol. 7, no. 25, pp. 13 987–13 995, 2015.

[119] Y.-J. Lim, D. Deo, T. P. Singh, D. B. Jones, and S. De, "In situ measurement and modeling of biomechanical response of human cadaveric soft tissues for physics-based surgical simulation," *Surgical endoscopy*, vol. 23, no. 6, p. 1298, 2009.

[120] J. Z. Wu, R. G. Dong, and A. W. Schopper, "Analysis of effects of friction on the deformation behavior of soft tissues in unconfined compression tests," *Journal of Biomechanics*, vol. 37, no. 1, pp. 147–155, 2004.

[121] S. Derler, R. Huber, H.-P. Feuz, and M. Hadad, "Influence of surface microstructure on the sliding friction of plantar skin against hard substrates," *Wear*, vol. 267, no. 5-8, pp. 1281–1288, 2009.

[122] M. Swindle, A. Makin, A. Herron, F. Clubb Jr, and K. Frazier, "Swine as models in biomedical research and toxicology testing," *Veterinary pathology*, vol. 49, no. 2, pp. 344–356, 2012.

[123] H. P. Haber and M. Stern, "Intestinal ultrasonography in children and young adults: bowel wall thickness is age dependent." *Journal of ultrasound in medicine*, vol. 19, no. 5, pp. 315–321, 2000.

[124] I. A. Stokes, S. Chegini, S. J. Ferguson, M. G. Gardner-Morse, J. C. Iatridis, and J. P. Laible, "Limitation of finite element analysis of poroelastic behavior of biological tissues undergoing rapid loading," *Annals of biomedical engineering*, vol. 38, no. 5, pp. 1780–1788, 2010.

[125] T. Krupski, C. Gundersen, W. Carson, C. Moskaluk, J. Harper, and G. Gerling, "Assessing mechanical properties of benign and malignant prostate tissue." *Journal of Clinical Oncology*, vol. 28, no. 15_suppl, pp. e15 109–e15 109, 2010.

[126] S. Phipps, T. Yang, F. Habib, R. Reuben, and S. McNeill, "Measurement of tissue mechanical characteristics to distinguish between benign and malignant prostatic disease," *Urology*, vol. 66, no. 2, pp. 447–450, 2005.

[127] A. E. Kubba and A. I. Kubba, "A micro-capacitive pressure sensor design and modelling," *Journal of Sensors and Sensor Systems*, vol. 5, no. 1, p. 95, 2016.

[128] W. Yang, "Design of electrical capacitance tomography sensors," *Measurement Science and Technology*, vol. 21, no. 4, p. 042001, 2010.

[129] M. I. Tiwana, A. Shashank, S. J. Redmond, and N. H. Lovell, "Characterization of a capacitive tactile shear sensor for application in robotic and upper limb prostheses," *Sensors and Actuators A: physical*, vol. 165, no. 2, pp. 164–172, 2011.

[130] F. L. Hammond, R. K. Kramer, Q. Wan, R. D. Howe, and R. J. Wood, "Soft tactile sensor arrays for force feedback in micromanipulation," *IEEE Sensors Journal*, vol. 14, no. 5, pp. 1443–1452, 2014.

[131] D. Alvares, L. Wieczorek, B. Raguse, F. Ladouceur, and N. H. Lovell, "Development of nanoparticle film-based multi-axial tactile sensors for biomedical applications," *Sensors and Actuators A: Physical*, vol. 196, pp. 38–47, 2013.

[132] M. Jagiella, S. Fericean, R. Droxler, and A. Dorneich, "New magneto-inductive sensing principle and its implementation in sensors for industrial applications," in *Sensors, 2004. Proceedings of IEEE.* IEEE, 2004, pp. 1020–1023.

[133] J. O. Fava and M. C. Ruch, "Calculation and simulation of impedance diagrams of planar rectangular spiral coils for eddy current testing," *NDT & e International*, vol. 39, no. 5, pp. 414–424, 2006.

[134] T. Instruments. Ti ldc spiral coil design tool. [Online]. Available: http://www.ti.com/design-tools/overview.html

[135] H. Wang and Z. Feng, "Ultrastable and highly sensitive eddy current displacement sensor using self-temperature compensation," *Sensors and Actuators A: Physical*, vol. 203, pp. 362–368, 2013.

[136] S. D. Roach, "Designing and building an eddy current position sensor," *Sensors-the Journal of Applied Sensing Technology*, vol. 15, no. 9, pp. 56–74, 1998.

[137] COMSOL Inc., USA. Comsol multiphysics 5.3. [Online]. Available: http://www.comsol.com/

[138] Dassault Systèmes SolidWorks Corporation. Solidworks 2015 x64 edition. [Online]. Available: http://www.solidworks.com/

[139] S. S. Mohan, M. del Mar Hershenson, S. P. Boyd, and T. H. Lee, "Simple accurate expressions for planar spiral inductances," *IEEE Journal of solid-state circuits*, vol. 34, no. 10, pp. 1419–1424, 1999.

[140] J. Wilde and Y. Lai, "Design optimization of an eddy current sensor using the finite-elements method," *Microelectronics Reliability*, vol. 43, no. 3, pp. 345–349, 2003.

[141] A. Reatti and M. K. Kazimierczuk, "Comparison of various methods for calculating the ac resistance of inductors," *IEEE Transactions on Magnetics*, vol. 38, no. 3, pp. 1512–1518, 2002.

[142] G. d. Boer, N. Raske, H. Wang, J. Kow, A. Alazmani, M. Ghajari, P. Culmer, and R. Hewson, "Design optimisation of a magnetic field based soft tactile sensor," *Sensors*, vol. 17, no. 11, p. 2539, 2017.

[143] S. Labs. Syntissue adult skin. [Online]. Available: http://syndaver.com/wp-content/uploads//Documents/Tear%20Sheets/Tear-Sheet-141500-Adult-Skin.pdf

[144] L. Bostan, Z. Taylor, M. Carré, S. MacNeil, S. Franklin, and R. Lewis, "A comparison of friction behaviour for ex vivo human, tissue engineered and synthetic skin," *Tribology International*, vol. 103, pp. 487–495, 2016.

[145] T. Baumberger and C. Caroli, "Solid friction from stick–slip down to pinning and aging," *Advances in Physics*, vol. 55, no. 3-4, pp. 279–348, 2006.

[146] E. R. Reale and A. C. Dunn, "Poroelasticity-driven lubrication in hydrogel interfaces," *Soft matter*, vol. 13, no. 2, pp. 428–435, 2017.

[147] M. Q. Nguyen, Z. Hughes, P. Woods, Y.-S. Seo, S. Rao, and J.-C. Chiao, "Field distribution models of spiral coil for misalignment analysis in wireless power transfer systems," *IEEE Transactions on Microwave Theory and Techniques*, vol. 62, no. 4, pp. 920–930, 2014.

[148] C. E. Reiley, T. Akinbiyi, D. Burschka, D. C. Chang, A. M. Okamura, and D. D. Yuh, "Effects of visual force feedback on robot-assisted surgical task performance," *The Journal of thoracic and cardiovascular surgery*, vol. 135, no. 1, pp. 196–202, 2008.

[149] M. B. C. Balcı, T. Ta, A. smet Hazar, M. Aydın, and Ö. Onuk, "Applicability and effectiveness of virtual realitysimulator training in urologic surgery: Adouble-blind randomised study," *Nobel Medicus Journal*, vol. 10, no. 2, 2014.

[150] E. M. Overtoom, T. Horeman, F.-W. Jansen, J. Dankelman, and H. W. Schreuder, "Haptic feedback, force feedback, and force-sensing in simulation training for laparoscopy: A systematic overview," *Journal of surgical education*, 2018.

[151] U. Kim, Y. B. Kim, J. So, D.-Y. Seok, and H. R. Choi, "Sensorized surgical forceps for robotic-assisted minimally invasive surgery," *IEEE Transactions on Industrial Electronics*, 2018.

[152] W. Lai, L. Cao, Z. Xu, P. T. Phan, P. Shum, and S. J. Phee, "Distal end force sensing with optical fiber bragg gratings for tendon-sheath mechanisms in flexible endoscopic robots," in *2018 IEEE International Conference on Robotics and Automation (ICRA)*. IEEE, 2018, pp. 1–5.

[153] L. Jamone, L. Natale, G. Metta, and G. Sandini, "Highly sensitive soft tactile sensors for an anthropomorphic robotic hand," *IEEE sensors Journal*, vol. 15, no. 8, pp. 4226–4233, 2015.

[154] L. Yu, Y. Yan, C. Li, and X. Zhang, "Three-dimensional nonlinear force-sensing method based on double microgrippers with e-type vertical elastomer for minimally invasive robotic surgery," *Robotica*, vol. 36, no. 6, pp. 865–881, 2018.

[155] L. Wang, Y. Han, and Y. Huang, "Usage of conductive polymer composite as the object film of eddy current gap sensor," *IEEE Transactions on Instrumentation and Measurement*, vol. 62, no. 12, pp. 3202–3208, 2013.

[156] E. Westebring-Van Der Putten, M. Hajian, R. Goossens, J. Van Den Dobbelsteen, and J. Jakimowicz, "A laparoscopic grasper handle with integrated augmented tactile feedback, designed for training grasp control," in *International Conference on Human Haptic Sensing and Touch Enabled Computer Applications*. Springer, 2010, pp. 243–250.

[157] S. Fouvry, P. Kapsa, and L. Vincent, "Analysis of sliding behaviour for fretting loadings: determination of transition criteria," *Wear*, vol. 185, no. 1-2, pp. 35–46, 1995.

[158] F. Motamen Salehi, A. Neville, and M. Bryant, "Bio-tribology of incontinence management products: additional complexities at the skin–pad interface," *Tribology-Materials, Surfaces & Interfaces*, pp. 1–7, 2018.

[159] A. Remes and D. Williams, "Immune response in biocompatibility," *The Biomaterials: Silver Jubilee Compendium*, pp. 79–91, 2006.

[160] A. B. Mathur, T. O. Collier, W. J. Kao, M. Wiggins, M. A. Schubert, A. Hiltner, and J. M. Anderson, "In vivo biocompatibility and biostability of modified polyurethanes," *Journal of biomedical materials research*, vol. 36, no. 2, pp. 246–257, 1997.